UNIVERSITÄT ZU LÜBECK

From the Institute for Endocrinology & Diabetes

of the University of Lübeck

Directors: Prof. Dr. rer. nat. Jens Mittag

and Prof. Dr. med. Sebastian Meyhöfer

"Mastering the Heat: The Role of Thyroid Hormone Receptor α1 in Thermoregulation"

Dissertation for Fulfillment of Requirements

for the Doctoral Degree

of the University of Lübeck

from the Department of Natural Sciences

Submitted by

Sarah Christine Sentis

from Witzenhausen, Germany

Lübeck, 2023

First referee: Prof. Jens Mittag

Second referee: Prof. Henrik Oster

Date of oral examination: March 18, 2024

Approved for printing: April 2, 2024

Eigenständigkeitserklärung

Ich versichere, dass ich die vorliegende Dissertation ohne fremde Hilfe angefertigt und keine anderen als die angegebenen Hilfsmittel verwendet habe. Weder vorher noch gleichzeitig habe ich andernorts einen Zulassungsantrag gestellt oder diese Dissertation vorgelegt. Ich habe mich bisher keinem Promotionsverfahren unterzogen.

_____

Sarah C. Sentis

Lübeck, den 22.12.2023

List of Publications

Parts of this thesis were already submitted to or published in peer-reviewed journals due to priority reasons:

1. **Sentis, S.C.**, Oelkrug, R., Mittag, J., 2021. Thyroid hormones in the regulation of brown adipose tissue thermogenesis. Endocr. Connect. 10, R106–R115. https://doi.org/10.1530/EC-20-0562
2. **Sentis, S.C.**, Dore, R., Oelkrug, R., Kolms, B., Iwen, K.A., Mittag, J., 2023. Hypothalamic thyroid hormone receptor α1 signaling controls body temperature. In press.

Publications that are not part of this thesis:

1. Dore, R., **Sentis, S.C.**, Johann, K., Lopez-Alcantara, N., Resch, J., Moeller, L.C., Fuehrer, D., Obermayer-Wasserscheid, B., Opitz, R., Mittag, J., 2023. Partial resistance to thyroid hormone-induced tachycardia and cardiac hypertrophy in mice lacking thyroid hormone receptor beta (preprint). Under review. https://doi.org/10.1101/2023.11.21.567193.
2. Dore, R., Watson, L., Hollidge, S., Krause, C., **Sentis, S.C.**, Oelkrug, R., Geißler, C., Johann, K., Pedaran, M., Lyons, G., Lopez-Alcantara, N., Resch, J., Sayk, F., Iwen, K.A., Franke, A., Boysen, T.J., Dalley, J.W., Lorenz, K., Moran, C., Rennie, K.L., Arner, A., Kirchner, H., Chatterjee, K., Mittag, J., 2023. Resistance to thyroid hormone induced tachycardia in RTHα syndrome. Nat. Commun. 14, 3312. https://doi.org/10.1038/s41467-023-38960-1
3. Lopez-Alcantara, N., Oelkrug, R., **Sentis, S.C.**, Kirchner, H., Mittag, J., 2023. Lack of thyroid hormone receptor beta is not detrimental for non-alcoholic steatohepatitis progression. iScience 26, 108064. https://doi.org/10.1016/j.isci.2023.108064
4. Land, R., **Sentis, S.C.**, Kral, A., 2022. Topographical EEG recordings of visual evoked potentials in mice using multichannel thin-film electrodes. J. Vis. Exp. 184, e64034. doi:10.3791/64034

Table of Contents

List of Figures

List of Tables

List of Abbreviations

AAV	Adeno-associated virus
ADP+P	Adenosine diphosphate and phosphate
Adrb2	ß2-adrenergic receptor
ADRB3	β3-adrenergic receptor
Adrb3	β3-adrenergic receptor
AHA	Anterior hypothalamic area
AMPK	Adenosine monophosphate-activated protein kinase
ANCOVA	Analysis of covariance
ANOVA	Analysis of variance
ARC	Arcuate nucleus
ATP	Adenosine triphosphate
Atp2a1	ATPase sarcoplasmic/endoplasmic reticulum Ca^{2+} transporting 1
Atp2a2	ATPase sarcoplasmic/endoplasmic reticulum Ca^{2+} transporting 2
BAT	Brown adipose tissue
BCA	Bicinchoninic acid
b-CL	CL 316243
BMR	Basal metabolic rate
BSA	Bovine serum album
cAMP	Cyclic adenosine monophosphate
Cd5l	CD5 molecule like
cDNA	Complementary deoxyribonucleic acid
CMV	Cytomegalovirus
Complex V	ATP synthase
CREB	Cyclic adenosine monophosphate response element-binding protein
DEE	Daily energy expenditure
DIO1	Iodothyronine deiodinase type I
Dio1	Iodothyronine deiodinase type I
DIO2	Iodothyronine deiodinase type II
Dio2	Iodothyronine deiodinase type II
DIO3	Iodothyronine deiodinase type III
Dio3	Iodothyronine deiodinase type III
ECG	Electrocardiogram
ECL	Enhanced chemiluminescence
eWAT	Epididymal white adipose tissue
Fasn	Fatty acid synthase
FBS	Fetal bovine serum
FFA	Free fatty acid
FGF21	Fibroblast growth factor 21
fT4	Free thyroxin
GFP	Green fluorescent protein

Gk	Glycerol kinase
Gpd2	Glycerol-3-phosphate dehydrogenase 2
Gys	Glycogen synthase 1
Hcrt	Hypocretin (orexin)
HPT	Hypothalamus-pituitary-thyroid axis
HSL	Hormone-sensitive lipase
iBAT	Interscapular brown adipose tissue
ICV	Intracerebroventricular
iWAT	Inguinal white adipose tissue
Klf9	Krueppel-like factor 9
KO	Knockout
LH	Lateral hypothalamus
Lpl	Lipoprotein lipase
MCT	Monocarboxylate transporter
Mstn	Myostatin
NCoR	Nuclear receptor corepressor
NE	Norepinephrine
Npy	Neuropeptide Y
NST	Non-shivering thermogenesis
OAPT	Organic anion transporting polypeptide
OXPHOS	Mitochondrial oxidative phosphorylation system
Pck1	Phosphoenolpyruvate carboxykinase 1
PFA	Paraformaldehyde
PKA	Protein kinase A
POA	Preoptic area
Pomc	Poopiomelanocortin
Ppargc1α	Peroxisome proliferator-activated receptor gamma coactivator 1-alpha
Prdm16	PR domain containing 16
PVDF	Polyvinylidene difluoride
PVN	Paraventricular nucleus
qPCR	Quantitative polymerase chain reaction
RMR	Resting metabolic rate
RNA	Ribonucleic acid
RQ	Respiratory quotient
rT3	Reverse 3,3’,5-triiodothyronine
RXR	Retinoid x receptor
SEM	Standard error of the mean
SERCA2	Sarco/endoplasmic reticulum-type calcium transport ATPase 2
SLC10A1	Solute carrier family 10-member 1
SMRT	Silencing mediator of retinoic acid and thyroid hormone receptor
SNS	Sympathetic nervous system

SVF	Stromal vascular fraction
T3	3,3’,5-triiodothyronine
T4	Thyroxine
TBS-T	Tris-buffered saline with Tween20
TH	Thyroid hormone
Thrb	Thyroid hormone receptor beta 1
Thrsp	Thyroid hormone responsive gene spot14
TR	Thyroid hormone receptor
TRE	Thyroid hormone response element
TRH	Thyrotropin-releasing hormone
TRα1	Thyroid hormone receptor α1
TRβ	Thyroid hormone receptor β
TSH	Thyroid-stimulating hormone
tT3	Total 3,3’,5-triiodothyronine
tT4	Total thyroxine
UCP1	Uncoupling protein 1
Ucp1	Uncoupling protein 1
VMH	Ventromedial hypothalamus
WAT	White adipose tissue

Abstract

Thyroid hormones (TH) are important regulators of body temperature and energy metabolism in both rodents and humans. Therefore, medical conditions such as hyper- and hypothyroidism can induce changes in body temperature and disrupt energy metabolism. Consequently, maintaining optimal levels of circulating TH is essential for proper tissue and organ functioning. Over the past decade, there has been growing interest in understanding the brain actions of THs and their respective nuclear receptors, TRα1 and TRβ, in the coordination of body temperature regulation and homeostasis. However, the exact contributions of the individual TR isoforms to the central and peripheral control of body temperature remain poorly understood. In mice, mutations in TRs may lead to defects in facultative thermogenesis but also whole-body temperature regulation. Interestingly, while TRα1+m mutants have a lower body temperature phenotype at room temperature due to excessive tail heat loss, TRβ knockout (KO) animals do not show any differences in body temperature. Whether the impaired body temperature phenotype observed in TRα1+m mice is solely the result of peripheral TRα1 actions, or whether defective central TRα1 signaling contributes to an altered body temperature set-point were addressed in this study. Additionally, this study investigated the underlying mechanisms at which TH-induced brown fat thermogenesis is differentially regulated in rats and mice as systemic TH treatment induces brown fat thermogenesis in rats but not in mice. First, by using radiotelemetry in freely moving mice at different ambient temperatures, including oral 3,3',5-triiodothyronine (T3) treatment, the contributions of mutant TRα1 and a TRβ KO to whole-body temperature regulation were dissected. Second, the effects of a dominant-negative TRα1 on body temperature after adeno-associated virus mediated expression in the hypothalamus, a region known to be involved in thermoregulation, were investigated. Lastly, to resolve the species-dependent effect of TH on brown fat thermogenesis in rats and mice, primary brown adipocytes were cultured and treated with T3, followed by thermogenic TH target gene expression analysis. However, T3 treatment of primary brown adipocytes did not induce changes in thermogenic marker gene expression, indicating that the effects of TH in brown fat are rather indirect. Interestingly, the *in vivo* experiments could show that TRβ signaling only plays a minor role in whole-body temperature regulation, whereas TRα1+m mutants had lower body temperature at 22°C and partially also at 30°C, despite reversed tail heat loss. Only oral T3 treatment fully rescued the defective body temperature phenotype of TRα1+m mice, implying that TRα1 signaling is involved in the regulation of the central temperature set-point. Additionally, the expression of hypothalamic dominant-negative TRα1 lowered body temperature at 22°C and 30°C. In conclusion, the results of this study suggest that hypothalamic TRα1 signaling is a central key player in the regulation of whole-body temperature homeostasis. Further research is required to identify the exact hypothalamic regions and neuroanatomical substrates that facilitate central TRα1 signaling.

Zusammenfassung

Schilddrüsenhormone sind wichtige Regulatoren der Körpertemperatur und des Energiestoffwechsels sowohl bei Nagetieren als auch beim Menschen. Daher können Krankheiten wie Hyper- und Hypothyreose zu Veränderungen der Körpertemperatur führen und den Energiestoffwechsel stören. Folglich ist die Aufrechterhaltung optimaler Schilddrüsenhormonspiegel für eine ordnungsgemäße Gewebe- und Organfunktion unerlässlich. In den letzten zehn Jahren ist das Interesse am Verständnis der Wirkung der Schilddrüsenhormone und ihrer jeweiligen nuklearen Rezeptoren, TRα1 und TRβ, im Gehirn bei der Koordinierung der Regulierung und Homöostase der Körpertemperatur gewachsen. Die genauen Beiträge der einzelnen Schilddrüsenhormonrezeptorisoformen zur zentralen und peripheren Kontrolle der Körpertemperatur sind jedoch nach wie vor nur unzureichend bekannt. Bei Mäusen können Schilddrüsenhormonrezeptormutationen zu Defekten in der fakultativen Thermogenese, aber auch in der Körpertemperaturregulation führen. Interessanterweise zeigen TRα1+m-Mutanten einen niedrigeren Körpertemperaturphänotypen bei Raumtemperatur aufgrund eines übermäßigen Wärmeverlusts über den Schwanz, während TRβ-Knockout (KO) Tiere keine Unterschiede in der Körpertemperatur aufweisen. In dieser Studie wurde untersucht, ob der bei TRα1+m-Mäusen beobachtete beeinträchtigte Körpertemperaturphänotyp ausschließlich auf periphere TRα1-Aktionen zurückzuführen ist, oder ob eine defekte zentrale TRα1-Signalgebung zu einem veränderten Sollwert der Körpertemperatur beiträgt. Da eine systemische Schilddrüsenhormonbehandlung die Thermogenese des braunen Fetts bei Ratten, nicht aber bei Mäusen induziert, wurden darüber hinaus in dieser Studie die zugrundeliegenden Mechanismen, durch die die Schilddrüsenhormon-induzierte Thermogenese des braunen Fetts bei Ratten und Mäusen unterschiedlich reguliert wird, untersucht. Zuerst wurden mit Hilfe von Radiotelemetrie bei frei beweglichen Mäusen bei verschiedenen Umgebungstemperaturen, einschließlich oraler 3,3',5-Triiodthyronin (T3) -Behandlung, die Beiträge von mutiertem TRα1 und einem TRβ-KO zur Regulierung der Körpertemperatur untersucht. Anschließend wurden die Auswirkungen der Adeno-assoziierten Virus-vermittelten Expression von dominant-negativem TRα1 auf die Körpertemperatur im Hypothalamus, einer Region, die bekanntermaßen an der Thermoregulation beteiligt ist, untersucht. Um schließlich die speziesabhängige Wirkung von Schilddrüsenhormonen auf die Thermogenese des braunen Fettgewebes bei Ratten und Mäusen zu klären, wurden primäre braune Adipozyten kultiviert und mit T3 behandelt, gefolgt von einer Analyse der thermogenen Schilddrüsenhormonzielgenexpression. Die Behandlung von primären braunen Adipozyten mit T3 führte jedoch nicht zu Veränderungen in der Expression thermogener Markergene, was darauf hindeutet, dass die Wirkung von Schilddrüsenhormonen im braunen Fett eher indirekt ist. Interessanterweise konnten die *In-vivo*-Experimente zeigen, dass die TRβ-Signalübertragung nur eine untergeordnete Rolle bei der Regulierung

der Körpertemperatur spielt, während TRα1+m-Mutanten, trotz aufgehobenem Wärmeverlust am Schwanz, eine niedrigere Körpertemperatur bei 22°C und teilweise auch bei 30°C aufwiesen. Nur eine orale T3-Behandlung rettete den defekten Körpertemperaturphänotypen der TRα1+m-Mäuse vollständig, was darauf hindeutet, dass die TRα1-Signalübertragung an der Regulierung des zentralen Temperatursollwerts beteiligt ist. Zusätzlich senkte die Expression von hypothalamischem dominant-negativem TRα1 die Körpertemperatur bei 22°C und 30°C. Die Ergebnisse dieser Studie deuten darauf hin, dass der hypothalamische TRα1-Signalweg eine zentrale Rolle bei der Regulierung der Homöostase der Körpertemperatur spielt. Weitere Forschung ist erforderlich, um die genauen hypothalamischen Regionen und die neuroanatomischen Substrate zu identifizieren, die die zentrale TRα1-Signalübertragung ermöglichen.

1 Introduction

Body temperature regulation is a highly complex and energy consuming process that takes place in homeotherms like rodents and humans. A stable core body temperature regardless of changes in ambient temperature is crucial for vital enzymatic activity (Peterson et al., 2007) and thus normal organ and tissue functioning. Most importantly, to achieve and maintain a constant body temperature, thermoregulatory processes like heat dissipation and heat production through thermogenesis need to be balanced at all times (Speakman and Król, 2010).

There are many important tools for body temperature regulation in humans, e.g., vasoconstriction to conserve heat and vasodilatation and sweating to get rid of excess heat. In rodents, vasoconstriction and vasodilation are also important regulators of body temperature, especially with regard to their ability to lose heat via their tails, as rodents are incapable of regulating their body temperature via sweating (Kennedy et al., 1984; Škop et al., 2020b). Other measures aimed at maintaining a constant body temperature may involve behavioral adjustments like reducing physical activity in high-temperature environments or seeking warmth through close contact in colder environments (Mota-Rojas et al., 2021).

1.1 Thermogenesis

In rodents and humans, multiple heat-producing processes contribute to thermogenesis, namely: basal metabolism, post-prandial and diet-induced thermogenesis, physical activity-induced thermogenesis, and facultative thermogenesis (Fristoe et al., 2015; Ricquier, 2006). Heat production through basal metabolism in particular is termed *obligatory thermogenesis* (Ricquier, 2006).

In the following chapter, the current knowledge about obligatory and facultative thermogenesis will be discussed.

1.1.1 Obligatory and facultative thermogenesis

Obligatory thermogenesis is the byproduct of cellular metabolic processes and takes place, among others, in homeotherms like rodents and humans. Subsequently, obligatory thermogenesis and therefore heat production in homeotherms greatly relies on oxygen consumption and cellular respiration to ensure sufficient heat production and the maintenance of constant body temperature (Fristoe et al., 2015; Ricquier, 2006; Soares and Müller, 2018). Consequently, homeothermic animals have a higher metabolic rate compared to poikilothermic animals that do not rely on thermal homeostasis (Van Der Meer, 2021).

The term *thermoneutrality* refers to the ambient temperature at which obligatory thermogenesis and thus the basal metabolic rate alone can sustain and defend body temperature without the need for additional thermoregulatory mechanisms (Fischer et al., 2019; Gordon, 2012). In mice and rats, the thermoneutral range is between 28 - 30 °C (Škop et al., 2020a). However, for humans, the thermoneutral temperature is 22 - 23°C due to the use of clothing or shelter (Pallubinsky et al., 2019). Below thermoneutral temperatures, rodents and humans have developed tightly regulated mechanisms to defend their body temperature (Fristoe et al., 2015; Škop et al., 2020b). In rodents, e.g., fur and also tail vasoconstriction limit heat loss at cooler temperatures to conserve heat (Mota-Rojas et al., 2021; Škop et al., 2020b). Additionally, sudden and rapid temperature drops activate heat generating processes which are summarized by the term *facultative thermogenesis* (Ricquier, 2006; Van Marken Lichtenbelt and Schrauwen, 2011).

Rodents and humans possess two forms of heat generating processes to adapt to colder ambient temperatures: shivering and non-shivering thermogenesis (NST). The extra heat production via shivering thermogenesis and/or NST during facultative or adaptive thermogenesis requires increased metabolic activity and energy expenditure (Blondin and Haman, 2018; Cannon and Nedergaard, 2004; Haman and Blondin, 2017; Silva, 2006). First, in response to sudden cold exposure, the body starts to shiver. Shivering is the most immediate thermogenic reaction to a rapid drop in temperature and is initiated by involuntary movements of skeletal muscles, e.g., gastrocnemius or soleus muscle (Blondin and Haman, 2018; Haman and Blondin, 2017). Second, in cases of prolonged cold exposure where shivering alone cannot cover the heat production demands of the body (Silva, 2006), heat production occurs through NST (Blondin and Haman, 2018). Importantly, the peripheral responses to cold, like shivering and NST, are regulated by the sympathetic central nervous system (SNS) (Nakamura and Morrison, 2011).

1.1.2 Adipose tissue thermogenesis

Brown adipose tissue (BAT) is a metabolically highly active tissue in rodents and also in humans that produces heat during NST (Bartelt and Heeren, 2014; Cannon and Nedergaard, 2004; Cheng et al., 2021).

The biggest BAT depot in rodents can be found in the interscapular neck region in close proximity to the aorta. Consequently, locally warmed blood can circulate through the body as one measure among others to defend body temperature in case of prolonged cold exposure (Thoonen et al., 2016). In turn, BAT depots are highly innervated by the SNS and well vascularized (Cannon and Nedergaard, 2004). In humans, vital BAT depots in newborns and infants mediate rapid heat production in response to cold as their skeletal muscle is not yet sufficiently developed to defend their body

temperature via shivering thermogenesis. The largest BAT depots in newborns and infants can be found in the interscapular neck region, around the kidneys, the adrenal glands, and smaller depots can be found, e.g., along the spine (Lidell, 2018). Also in some adult humans, BAT can be found as small fat pads in the neck region, near the kidneys, and near the adrenal glands (Cypess et al., 2009; Gaspar et al., 2021; Lee et al., 2011; Virtanen et al., 2009).

The activation of brown fat thermogenesis requires the release of norepinephrine (NE) by the SNS innervating BAT. As the main central regulator of body temperature homeostasis and thermogenesis, the brain releases NE in response to cold exposure to directly trigger BAT thermogenesis (Figure 1). In rats and mice, SNS signaling in BAT is mainly mediated by the β3-adrenergic receptor (ADRB3) isoform (Collins et al., 2014; Grujic et al., 1997; Zhao et al., 1997). In turn, the body's response to prolonged cold exposure in rodents is predominantly facilitated by the uncoupling protein 1 (UCP1) initiating NST (Ikeda and Yamada, 2020; Jacobsson et al., 1985; Kozak et al., 1988). Upon NE-binding, β-adrenergic receptors induce second messenger signaling cascades, leading to the transcriptional upregulation of the gene *Ucp1*. UCP1 is a transmembrane protein located at the inner mitochondrial membrane of brown adipocytes (Jacobsson et al., 1985; Kozak et al., 1988) and harbors six α-helical domains with a single substrate binding site, a proton binding site, and several hydrophobic residues (Kozak et al., 1988; Ricquier, 2017; Ricquier et al., 1991). In order to activate UCP1, β-adrenergic receptors mediate the increase of intracellular cyclic adenosine monophosphate (cAMP) concentration and therefore the stimulation of protein kinase A (PKA) activity (Wicksteed and Dickson, 2017; Zhao et al., 1997). Examples of downstream targets of PKA are the cAMP-response-element-binding protein (CREB) and the hormone-sensitive lipases (HSL), which provide free fatty acids (FFA) after breaking down triacylglycerol (Divakaruni et al., 2012; Fedorenko et al., 2012), ultimately leading to the activation of UCP1 (Figure 1).

On the molecular level, the energy currency in the body is adenosine triphosphate (ATP) that is generated during oxidative respiration (Dunn and Grider, 2023; Smeitink et al., 2001; Vercellino and Sazanov, 2022). Consequently, the release of energy during the hydrolysis of ATP to adenosine diphosphate and phosphate (ADP+P) serves important cell functions in every tissue and organ (de Meis et al., 1997; Nelson and Cox, 2001). During BAT thermogenesis, ATP production is uncoupled by UCP1. In detail, upon the activation by FFAs, UCP1 facilitates the uncoupling of oxidative phosphorylation from ATP production during mitochondrial respiration by dissipating the proton gradient from the electron transport chain (Demine et al., 2019; Silva, 2006). The necessary increase in oxidation of substrates consequently releases more energy in the form of heat giving BAT its thermogenic features (Ikeda and Yamada, 2020). BAT possesses high amounts of mitochondria and thus provides an exclusive environment for heat production via controlled uncoupling of the oxidative ADP phosphorylation via UCP1. Hence, UCP1 protein content is most abundantly found in the mitochondria of brown adipocytes,

but cold exposure may also trigger *Ucp1* expression in white adipocytes (Bartesaghi et al., 2015; Sepa-Kishi et al., 2019).

White adipose tissue (WAT) stores energy as large triglyceride-containing lipid droplets inside of white adipocytes. Two major WAT depots in rodents are epididymal (eWAT), which can be found in the central cavity, and subcutaneous inguinal WAT (iWAT). White adipocytes and thus, WAT, likewise harbor energy storing properties in humans. The two main white fat depots in humans are visceral and subcutaneous fat (Börgeson et al., 2022). Similar to BAT, also WAT is innervated by the SNS and vascularized (Bartness et al., 2014; Rayner, 2001).

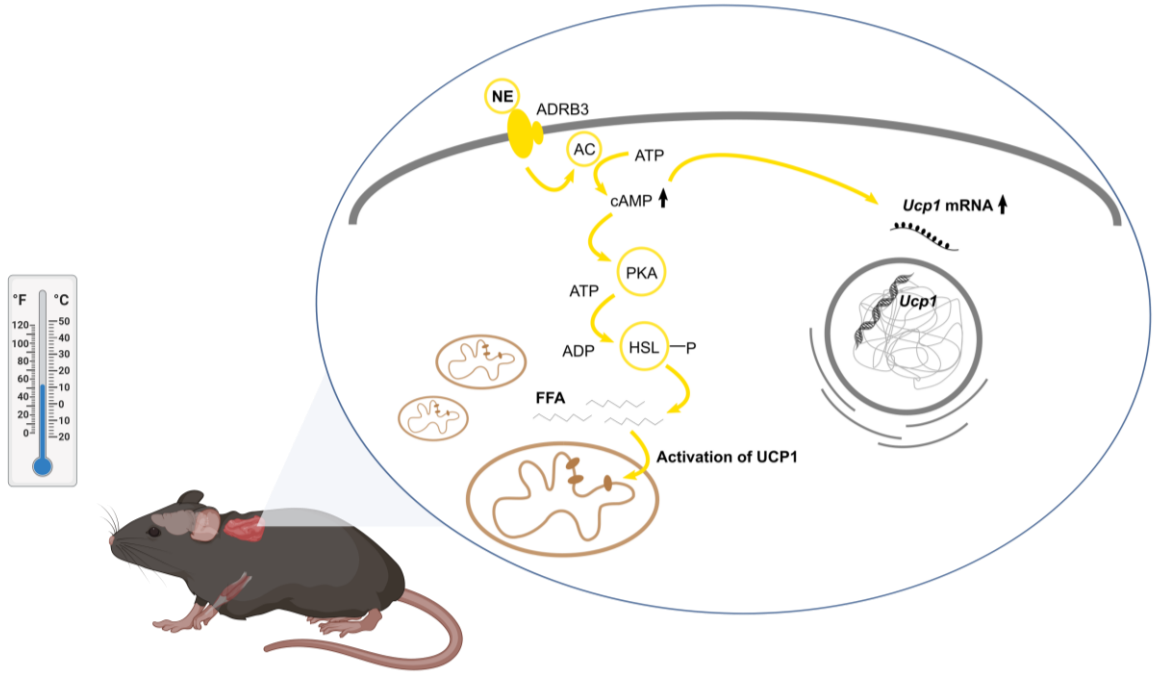

Figure 1: Molecular pathways in BAT thermogenesis in response to prolonged cold exposure in mice. Upon SNS signaling into BAT, norepinephrine (NE) binds to β3-adrenoreceptors (ADRB3), which in turn will lead to increased intracellular cyclic adenosine monophosphate (cAMP) levels due to the activation of adenylyl cyclase (AC). cAMP stimulates protein kinase A (PKA), which subsequently activates the hormone-sensitive lipase (HSL) and will lead to the breakdown of free fatty acids (FFA). FFAs can activate uncoupling protein 1 (UCP1) that is located at the inner mitochondrial membrane, ultimately leading to NST. The schematic molecular overview of brown fat thermogenesis was adapted from Sentis et al., 2021.

Interestingly, cold exposure and SNS signaling can trigger lipolysis in WAT which leads to the release of FFAs that can potentially active UCP1 (Bartelt et al., 2011; Khedoe et al., 2015). More importantly, UCP1 protein can also be found in WAT of rodents and humans, albeit in smaller quantities compared to BAT (Bartesaghi et al., 2015; Martínez-Sánchez et al., 2017a; Sepa-Kishi et al., 2019). Furthermore, cold exposure and other cues can trigger the occurrence of cells that harbor higher amounts of mitochondria compared to white adipocytes within WAT depots. These cells are called

beige cells and may acquire thermogenic potential during a process called *browning* (Fisher et al., 2012; Ishibashi and Seale, 2010; Petrovic et al., 2010). The thermogenic feature of beige cells, namely the ability to contribute to NST, is of great interest in obesity research due to their origin in WAT depots and their ability to burn excess calories (Bartelt and Heeren, 2014; Petrovic et al., 2010). Browning within WAT can be triggered by cold and β-adrenergic agonists (Cannon and Nedergaard, 2004). However, another trigger of browning in WAT is hormones, such as thyroid hormone (Johann et al., 2019; Silva, 2003, 2001, 1995).

1.2 Thyroid hormones

Thyroid hormones (TH) are crucial players in whole-body homeostasis, controlling, e.g., growth, thermogenesis, and metabolism in mammals, such as rodents and humans. Target tissues of TH are, e.g., the liver, heart, muscle tissue, and also BAT (Anyetei-Anum et al., 2018).

1.2.1 Thyroid hormone regulation and action

The release of TH by the thyroid gland is tightly regulated by the hypothalamus-pituitary-thyroid (HPT) axis (Duntas, 2016). Additionally, the release of TH is highly self-regulated via a negative feedback circuit (Gothe et al., 1999; Shupnik et al., 1989; Yen, 2001). Upon signaling from the hypothalamus via the thyrotropin-releasing hormone (TRH), the pituitary releases the thyroid-stimulating hormone (TSH). TSH in turn binds to the thyrotropin receptor of thyroid follicular cells of the thyroid gland initiating the releases of thyroxine (T4) and small amounts of the physiologically more active 3,3',5-triiodothyronine (T3) into the bloodstream (Shupnik et al., 1989, 1985; Yen, 2001; Figure 2).

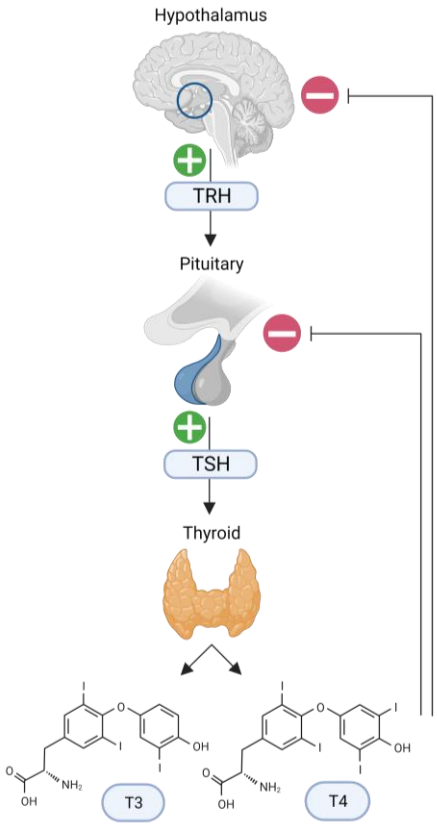

Figure 2: Hypothalamus-pituitary-thyroid (HPT) axis. The release of thyroxine (T4) and 3,3',5-triiodothyronine (T3) by the thyroid gland is tightly regulated by the HPT-axis. The hypothalamus releases thyrotropin-releasing hormone (TRH), which in turn initiates the release of thyroid-stimulating hormone (TSH) from the pituitary. Finally, TSH induces the release of T3 and T4 from the thyroid gland. TH demands in the periphery are regulated via a negative feedback circuit.

T4 and T3 enter the cell via TH transporters, such as the monocarboxylate transporter (MCT) 8, MCT10, the organic anion transporting polypeptide (OAPT) 1C1, and the solute carrier family 10 member 1 (SLC10A1) (Groeneweg et al., 2020). TH target tissues express iodothyronine deiodinases (DIO) which regulate the intracellular availability of TH (Bianco and Da Conceição, 2018; Bianco and Kim, 2006; Sabatino et al., 2021). DIO1 and DIO2 mediate the intracellular conversion of the prohormone T4 to T3 by outer ring deiodination in a tissue-specific manner. DIO1 is most abundantly found in the liver, whereas DIO2 mediates TH actions in, e.g., BAT, skeletal muscle, and the hypothalamus (Sabatino et al., 2021). In turn, DIO3 inactivates T3 to reverse T3 (rT3) restricting the tissue-specific demands of TH (Bianco and Da Conceição, 2018; Hernandez and Stohn, 2018).

Upon entry into the cell, T3 also enters the nucleus to bind to thyroid hormone receptors (TRs). Two main types of nuclear receptors, which are expressed by two different genes, can be found throughout the body: TRα1 and TRβ1/2 (Ortiga-Carvalho et al., 2014). TRα1 is most abundantly located, e.g., in the heart mediating heart rate changes via ionotropic effects, in the muscle increasing energy metabolism, and in the hypothalamus regulating body temperature (Anyetei-Anum et al., 2018; Zekri et al., 2022a). By contrast, TRβ isoforms are most abundantly found in the liver mediating important metabolic liver processes and play a role in TSH regulation, as well as during the embryonic development of hearing and color vision (Anyetei-Anum et al., 2018; Ng et al., 2001; Zekri et al., 2022a). Brown and white adipocytes accommodate both, TRα1 and TRβ isoforms (Anyetei-Anum et al., 2018; Hernández and Obregón, 1996; Zekri et al., 2022a). TRβ is thought to mediate the direct actions of TH in BAT in response to a cold trigger (Ribeiro et al., 2010, 2001; Villicev et al., 2007), whereas TRα1 is crucial for the overall adrenergic responsiveness of BAT needed for the induction of NST (Ribeiro et al., 2010; Sjögren et al., 2007). However, the exact contributions of both receptor isoforms to adaptive BAT thermogenesis and whole-body thermogenesis are yet to be fully elucidated (Sentis et al., 2021).

Nuclear TRs act as ligand-dependent transcription factors inducing or repressing target gene expression via canonical pathways, thus mediating the actions of TH signaling. Furthermore, TRs can bind to TH response elements (TREs) that unfold their action by forming heterodimers with, e.g., retinoid x receptors (RXRs) (Paquette et al., 2014; Yen, 2001). Ultimately, target gene transcription is initiated upon the recruitment of coactivator complexes and histone acetyl transferases (Koenig, 1998; Shabtai et al., 2021; Sinha and Saiz, 2014). Additionally, TRs can also act on gene transcription in the unliganded state as aporeceptors (Brent et al., 1989). Unliganded aporeceptors can interact with corepressors, e.g., the nuclear receptor corepressor (NCoR) or the silencing mediator of retinoic acid and thyroid hormone receptor (SMRT) to repress or also induce target gene transcription (Astapova et al., 2008; Saponaro et al., 2020). Recent studies suggest that TH aporeceptors play a physiological role and may mediate developmental actions in the absence of TH (Bernal and Morte, 2013). However, most TR actions are still poorly understood, as studies suggest that also non-canonical cellular

pathways may be initiated by T3 signaling (Flamant et al., 2017).

Most importantly, balanced levels of circulating TH are crucial for normal tissue and organ functioning in rodents, but also in humans. In the case of hyperthyroidism, excess circulating TH levels implicate a faster metabolism and hyperthermia, ultimately leading to weight loss (De Leo et al., 2016; Sulman et al., 1975). In turn, too little circulating TH, as in hypothyroidism, results in a slower metabolic rate and subsequent weight gain (Chaker et al., 2022). The consequent changes of the metabolic rate during clinical hypo- or hyperthyroidism can most likely be attributed to the effects of TH in metabolically highly active muscle tissue, but also in the liver (Lahesmaa et al., 2014; Sawicka-Gutaj et al., 2022; Sinha et al., 2018).

1.2.2 Thyroid hormones in thermogenesis

Thyroid hormones act in various tissues and organs of rodents and humans to exert, e.g., metabolic and thermoregulatory functions (Figure 3).

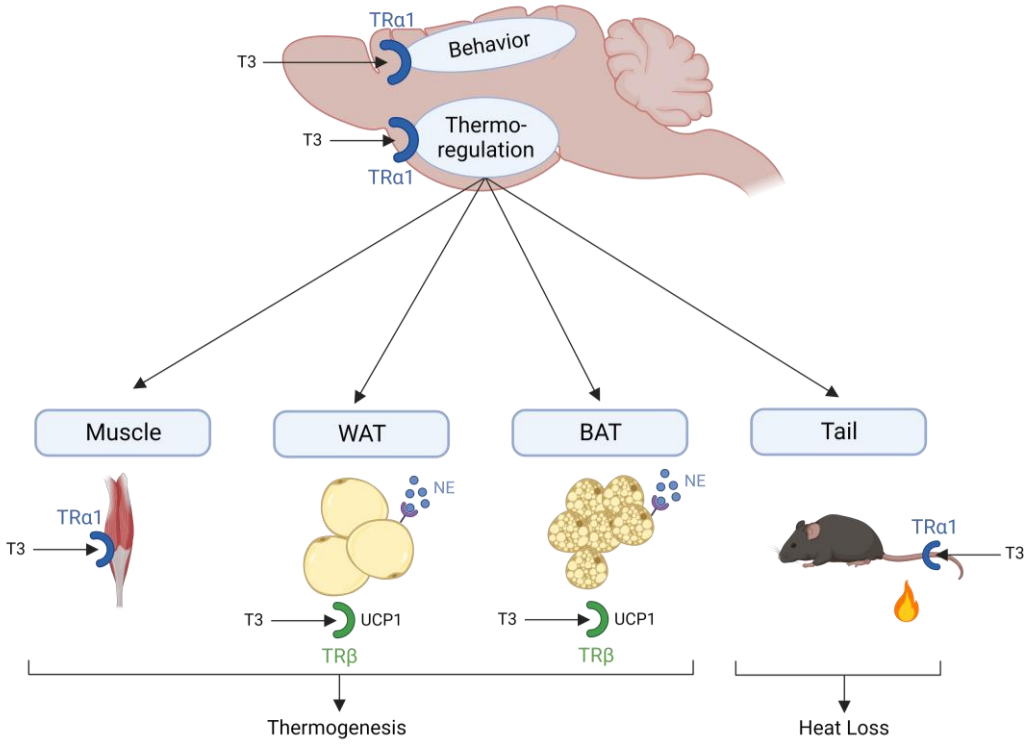

Figure 3: Thyroid hormones (TH) act in various tissues and organs of rodents. The nuclear thyroid hormone receptors (TRα1 and TRβ isoforms) can be found (i) in the brain, to regulate whole-body temperature regulation and thermogenesis; (ii) in the muscle, to increase energy metabolism; (iii) in white adipose tissue (WAT), to improve thermogenic potential by increasing Ucp1 expression; (iv) in brown adipose tissue (BAT) to induce thermogenesis via UCP1; and (v) in epithelial cells, where THs influence vasoconstriction and vasodilatation in the tail of mice. The schematic overview of thyroid hormone target organs and tissues was adapted from Sentis et al., 2021.

Following the effects of TH imbalances on whole-body thermoregulation, studies on thyroidectomized rats have long established an important role for TH in brown fat thermogenesis (Figure 3) and thus adequate BAT function (Triandafillou et al., 1982). On the molecular level, TH elicits two crucial effects in BAT: the activation of *Ucp1* transcription and the enhancement of BAT sensitivity to NE. The latter is particularly noteworthy, as NE boosts DIO2 activity (Silva and Larsen, 1983), leading to the increased conversion of intracellular T4 to T3 in BAT (Figure 4). Upon NE-stimulation, elevated DIO2 activity results in a 3- to even 4-fold increase of intracellular T3 concentration (Silva and Larsen, 1983). In turn, high intracellular T3 levels lead to nuclear TR saturation and the rapid induction of *Ucp1* expression via TREs that can be found in the 5'-flanking region of *Ucp1* (Rabelo et al., 1995).

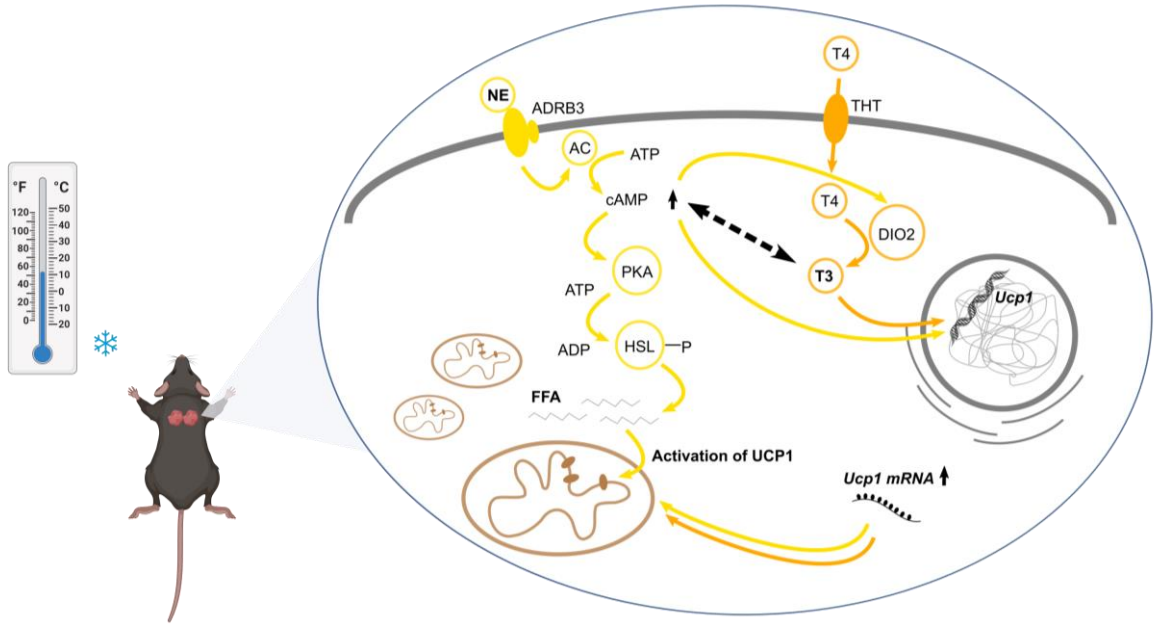

Figure 4: Thyroid hormone in brown fat thermogenesis. In synergism with SNS signaling, thyroid hormones (thyroxine, T4) can enter the cell via thyroid hormone transporters (THT). Upon conversion of T4 to physiological more active triiodothyronine (T3) by the iodothyronine deiodinase 2 (DIO2), T3 can initiate Ucp1 expression during brown fat thermogenesis. The schematic molecular overview of brown fat thermogenesis was adapted from Sentis et al., 2021.

Furthermore, observations about UCP1 protein content in BAT mitochondria of euthyroid rats compared to hypothyroid rats housed at thermoneutrality revealed that UCP1 protein content is significantly reduced in the latter when TH is not available. Interestingly, *Ucp1* expression in rats cannot be upregulated in absence of TH when exposed to cold, which ultimately leads to an impaired thermogenic response (Bianco and Silva, 1988, 1987; Rehnmark et al., 1992). Thus, TH actively contributes to the thermogenic potential of brown fat by inducing thermogenic target gene expression during cold exposure (Figure 4).

Besides the direct effects of TH on *Ucp1* expression during NST, β-adrenergic receptors that

mediate NE-signaling in BAT are also indirect targets of TH signaling (Bahouth, 1991). In absence of sympathetic stimulation, TH does not trigger *Ucp1* upregulation in BAT (Bianco and Silva, 1988). In turn, NE-induced thermal responsiveness depends likewise on the availability of TH in BAT (Zekri et al., 2022b). Although the importance of the indirect influence of TH on β-adrenergic receptor expression has been suggested, the degree at which β-adrenergic receptors can be seen as a sensitive target of TH-SNS crosstalk and interaction remains enigmatic (Alvarez-Crespo et al., 2016; Guilherme et al., 2020; Johann et al., 2019; López et al., 2013, 2010; Silva and Bianco, 2008). Eventually, the synergistic interplay of TH signaling, β-adrenergic signaling, and the expression of *Ucp1* and following activation of UCP1 via FFAs is required for proper BAT functioning and therefore NST (Ribeiro et al., 2001; Schweizer et al., 2018; Silva and Larsen, 1983; Yau and Yen, 2020).

Interestingly, systemic TH treatment in rats at room temperature promotes BAT thermogenesis (Abelenda and Puerta, 1992; Rial-Pensado et al., 2022), whereas hyperthyroidism in mice leads to shut-down of BAT thermogenesis that is also accompanied by a downregulation of *Adrb3* expression (Johann et al., 2019). However, the molecular mechanisms that mediate these contradictory findings are yet to be identified.

1.2.3 Thyroid hormone receptors and their role in thermoregulation

Due to the important role of THs in whole-body temperature homeostasis and brown fat thermogenesis, mutations in TRs may lead to defects in thermoregulation, e.g., during cold exposure.

Studies in TRβ knockout (KO) mice revealed that their body temperature phenotype is normal at 22°C ambient temperature (Forrest et al., 1996; Forrest and Vennström, 2000). Opposite to that, TRα1+m mutants and TRα1 KO mice display a significantly reduced body temperature when housed at room temperature and fail to sufficiently defend their body temperature during cold exposure (Marrif et al., 2005; Tinnikov et al., 2002). Additional studies aiming at investigating the underlying causes of the lower body temperature phenotype in TRα1+m mice found that defective TRα1 signaling leads to excessive heat loss via the tail due to defective vasoconstriction. To compensate for the excessive heat loss via the tail, BAT of TRα1+m mutants is highly active (Warner et al., 2013). Furthermore, TRα1+m mice harbor a mutant TRα1 with a 10-fold reduced binding affinity to T3, rendering organs and tissues where TRα1 is most abundant hypothyroid. However, by treating the TRα1+m mice with sufficient concentrations of TH, the defective TRα1 can be reactivated (Tinnikov et al., 2002; Warner et al., 2013).

Whether the defective body temperature phenotype of TRα1+m mice is exclusively provoked by peripheral TRα1 actions or whether defective central TRα1 signaling leads to changes in the centrally regulated body temperature set-point is, however, yet to be investigated.

1.2.4 Central effects of thyroid hormones

In addition to the direct effects on peripheral organs like the liver and BAT, THs also elicit direct central actions, thereby mediating peripheral effects such as thermogenesis and metabolic changes (Klieverik et al., 2009; Warner and Mittag, 2012; Zhang and Bi, 2015; Zhang et al., 2018).

The hypothalamus was identified as the central key player in body temperature regulation and homeostasis in rodents and humans, influencing peripheral thermogenesis (Contreras et al., 2017, 2016; Hameed et al., 2017; López et al., 2016; Warner and Mittag, 2012). Already in the late 1990s, the altered-body temperature set-point hypothesis was proposed, suggesting that the central body temperature set-point is modulated and adjusted by centrally acting TH (Nedergaard et al., 1997).

A decade later, it was shown that the intracerebroventricular (ICV) administration of T3 triggers BAT thermogenesis by decreasing the levels of hypothalamic adenosine monophosphate-activated protein kinase (AMPK) in the ventromedial hypothalamus (VMH), subsequently inducing increased SNS signaling to BAT (López et al., 2010). Furthermore, thermogenic markers, such as *Ucp1* gene expression and *Dio2* gene expression are upregulated in brown fat in response to central T3 administration. Consequently, centrally acting T3 leads to an enhanced thermogenic capacity of BAT (Alvarez-Crespo et al., 2016; López et al., 2016, 2013, 2010; Martínez-Sánchez et al., 2017b). These findings highlight the important role of centrally acting TH in the broader context of activating thermogenesis and brown fat thermogenesis in particular. However, recent findings suggest a more complicated interplay of centrally acting T3 and the diverse peripheral actions of TH in different tissues and organs (Sentis et al., 2021). Despite elevated body temperature upon systemic hyperthyroidism, NE turnover rates imply a reduced adrenergic responsiveness of BAT in hyperthyroid mice at thermoneutrality (Johann et al., 2019).

Furthermore, whether the hypothalamic effects of TH on body temperature regulation are mediated via TRα1 or TRβ action remains mostly unknown.

1.3 Aims of this study

Due to the incomplete understanding of the individual contributions of TRα1 and TRβ action to body temperature regulation, this thesis aims at dissecting the peripheral and central contributions of TRα1 and TRβ signaling to body temperature homeostasis in mice (Figure 5A+B). While TRα1+m mutants have a lower body temperature phenotype at room temperature due to excessive tail heat loss (Warner et al., 2013), TRβ KO animals do not show any differences in body temperature when compared to wildtype controls (Forrest and Vennström, 2000). Whether the impaired body temperature phenotype observed in TRα1+m mice is solely the result of peripheral TRα1 actions, or whether defective central TRα1 signaling contributes to, e.g., an altered body temperature set-point, will be addressed in this study.

Additionally, the underlying mechanisms at which TH-induced brown fat thermogenesis are differentially regulated in rats and mice are still vastly unknown. Systemic TH treatment induces brown fat thermogenesis in rats (Rial-Pensado et al., 2022) but fails to recruit BAT in mice at room temperature, which is accompanied by a downregulation of *Adrb3* (Johann et al., 2019; Lombardi et al., 2015). Interestingly, no mechanism that promotes the species-specific differences in BAT recruitment following systemic hyperthyroidism in rats and mice has been described yet (Figure 5C).

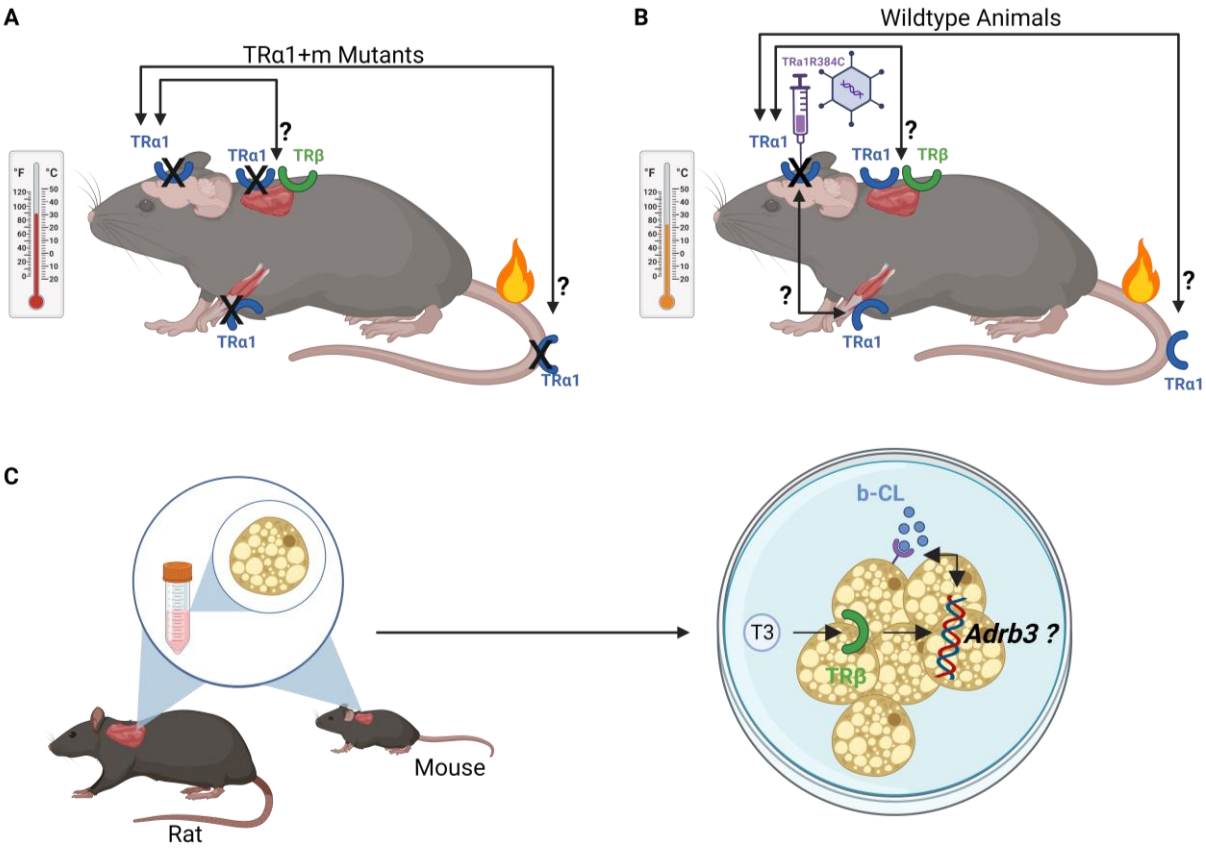

Figure 5: Aims of the study. A) Is the heat loss defect in TRα1+m mice the main driver of lower body temperature or is there a central contribution of TRα1 signaling to body temperature regulation? B) Is the expression of dominant-negative TRα1 in the hypothalamus of wildtype mice sufficient to alter the body temperature phenotype and thus the central body temperature set-point? C) Is Adrb3 expression differentially regulated in vivo and in vitro in response to thyroid hormone treatment in rats and mice?

By first using TRα1+m mutants, TRβ KO mice, and wildtype mice expressing dominant-negative TRα1 in the hypothalamus to investigate TR-dependent thermoregulation *in vivo*, and second by using cultured murine primary brown and white adipocytes *in vitro*, I will address following questions in this thesis:

1. Is TRα1 the main receptor isoform for body temperature regulation or does TRβ contribute to body temperature homeostasis?
2. Is the heat loss defect in TRα1+m mice the main driver of the lower body temperature or is there also a central contribution of TRα1 signaling to body temperature regulation (Figure 5A)?
3. Does the reactivation of the mutated TRα1 at thermoneutrality in TRα1+m mice alter the body temperature phenotype compared to controls by recruiting BAT?
4. Is the expression of dominant-negative TRα1 in the hypothalamus of wildtype mice sufficient to alter the basal metabolic rate and the body temperature phenotype and thus the central body temperature set-point (Figure 5B)?
5. Is *Adrb3* expression differentially regulated *in vivo* and *in vitro* in response to TH treatment in rats and mice (Figure 5C)?

2 Material and Methods

The following chapter lists all materials (see section 2.1) and methods (see section 2.2) used in this study.

2.1 Material

2.1.1 Chemicals, drugs, and reagents used in this study

Table 1 lists all commercially available chemicals, drugs, and reagents that were used in this study to conduct the experiments.

Table 1: List of chemicals, drugs, and reagents

Chemicals/reagents	**Company**
0.05 % Trypsin-EDTA (1x)	Thermo Fisher Scientific Inc., Germany
2-Amino-2-(hydroxymethyl)propane-1,3-diol (Tris)	Carl Roth GmbH + Co. KG, Germany
2-Propanol	Carl Roth GmbH + Co. KG, Germany
3,3',5-Triiodo-L-Thyronine sodium salt (T3; T6397)	Sigma Aldrich Chemie GmbH, Germany
3-isobutyl-1-methylxanthine (IBMX)	Sigma Aldrich Chemie GmbH, Germany
Ammonium peroxodisulfate (APS)	Carl Roth GmbH + Co. KG, Germany
Bepanthen eye oinment	Bayer, Germany
Bicinchoninic acid reagent (BCA)	Sigma Aldrich Chemie GmbH, Germany
Bovine serum albumin (BSA; A7030 & A7906)	Sigma Aldrich Chemie GmbH, Germany
Bromophenol blue	Sigma Aldrich Chemie GmbH, Germany
Carprofen (Rimadyl® Vnr462986)	Pfizer Inc., USA
Chloroform	Sigma Aldrich Chemie GmbH, Germany
CL 316,243 (β3-adrenergic receptor agonist)	Sigma Aldrich Chemie GmbH, Germany
Collagenase type II	Worthington Biochemical Corp, USA
Copper(II) sulfate ($CuSO_4$; 4 %)	Merck KGaA, Germany
D(+)-Saccharose ($C_{12}H_{22}O_{11}$)	Carl Roth GmbH + Co. KG, Germany
D-Biotin	Sigma Aldrich Chemie GmbH, Germany
Dexamethasone	Sigma Aldrich Chemie GmbH, Germany
Diethyl ether	Carl Roth GmbH + Co. KG, Germany

Chemicals/reagents	Company
Dimethyl sulfoxide (DMSO)	AppliChem GmbH, Germany
Disodium phosphate (Na_2HPO_4)	Carl Roth GmbH + Co. KG, Germany
Dispase II	Roche Diagnostics GmbH, Germany
D-Panthotenic acid hemicalcium salt	Sigma Aldrich Chemie GmbH, Germany
Dulbecco's phosphate buffered saline (DPBS (1x), sterile)	Thermo Fisher Scientific Inc., Germany
Erythrocyte lysis buffer	QIAGEN GmbH, Germany
Ethanol (denaturated)	Carl Roth GmbH + Co. KG, Germany
Ethanol 99 % (extra pure)	Th. Geyer GmbH, Germany
Ethylene glycol	Th. Geyer GmbH, Germany
Ethylenediaminetetraacetic acid (EDTA)	AppliChem GmbH, Germany
Fetal bovine serum (FBS; F7524)	Sigma Aldrich Chemie GmbH, Germany
Gibco™ Dulbecco's modified eagle medium (DMEM/F-12, without glutamine)	Thermo Fisher Scientific Inc., Germany
Glycerol	Sigma Aldrich Chemie GmbH, Germany
Glycine (G8898)	Sigma Aldrich Chemie GmbH, Germany
Hydrochloric acid (HCl; 37 %)	Carl Roth GmbH + Co. KG, Germany
Indomethacin	Sigma Aldrich Chemie GmbH, Germany
Insulin	Novo Nordisk, Denmark
Isoflurane	Zoetis Inc., USA
Isopropanol 99 % (17024)	Th. Geyer GmbH, Germany
L-Glutamine	Life Technologies, USA
Methanol	Carl Roth GmbH + Co. KG, Germany
Mineral oil	SERVA Electrophoresis GmbH, Germany
Monosodium phosphate (NaH_2PO_4)	Carl Roth GmbH + Co. KG, Germany
Nonidet P40	Honeywell Fluka, USA
Normal donkey serum (END9010-10)	BIOZOL Diagnostics, Germany
Page Ruler™ Plus Prestained protein ladder	Thermo Fisher Scientific Inc., Germany
Penicillin-Streptomycin (10000 U/mL; 15140122)	Thermo Fisher Scientific Inc., Germany
Perfluoroalkoxy alkanes (PFA in PBS; 4 %)	Thermo Fisher Scientific Inc., Germany
Phenylmethylsulfonyl fluoride (PMSF)	Sigma Aldrich Chemie GmbH, Germany
Potassium chloride (KCl)	Carl Roth GmbH + Co. KG, Germany
Potassium dihydrogen phosphate (KH_2PO_4)	Carl Roth GmbH + Co. KG, Germany
Powdered milk	Carl Roth GmbH + Co. KG, Germany
ProLong Diamond Antifade Mountant with DAPI (P36971)	Life Technologies, USA
Protease inhibitors (5892970001)	Roche Diagnostics GmbH, Germany

Chemicals/reagents	Company
QIAzol	QIAGEN GmbH, Germany
Restore™ stripping buffer	Thermo Fisher Scientific Inc., Germany
RNase ZAP™	Th. Geyer GmbH, Germany
Rosiglitazone	Cayman Chemical, USA
Sodium chloride (NaCl; 0.9 % sterile)	Carl Roth GmbH + Co. KG, Germany
Sodium deoxycholate ($C_{24}H_{39}NaO_4$)	AppliChem GmbH, Germany
Sodium fluoride (NaF)	Sigma Aldrich Chemie GmbH, Germany
Sodium hydrogen carbonate (Na_2HPO_4)	Carl Roth GmbH + Co. KG, Germany
Sodium hydroxide (NaOH)	Carl Roth GmbH + Co. KG, Germany
Sodium lauryl sulfate (SDS)	Sigma Aldrich Chemie GmbH, Germany
Sodium orthovanadate (Na_3VO_4)	Sigma Aldrich Chemie GmbH, Germany
ß-Mercapthoethanol	Sigma Aldrich Chemie GmbH, Germany
Standard chow diet (1314)	Altromin, Germany
Tetramethylethylenediamine (TEMED)	Carl Roth GmbH + Co. KG, Germany
Triton™X-100	Th. Geyer GmbH, Germany
Tween® 20	Sigma Aldrich Chemie GmbH, Germany
Vaseline	Balea; dm-Drogeriemarkt GmbH + Co. KG, Germany
Xylocain (10 mg/mL)	AstraZeneca, UK

2.1.2 Consumables, devices, and equipment used in this study

The following table (Table 2) lists all commercially available consumables, devices, and additional equipment that were used in this study to conduct the experiments.

Table 2: List of consumables, devices, and equipment

Devices/consumables	Company
96-PCR plate	Sarstedt AG & Co., Germany
Absorbable suture (V396H Coated Vicryl)	Ethicon, Germany
Adhesive clear PCR seal sheets	BiozymScientific GmbH, Germany
Alcohol pads	Braun, Germany
Aluminium foil	Th. Geyer GmbH, Germany
Anaesthesia Unit 410	High Precision Instruments, Univentor, Malta
Benchtop centrifuge (MC6 centrifuge)	Sarstedt AG & Co., Germany

Devices/consumables	Company
Bright field microscope (Axiovert 40 CFL)	Carl Zeiss AG, Germany
Cell scraper (sterile)	Sarstedt AG & Co., Germany
Cell strainer (70 µm)	Corning Incorporate – Life Sciences, USA
Centrifuge (5430, 5430 R, and multifuge 3 S-R)	Eppendorf AG, Germany
Ceramic beads (1.4 mm, 325 g)	VWR International, Germany
ChemiDoc™ Touch Imaging System	BioRad Laboratories, Germany
Climate chamber MKKL1200	Flohr Instruments, Netherlands
Cotton swaps	Nobamed, Germany
Cover glasses	Th. Geyer GmbH, Germany
Cryostat	Leica Biosystems, Germany
DMI6000B Fluorescence microscope	Leica Biosystems, Germany
Dräger Isoflurane Vapor® 19.3	Drägerwerk AG & Co. KGaA, Germany
Dremel® 200 Multitool System	Dremel, USA
DVOMAX 1030	Heidolph Instruments, Germany
ECGenie Clinic System	Mouse Specifics Inc., USA
Eppendorf tubes (5 mL)	Eppendorf AG, Germany
ER-4000 receiver plates	PhilipsRespironics, USA
Falcon tubes (15 mL, 50 mL)	Sarstedt AG & Co., Germany
Filter tips (10 µL, 100 µL, 1000 µL; 701114210, 70760212, 70762211)	Sarstedt AG & Co., Germany
Filtropur S 0.2 (Syringe filters 0.2 µm)	Sarstedt AG & Co., Germany
Fisherbrand™ Homogenizer Bead Mill 24	Fisher Scientific GmbH, Germany
Fluorescence microscope (AxioVision)	Carl Zeiss AG, Germany
G2-E-Mitter	PhilipsRespironics, USA
Gel Chamber	BioRad Laboratories, Germany
Glass capillaries (1.14 mm; 504949)	World Precision Instruments, USA
Heating pad (Thermolux)	Witte + Sutor GmbH, Germany
Hood	Waldner Laboreinrichtungen GmbH & Co. KG, Germany
Incubator (HERA Cell)	Heraeus, Germany
INCU-LINE ILS6	VWR International, Germany
Inject®-FLuerSolo	Braun, Germany
Magnetic stirrer (Rct basic)	IKA®-Werke GmbH & Co. KG, Germany
Micro tube 1.5 mL SafeSeal	Sarstedt AG & Co., Germany
Micro tube 2 mL SafeSeal	Sarstedt AG & Co., Germany
Microscope slides	Thermo Fisher Scientific Inc., Germany
NanoDrop™ One C	Thermo Fisher Scientific Inc., Germany

Devices/consumables	Company
Nanoliter 2020 injector	World Precision Instruments, USA
Parafilm	American National Con., USA
Permanent suture (EH7823H)	Ethicon, Germany
pH-meter (PB-11)	Sartorius Lab Instruments GmbH & Co. KG, Germany
Pipetboy (Pipetus red dot)	Hirschmann Laborgeräte GmbH & Co. KG, Germany
Pipettes (Research Plus and Multipette)	Eppendorf AG, Germany
PluriStrainer (300 µm)	pluriSelect, Germany
PV-1 Grantbio	Grant Instruments Ltd, UK
QuantStudio Applied Biosystems real-time PCR system	Thermo Fisher Scientific Inc., Germany
Rectal thermometer probe (BAT-12)	Physitemp Inc., USA
Sample concentrator	Biostep GmbH, Germany
Savant™ SpeedVac™ Concentrator SPD111V	Savant Group, USA
Scale (ACCULAB)	Sartorius Lab Instruments GmbH & Co. KG, Germany
SPECTROstar Nano Microplate Reader	BMG Labtech, Germany
Stereotaxic Apparatus (963205A, 957)	Kopf®, USA
Sterile bench (HERA Safe 2020)	Heraeus, Germany
T335 and T540 infrared cameras	FLIR Systems Termisk Systemteknik, Sweden
TC dish 100, standard	Sarstedt AG & Co., Germany
TC plate, 6 well, standard F	Sarstedt AG & Co., Germany
Thermocycler (PTC-200)	Biozym Scientific GmbH, Germany
Thermomixer (5436)	Eppendorf AG, Germany
Titramax100	Heidolph Instruments, Germany
Transfer membranes Immobilion®-PVDF (IPVH00010)	Merck KGaA, Germany
TSE PhenoMaster	TSE Systems, Germany
VMS-C4	VWR International, Germany
Water bath (OLS 200)	Grant Instruments Ltd, UK
Western Blot apparatus	BioRad Laboratories, Germany
Western Blotting filter paper	Thermo Fisher Scientific Inc., Germany

2.1.3 Commercially available kits

Table 3 lists all commercially available kits and the respective catalogue numbers that were used in this study.

Table 3: List of commercially available kits

Kits	**Company**	**Catalogue #**
cAMP assy kit	Cytiva, USA	RPN225
Clarity™ Max Western ECL Substrate	BioRad Laboratories, Germany	1705062
Free fatty acid assay kit	Abcam, UK	ab65341
Free T4 ELISA	DRG Instruments GmbH, Germany	EIA-3775
Glycogen assay kit	Sigma Aldrich Chemie GmbH, Germany	MAK016
GoTaq® qPCR Mastermix	Promega GmbH, Germany	M7112
RevertAid First Strand cDNA Synthesis kit	Thermo Fisher Scientific Inc., Germany	K1621
RNaesyMini kits	QIAGEN GmbH, Germany	74106, 74704, 74804
TGX Stain Free FastCast acrylamide kit	BioRad Laboratories, Germany	1610183, 1610185
Total T3 ELISA	NovaTec Immundiagnostica GmbH, Germany	DNOV053
Total T4 ELISA	DRG Instruments GmbH, Germany	EIA-1781

2.1.4 Buffer recipes used in this study

Table 4 lists all buffers and their respective compositions and concentrations that were used in this study to conduct the experiments.

Table 4: List of buffers and recipes

Buffer	**Concentration**	**Substances**
Cryo-protection solution (CPS; pH = 7.4, for 250 mL)	75 mL	Ethylene glycol
	75 mL	Glycerol
	19 mL	NaH_2PO_4 (0.1 M)
	81 mL	Na_2HPO_4 (0.1 M)

Buffer	Concentration	Substances
Lysis buffer	50 mM 150 mM 1 % v/v 0.25 % w/v 1 mM 1 Tablet 1 mM 1 mM 1 mM	Tris-HCl (pH 7.4) NaCl Nonidet P40 $C_{24}H_{39}NaO_4$ Ethylenediaminetetraacetic acid (EDTA) Protease inhibitor PMSF Na_3VO_4 NaF
Phosphate buffered saline (PBS, 10x) pH = 7.4	27 mM 17.6 mM 188.8 mM 1370 mM	KCl KH_2PO_4 Na_2HPO_4 NaCl
Resolving gel: for 1 Gel with TGX Stain-Free™ FastCast™ Acrylamide Kit (Table 3)	1 part 1 part 0.5 % 0.08 %	Resolver 1 Resolver 2 Ammonium peroxodisulfate (APS; 10 %) Tetramethylethylenediamine (TEMED)
Running buffer	0.25 M 1.92 M 1 % (w/v)	Tris Glycin Sodium lauryl sulfate (SDS)
Sample buffer (4x Lämmli Buffer)	50 % (v/v) 10 % (w/v) 312.5 mM 1 spatula Before use: 1 part for 4 parts of buffer	Glycerol SDS Tris-HCl (pH 6.8) Bromphenol blue β-Mercaptoethanol
Stacking gel: for 1 Gel with TGX Stain-Free™ FastCast™ Acrylamide Kit (Table 3)	1 part 1 part 0.5 % 0.15 %	Stacker 1 Stacker 2 APS (10 %) TEMED
TBS (Tris-buffered saline, 10x, pH 7.4)	100 mM 1.5 M	Tris-HCl NaCl
TBS-T (TBS-Tween20, 1x)	1 part 9 parts 0.1 %	TBS (10x) Distilled water Tween-20
Transfer buffer	0.025 M 0.192 M 20 %	Tris Glycine Methanol

2.1.5 Analysis software

The following table (Table 5) lists all software and their respective analysis purpose that were used in this study to conduct the experiments.

Table 5: List of software used in this study

Software name	**Purpose**	**Company**
CorVita	ECG signal preprocessing and analysis	Mouse Specifics Inc., USA
FLIR Tools	Infrared picture analysis	FLIR Systems Termisk Systemteknik, Sweden
GraphPad PRISM 9	Statistical analysis	GraphPad Software Inc., USA
ImageLab™ Software	Western Blot analysis	BioRad Laboratories, Germany
MARS Datenanalyse-Software	Microplate reader software	BMG Labtech, Germany
MATLAB® R2018a	Analysis of physiological mouse data	The MathWorks Inc., USA
Microsoft Office Excel	Data preprocessing and statistical analysis	Microsoft, USA
QuatStudio™ Design & Analysis v1.5.1	qPCR analysis	Thermo Fisher Scientific Inc., Germany
TSE PhenoMaster Software V6.5.3	Recording and analysis of indirect calorimetry parameters	TSE Systems, Germany
Vital View 4.200.2	Telemetry recording software	PhilipsRespironics, USA

2.2 Methods

2.2.1 *In vivo* experiments

2.2.1.1 Animal husbandry

Male TRα1+m mutant mice (Tinnikov et al., 2002), TRβ KO mice (Forrest et al., 1996), and control animals on a C57Bl/6NCr background were obtained from in-house breeding from Gemeinsame Tierhaltung, University of Lübeck, Germany. Additional male wildtype C57Bl/6NCr animals for hypothalamic viral vector injections were purchased from Charles River Laboratories (CharlesRiver, Germany). Before any interventions, all mice were 3-6 months old, single-housed at 22 ± 1°C ambient temperature, exposed to a constant 12 h light-/dark cycle, and fed ad libitum with chow food and water. All animal experiments were performed according to EU guideline regulations (210/63/EU) and approved by the MEKUN (Ministerium für Energiewende, Klimaschutz, Umwelt und Natur) Schleswig-Holstein (Germany).

After sacrifice, tissues and organs of interest were collected, snap-frozen, and stored at -80°C for further analysis. Blood was collected from the aorta and allowed to clot on ice for 20 min. Subsequent centrifugation of the blood at 4°C and 2000 rfc for 10 min was repeated twice before the supernatant was transferred into fresh tubes and stored at -20°C until further use.

2.2.1.2 Radiotelemetry transmitter implantation

Body temperature, heart rate, and activity of freely moving mice were recorded with the help of implanted radiotelemetry transmitters and radiotelemetry receiver plates (Table 2).

The surgical procedure was previously described and adjusted for all following experiments (Dore et al., 2023b; Herrmann et al., 2020). First, mice were placed on a heating pad (Table 2) and body temperature was controlled via a rectal probe during all surgeries. Anesthesia was induced using 4 % isoflurane (Table 1) at a 400 mL/min flow rate which was reduced to 2 % isoflurane at 200 mL/min for the duration of surgery. Before the start of the telemetry transmitter implantation surgeries, pain medication was administered s.c. (5 mg/kg Carprofen (Table 1) in 1x sterile NaCl (Table 1)) and eye ointment (Table 1) was applied to avoid drying of the eyes. Physiological parameters, such as body temperature, regular heart rate, and reflexes were constantly monitored. The toe-pinch reflex was used to check the anesthesia depth.

The surgical procedure itself started by making a vertical incision into the skin at the lower rips level, followed by separation of the connective tissue from the superincumbent skin to reveal the cavity. A second incision was made following the linea alba to avoid excessive bleeding. A sterilized radiotelemetry transmitter was implanted into the abdominal cavity and the cavity was closed using

absorbable sutures (Table 2). Electrodes for continuous heart rate recordings were placed near the right shoulder (negative electrode) and close to the lower left costal arch (positive electrode) to create a diagonal plane embedding the heart. Both electrodes were fixated with non-absorbable sutures (Table 2). The outer skin incisions were closed with absorbable suture and all mice were allowed to wake up in their cages. For the next three days, water-soaked food in petri dishes was placed into the cages and pain medication (5 mg/kg Carprofen (Table 1) in 1x sterile NaCl (Table 1)) was administered s.c. for two more days after surgery. After a recovery period of a minimum of seven days, baseline measurements of core body temperature, heart rate, and activity were recorded.

2.2.1.3 Induction of systemic hyperthyroidism: oral T3 treatment

Wildtype control animals, TRβ KO animals, and TRα1+m mutant mice were treated with 0.5 mg/L T3 (Table 1) in 0.01 % bovine serum albumin (BSA; Table 1) in tap water for 12 days to induce systemic hyperthyroidism (Dore et al., 2023b; Johann et al., 2019). All water bottles were freshly prepared in the morning and replaced every day.

2.2.1.4 Adeno-associated viral vector (AAV) delivery

Wildtype C57Bl/6NCr animals were used to perform stereotaxic injections of adeno-associated viral vectors (AAV1/2) carrying dominant-negative TRα1 (TRα1R384C-IRES-mCherry, $2.81*10^{12}$ GC/mL) or green fluorescence protein (GFP, $2.17*10^{12}$ GC/mL) that were commercially purchased from VectorBuilder (VectorBuilder GmbH, Germany). Both vectors were cytomegalovirus (CMV) immediate-early promoter-driven and thus promoted the expression of dominant-negative TRα1 and control GFP in cells close to the injection site (Bäck et al., 2019).

The surgical procedure started by anesthetizing the animals using 4 % isoflurane (Table 1) at a 400 mL/min flow rate to induce anesthesia. Subsequently, the isoflurane flow rate was reduced to 2 % (Table 1) at 200 mL/min for the duration of the surgery. Mice were placed on a temperature-controlled heating pad (Table 2) and mounted into a stereotaxic frame (Table 2). The ear bars of the stereotaxic frame were adjusted to position the head horizontally and to prevent any lateral movement of the head during surgery. Next, the teeth of the mouse were mounted into the tooth bar and nose and tooth bar were individually adjusted according to the size of the mouse. To avoid head size variance, only mice aged three months and older were considered for stereotaxic AAV delivery, as the brain size had matured at that age. The toe-pinch reflex was checked regularly during the procedure and drying of the eyes was prevented by applying eye ointment (Table 1). Pain medication was administered s.c. (5 mg/kg Carprofen (Table 1) in 1x sterile NaCl (Table 1)) and the skin of the head was cleansed with

sterile alcohol-soaked pads (Table 2) before any invasive procedure.

To start the invasive procedure, the skin of the head was carefully lifted, and a 1 cm incision was cut vertically into the skin to expose the skull. The meninges was removed and the skull was treated with xylocaine (Table 1). Afterwards, the coordinates of bregma and lambda were determined before drilling a small hole (Table 2) at the desired site of injection. The viral vectors were administered bilaterally and relative to bregma (250 nL per side; injection rate: 4 nL/s) into the hypothalamus at the coordinates anterior-posterior -0.1 mm, lateral-medial ±0.2 mm, and dorsal-ventral -5.5 mm via an automatic injector (Table 2). All coordinates were determined according to a mouse brain atlas (Paxinos and Franklin, 2019). To avoid spreading of the virus to other parts of the brain, the needle attached to the injector was kept in place for eight minutes before retraction. The outer skin incisions were closed with absorbable suture and mice were allowed to wake up in their cages. Water-soaked food in petri dishes was provided for three days. Pain medication (5 mg/kg Carprofen (Table 1) in 1x sterile NaCl (Table 1)) was administered s.c. for two days following surgery. All mice were allowed to recover for two weeks to allow for the expression of dominant-negative TRα1 and control-GFP.

2.2.1.5 Infrared thermography

Infrared pictures were taken of freely moving animals using T335 and T540 infrared cameras by FLIR Systems Termisk Systemteknik, Sweden (Table 2) followed by data analysis using the software FLIR Tools (Table 5). The day before experiment, vaseline (Table 1) was applied and brushed into the fur between the shoulder blades to reveal the skin above the BAT (Oelkrug and Mittag, 2021). Before taking the infrared pictures, animals were allowed to wake up in their cages for one minute. Infrared pictures of tail and BAT were taken in random order and the duration of image acquisition did not exceed two minutes. All pictures were daily taken at the same time in the morning and during the inactive phase of the animals.

2.2.1.6 Indirect calorimetry

To assess any changes in metabolic parameters and the metabolic rate upon the delivery of dominant-negative TRα1 compared to control virus into the hypothalamus, oxygen (VO_2) and carbon dioxide (VCO_2) exchange of these mice were measured. The assessment was performed via indirect calorimetry using an open respirometry climate chamber (Table 2). Mice were trained and accustomed to the temperature-controlled climate chamber before measurements for three days. Food intake, water intake, and activity of freely moving animals were measured at 20-minute intervals.

Metabolic parameters, such as daily energy expenditure (kJ/day) of a 24 h interval at 22°C ambient baseline temperature, were calculated using the respiratory quotient

$$RQ = \frac{carbon\ dioxide\ produced}{oxygen\ consumed},$$

the metabolic rate VO_2 and the caloric equivalents given by (Heldmaier, 1975)

$$heat\ production\ (HP) = (4.44 + 1.43 \cdot RQ) \cdot VO_2$$

with $[HP] = \mathrm{mW}$ and $[VO_2] = \mathrm{mL}\ O_2/\mathrm{h}$.

Furthermore, the resting metabolic rate (RMR) was calculated considering only values from the inactive phase of the mice at room temperature (1 h interval without movement and consistently low oxygen consumption). Respectively, the basal metabolic rate (BMR) at thermoneutrality (30°C) was calculated considering only values of the lowest mean oxygen consumption (1 h interval without movement). To measure the BMR, animals were fasted for 6 h during data acquisition. Subsequent data analysis was performed using Microsoft Office Excel (Table 5) and TSE PhenoMaster Software V6.5.3 (Table 5).

2.2.1.7 Electrocardiogram

Electrocardiograms (ECG) of awake and freely moving mice were recorded using ECGenie Clinic System, Mouse Specifics Inc., USA (Table 2). Mice were trained and accustomed to the electrode towers for 10 min prior to the experiment. The recording was started as soon as the mice stopped extensive exploring inside the electrode tower. An average of 190 heart beats was recorded for each animal. ECG data was preprocessed and analyzed using ECGenie CorVita Software (Table 5).

2.2.2 *In vitro* experiments

As part of an international collaboration with the University of Southern Denmark (SDU), Denmark (collaborator: Prof. Jan-Wilhelm Kornfeld) and the University of Santiago de Compostela, Spain (collaborator: Prof. Miguel Lopez), primary cell culture experiments were conducted in the laboratories of Prof. Jan-Wilhelm Kornfeld. Parts of the *in vitro* experiments were conducted under my supervision by Berenike Soehl, M.Sc., as part of her master's studies (study program: Molecular Life Science) at the University of Lübeck, Germany.

2.2.2.1 Primary mouse and rat preadipocyte isolation

Preadipocytes from mice, aged 32-66 days, or rats, aged 10 days, were used for all primary cell culture experiments (Engelhard et al., 2022; Galmozzi et al., 2021). iWAT and interscapular BAT (iBAT) depots were immediately removed following sacrifice. The fat depots were dissected, minced, and transferred into pre-warmed serum-free media (Table 1). Serum-free media, supplemented with biotin (33 mM), D-panthotenate (17 mM), glutamine (1 %) and Penicillin-Streptomycin (1 %), was used for all further steps during cell isolation and for all following *in vitro* experiments (Table 1). To increase the number of isolated cells, the fat depots of at least two mice or rats were pooled before enzymatic digestion (BSA (34 mg/mL), collagenase II (2 mg/mL), and dispase II (1.5 mg/mL; only for iBAT; Table 1)). Next, the minced tissue was incubated in a horizontal shaker at 37°C for 45-60 min. All following steps were performed under sterile conditions.

After digestion, preadipocytes in solution were filtrated (sterilized mesh, 300 µm; Table 2) and centrifuged two times (room temperature, 5 min, 300 g) to separate the stromal vascular fraction (SVF) from adult cells. The cell pellet was resuspended in pre-warmed media containing 10 % fetal bovine serum (FBS; Table 1) to inactivate enzymes. The resuspension was centrifuged at 500 g two times (room temperature, 5 min) and the supernatant was discarded. The cell pellet was resuspended in erythrocyte lysis buffer (Table 1) and incubated at room temperature for 1 min to lyse all remaining erythrocytes. After the erythrocyte lysis buffer incubation, pre-warmed media containing 20 % FBS (Table 1) was added and the cell suspension was centrifuged at 300 g (5 min, room temperature). Finally, the cell pellet was resuspended in pre-warmed media (20 % FBS (Table 1)) and filtered through a 70 µm cell strainer (Table 2), followed by seeding into a 10 cm petri dish (Table 2). The freshly isolated primary cells were incubated at 37°C, 5 % CO_2, and 101.3 kPa (Table 2) for the entire duration of the experiment.

2.2.2.2 Differentiation of preadipocytes to mature adipocytes

The isolated preadipocytes in culture were checked daily for confluency and viability using light microscopy (Table 2). Preadipocytes were washed with pre-warmed 1x phosphate buffered saline (PBS; Table 1) every other day to remove debris and dead cells before adding new pre-warmed media containing 20 % FBS (Table 1). Once the adherently growing cultures had reached 80 % confluency, differentiation from preadipocytes to mature brown or white adipocytes was induced. Differentiation progression was confirmed by light microscopy (Table 2). Differently supplemented media were added to the cultures for six days to ensure differentiation (Table 6).

At day four of differentiation, the primary cells were passaged into 6-well plates (Table 2; see section 3.3.2 for detailed experimental layout information). For that, a trypsin/ ethylenediaminetetraacetic acid (EDTA)-solution (Table 1) was added and the cells were incubated at

37°C for 5 min. The detachment of the cells was confirmed using light microscopy (Table 2). To stop the enzymatic trypsin reaction, differentiation media (D4-media, Table 6) was added. Starting on day four after induction of differentiation, iBAT cells were T3-starved (D4-media, Table 6). On day six after induction of differentiation, accumulation of lipid droplets was confirmed via light microscopy (Table 2) and subsequent treatment of the mature adipocytes with T3 and CL 316243 was initiated (see section 3.3.2 for detailed experimental layout information). After exactly 24 h of treatment, the cells were harvested and stored at -80°C until further processing.

Table 6: Differentiation media

Day after induction of differentiation	**Added supplements**
D0-media	Serum-free media 10 % FBS Rosiglitazone (1 µM) Insulin (850 nM) Dexamethasone (1 µM) 3-isobutyl-1-methylxanthine (IBMX; 250 µM) Indomethacin (125 µM) T3 (1 nM) - only iBAT cells
D2-media	Serum-free media 10 % FBS Rosiglitazone (1 µM) Insulin (850 nM) – only for iBAT cells T3 (1 nM) – only iBAT cells
D4-media (T3 starvation of iBAT)	Serum-free media 10 % FBS Rosiglitazone (1 µM) Insulin (850 nM) – only for iBAT cells
D6-media	Serum-free media 10 % FBS Rosiglitazone (1 µM) Insulin (850 nM) – only for iBAT cells

2.2.3 Molecular methods

2.2.3.1 Immunofluorescence staining

Brains of animals were collected and fixed in 4 % perfluoroalkoxy alkanes solution (PFA; Table 1) overnight at 4°C followed by the incubation in 30 % w/v sucrose (Table 1) in 1x PBS (Table 4) for 48 h at

room temperature. After fixation, brains were stored at -80°C until further processing with the cryostat (Table 2). Fixed free-floating cryostat coronal sections (40 µm) of the area of interest were stored in cryo protection solution (Table 4) and used for immunofluorescence staining. All following reagents were diluted in 1x PBS. First, all sections were blocked with 5 % normal donkey serum (Table 1) in 0.3 % Triton-X 100 (Table 1). Sections of animals that received dominant-negative TRα1 were incubated with primary anti-mCherry antibody (1:1000; Table 7) and control sections were incubated with primary anti-GFP antibody (1:1000; Table 7) overnight at 4°C. Next, sections of transgenic dominant-negative TRα1 animals were incubated in Alexa Fluor 594™ (1:800) labelled secondary antibody (Table 7) and sections of control animals were incubated in Alexa Fluor 488™ (1:800) labelled secondary antibody (Table 7), respectively. The stained sections were finally mounted on object slides using ProLong Diamond Antifade Mountant with 4',6-diamidino-2-phenylindole (DAPI; Table 1). If only weak or no hypothalamic staining (mCherry or GFP) was found, animals were excluded from analysis.

Table 7: List of immunofluorescence antibodies

Purpose	**Antibody**	**Company**
Primary antibodies	Anti-GFP antibody (ab290)	Abcam, UK
	Anti-mCherry antibody (AB0040)	OriGene, Germany
Secondary antibodies	Alexa Fluor 488™ (A-21206)	Invitrogen, Thermo Fisher Scientific Inc., Germany
	Alexa Fluor 594™ (A-11058)	Invitrogen, Thermo Fisher Scientific Inc., Germany

2.2.3.2 RNA isolation, cDNA synthesis, and qPCR

Tissue samples, organs, or cells for ribonucleic acid (RNA) isolation were immediately snap-frozen after harvesting and stored at -80°C until further processing. Liver, kidneys, and gastrocnemius muscle tissue were ground before RNA isolation. Cells were harvested, spun down at 4°C, and resuspended in 250 µL QIAzol (Table 1) before stored at -80°C. RNA isolation was performed using QIAGEN RNeasy mini kits (Table 3) following manufacturer's instructions (muscle: RNeasy fibrous tissue mini kit; eWAT, iWAT, iBAT: RNeasy lipid tissue mini kit; liver, kidney, cells: RNeasy mini kit). RNA concentration was determined using Nanodrop (Table 2).

Subsequent complementary deoxyribonucleic acid (cDNA) synthesis was conducted using RevertAid first strand cDNA synthesis kit (Table 3). The synthesized cDNA was diluted in nuclease-free water to achieve a final concentration of 5 ng per quantitative polymerase chain reaction (qPCR).

Subsequent qPCR measurements were performed using GoTaq Master Mix (Table 3) and the QuantStudio Applied Biosystems real-time PCR system (Table 2). Details of the two-step qPCR protocol with 40 cycles can be found in Table 8. After the PCR reaction, a melting curve was measured to ensure primer specificity. Additionally, standard curves were determined to correct for primer efficiency (E) using the slope (Pfaffl et al., 2004)

$$E = 10^{-\frac{1}{\text{slope}(standard\ curve)}}.$$

Housekeeping genes for qPCR analysis were selected according to NormFinder for each tissue (Andersen et al., 2004) and can be found in Table 9. Due to low RNA yield from harvested cells, only one housekeeping gene was selected for qPCRs performed on cell material (for iWAT and iBAT: *Hprt* (hypoxanthine-guanine phosphoribosyltransferase)). All primer sequences can be found in Table 10 and Table 11. qPCR data were analyzed using the $\Delta\Delta Ct\ (cycle\ threshold)$-method (Livak and Schmittgen, 2001) and QuatStudio™ Design & Analysis software (Table 5):

$$\Delta Ct\ = mean\ Ct_{target\ gene} - mean\ Ct_{housekeeping\ gene}.$$

Table 8: Two-step qPCR protocol

Step	**Temperature (°C)**	**Time (min)**	**# of replications**
Hold stage	50	2	1
	95	10	1
PCR replication	95	0.15	40
	60	1	
Melt curve stage	95	0.15	1
	60	0.30	1
	95	0.15	1

Table 9: List of analyzed murine tissues and their respective housekeeping genes

Tissue	**Housekeeping genes**
eWAT	*Rplp0, Hprt* (3.1 and 3.2)
Gastrocnemius muscle	*Hprt, Ppia* (3.2)
Hypothalamus	*Cyclophilin, Hprt* (3.1)
iBAT	*Rplp0* (3.1); *Hprt* (3.2 and 3.3.1)
iWAT	*Cyclophilin, Hprt* (3.1); *Cyclophilin, Rplp0* (3.2)
Liver	*Gapdh* (3.1); *Gapdh, Hprt* (3.2)
Soleus muscle	*Hprt, Ppia* (3.2)

Table 10: List of primer sequences used for mouse organs and tissues, and brown and white adipocytes isolated from mice

Gene	**Abbreviation**	**Sequences 5' → 3' (forward and reverse)**
ATPase sarcoplasmic/endoplasmic reticulum Ca^{2+} transporting 1	*Atp2a1*	TGTTTGTCCTATTTCGGGGTG AATCCGCACAAGCAGGTCTTC
ATPase sarcoplasmic/endoplasmic reticulum Ca^{2+} transporting 2	*Atp2a2*	TCCGCTACCTCATCTCATCC CAGGTCTGGAGGATTGAACC
CD5 molecule like	*Cd5l*	GATCGTGTTTTTCAGAGTCTCCA TGCAGTCAACCCCTTGAATAAG
Cell death-inducing DNA fragmentation factor alpha subunit-like effector A	*Cidea*	TGACATTCATGGGATTGCAGA GGCCAGTTGTGATGACTAAGA
Fatty acid synthase	*Fasn*	GGAGGTGGTGATAGCCGGTAT TGGGTAATCCATAGAGCCCAG
Fibroblast growth factor 21	*Fgf21*	CTGCTGGGGGTCTACCAAG CTGCGCCTACCACTGTTCC
Glyceraldehyde-3-phosphate dehydrogenase	*Gapdh*	AGGTCGGTGTGAACGGATTTG TGTAGACCATGTAGTTGAGGTCA
Glycerol kinase	*Gk*	CTGTGGACTCACTCAGTTCACC TGAGTGGAATTCCACAGTCG
Glycerol-3-phosphate dehydrogenase 2	*Gpd2*	GAAGGGGACTATTCTTGTGGGT GGATGTCAAATTCGGGTGTGT
Glycogen synthase 1	*Gys*	CGACATGCTCATATTTGGGTCT GCCTGCCATTCATGGAATTGG
Hypocretin (orexin)	*Hcrt*	ATCTTCTATCCTTGTCCTGATCC AGTCACACCACCAGAGAATCG

Gene	Abbreviation	Sequences 5' → 3' (forward and reverse)
Hypoxanthine-guanine phosphoribosyltransferase	*Hprt*	GCAGTACAGCCCCAAAATGG AACAAAGTCTGGCCTGTATCCAA
Iodothyronine deiodinase type I	*Dio1*	GCTGAAGCGGCTTGTGATATT GTTGTCAGGGGCGAATCGG
Iodothyronine deiodinase type II	*Dio2*	CCTGCCAGTCTTTTTCTCCA ACACTGGAATTGGGAGCATC
Iodothyronine deiodinase type III	*Dio3*	CACGGCCTTCATGCTCTGG CGGTTGTCGTCTGATACGCA
Krueppel-like factor 9	*Klf9*	TTATTGCACGCTGGTCACTATC CTCATCGGGACTCTCCAGAC
Lipoprotein lipase	*Lpl*	GGTTGCGCGTAGAGAGGATG CTCACGCTCTGACATGCCTTC
Myosin heavy chain 1	*Myh1*	CTCTTCCCGCTTTGGTAAGTT CAGGAGCATTTCGATTAGATCCG
Myosin heavy chain 4	*Myh4*	CTTTGCTTACGTCAGTCAAGGT AGCGCCTGTGAGCTTGTAAA
Myostatin	*Mstn*	CCCAGGACCAGGAGAAGATGGGC TCGACCGTGAGGGGGTAGCG
Neuropeptide Y	*Npy*	AAAATGGGTCCGGTCTTGTG GGTAGACAATGCAACGATGGC
Peptidylprolyl isomerase A	*Ppia*	GAGCTGTTTGCAGACAAAGTTC CCCTGGCACATGAATCCTGG
Peptidylprolyl isomerase D (Cyclophilin D)	*Cyclophilin*	TCACAACAGTTCCGACTCCTC ACCTCTACATTTTCAAGCGTCC
Peroxisome proliferator-activated receptor gamma	*Pparg*	TCGCTGATGCACTGCCTATG GAGAGGTCCACAGAGCTGATT
Peroxisome proliferator-activated receptor gamma coactivator 1-alpha	*Ppargc1a*	TTGTCAGGCTGGAGTGTACC CACCATGGTCGTATCAGAGG
Phosphoenolpyruvate carboxykinase 1	*Pck1*	ATCTTTGGTGGCCGTAGACCT GCCAGTGGGCCAGGTATTT
Poopiomelanocortin	*Pomc*	TCATGACCTCCGAGAAGAGC GCCTTGGAATGAGAAGACC
PR domain containing 16	*Prdm16*	CCCCACATTCCGCTGTGAT CTCGCAATCCTTGCACTCA
Ribosomal protein lateral stalk subunit P0	*Rplp0*	TCGGGTCCTAGACCAGTGTTC AGATTCGGGATATGCTGTTGGC
Ryanodine receptor 1	*Ryr1*	CAGTTTTTGCGGACGGATGAT CACCGGCCTCCACAGTATTG
Sarcolipin	*Sln*	GAGGTGGAGAGACTGAGGTCCTTGG GAAGCTCGGGGCACACAGCAG

Gene	Abbreviation	Sequences 5' → 3' (forward and reverse)
ß-adrenergic receptor 1	*Adra1a*	CTCATCGTGGTGGGTAACGTG ACACACAGCACATCTACCGAA
ß-adrenergic receptor 2	*Adrb2*	GGGAACGACAGCGACTTCTT GCCAGGAGCATAACCGACAT
ß-adrenergic receptor 3	*Adrb3*	AGAAACGGCTCTCTGGCTTTG TGGTTATGGTCTGTAGTCTCGG
Thyroid hormone receptor beta 1	*Thrb*	ACACCTTATCCAGGCCACTT GTGGTACCCTGTGGCTTTGT
Thyroid hormone responsive gene spot14	*Thrsp*	AAGGTGGCTGGCAACGAAA GGGTCAGGTGGGTAAGGATG
Uncoupling protein 1	*Ucp1*	ACTCAGGATTGGCCTCTACG CCACACCTCCAGTCATTAAGC
Uncoupling protein 3	*Ucp3*	GAGATGGTGACCTACGACATCA GCGTTCATGTATCGGGTCTTTA

Table 11: List of primer sequences used for rat tissues, and adipocytes isolated from rats

Gene	Abbreviation	Sequences 5' → 3' (forward and reverse)
Hypoxanthine-guanine phosphoribosyltransferase	*Hprt*	GCAGTACAGCCCCAAAATGG AACAAAGTCTGGCCTGTATCCAA
Iodothyronine deiodinase type II	*Dio2*	CCTGCCAGTCTTTTTCTCCA ACACTGGAATTGGGAGCATC
Ribosomal protein lateral stalk subunit P0	*Rplp0*	TCGGGTCCTAGACCAGTGTTC AGATTCGGGATATGCTGTTGGC
ß-adrenergic receptor 1	*Adra1a*	CTACAACGACCCCAAGTGCT ACGTAGAAGGAGACGACGGA
ß-adrenergic receptor 3	*Adrb3*	AGAAACGGCTCTCTGGCTTTG TGGTTATGGTCTGTAGTCTCGG
Uncoupling protein 1	*Ucp1*	CAATGACCATGTACACCAAGGA GATCCGAGTCGCAGAAAAGAA

2.2.3.3 T3/T4 ELISA

Total T3 (tT3; free T3 and protein-bound T3) and total T4 (tT4; free T4 and protein-bound T4) serum concentrations were determined using commercially available enzyme-linked immunoabsorbent assays (ELISA) following manufacturer's instructions (Table 3). For analysis, mean values of absorbance

of the standards were plotted against concentration. The measured intensity of the samples was inversely proportional to the amount of tT3 or tT4 in the sample, respectively. By drawing a best-fit curve through the plotted standard values (four parameter logistics), sample data was interpolated on the standard curve to obtain the corresponding concentration values of the samples.

2.2.3.4 Glycogen assay

Glycogen concentration in the gastrocnemius and lower limb soleus muscle, as well as in the liver was determined according to manufacturer's instructions using a commercially available glycogen assay kit (Table 3). For analysis, mean values of absorbance of the standards were plotted against concentration. Linear regression analysis was used for interpolation of the sample data on the standard curve, followed by normalization to tissue weight.

2.2.3.5 Free fatty acid (FFA) assay

FFA concentration in iBAT tissue was determined according to manufacturer's instructions using a commercially available FFA assay kit (Table 3). For analysis, mean values of absorbance of the standards were plotted against concentration. By drawing a best-fit curve through the plotted standard values (four parameter logistics), sample data was interpolated on the standard curve to obtain the corresponding concentration values of the samples, followed by normalization to tissue weight.

2.2.3.6 Cyclic adenosine monophosphate (cAMP) assay

cAMP concentration in iBAT tissue was determined according to manufacturer's instructions using a commercially available cAMP assay kit (Table 3). The standard curve was generated plotting the percentage

$$\frac{B}{B_0} = \frac{(standard\ OD - NSB\ OD)}{(zero\ standard\ OD - NSB\ OD)} \cdot 100$$

with $OD = \text{optical density}$ and $NSB = \text{non} - \text{specific binding}$ as a function of the logarithmic cAMP concentration. Finally, sample data was interpolated on the standard curve to obtain the corresponding concentration values of the samples, followed by normalization to tissue weight.

2.2.3.7 Western Blot

For protein quantification, 5-10 mg of the tissue of interest was snap-frozen and homogenized in lysis buffer (Table 4) with protease inhibitors (Table 1). Protein quantification was performed using a bicinchoninic acid solution (BCA) assay (Table 1). Subsequent SDS-gel (TGX stain free FastCast acrylamide gels; 12 %) electrophoresis was performed (Table 3) using 15-20 µg of protein. Afterwards, proteins were transferred to a polyvinylidene difluoride (PVDF) membrane for 1 h at 100 V (Table 2). To minimize the unspecific binding to proteins, the PVDF membranes (Table 2) were blocked in 5 % milk (Table 1) in tris-buffered saline-Tween20 (TBS-T (Table 4)). After blocking, the PVDF membranes were incubated with primary antibodies (anti-UCP1, anti-SERCA2 (sarco/endoplasmic reticulum-type calcium transport ATPase 2), anti-OXPHOS (mitochondrial oxidative phosphorylation system); Table 12) overnight at 4°C. The next day, the membranes were washed five times in TBS-T before incubation with the secondary antibodies (Table 12) for 1 h at room temperature. Chemiluminescence was induced using Clarity Max Western ECL (enhanced chemiluminescence) Substrate (Table 3) and recorded with ChemiDoc™ Touch Imaging System, BioRad Laboratories, Germany (Table 2). After detection, blots were stripped with Restore PLUS Western Blot stripping buffer (Table 1) for 20 min at room temperature for reprobing purposes. Eventually, band intensities were quantified using ImageLab™ Software (Table 5) and single band intensities were normalized to total protein content.

Table 12: List of western blot antibodies

Purpose	**Antibody**	**Company**
Primary antibody	Mouse-anti-OXPHOS (45-8099)	Invitrogen, Thermo Fisher Scientific, Germany
	Rabbit-anti-SERCA2 (4388)	Cell Signaling Technology, Inc., USA
	Rabbit-anti-UCP1	(Jastroch, 2012)
Secondary antibody	Goat-anti-mouse polyclonal HRP-conjugated antibody (P0447)	DAKO, Denmark
	Goat-anti-rabbit polyclonal HRP-conjugated antibody (P0448)	DAKO, Denmark

2.2.4 Statistics and software

All physiological and molecular data were preprocessed using MATLAB (R2018a, MathWorks Inc., USA) or Excel (2021, Version: 2308; Microsoft Corporation, USA). Subsequent statistical analysis of the data was performed using GraphPad Prism 8 (GraphPad, USA). Information on statistical tests can be found in Supplementary Table 1. Post hoc test information can be found in the respective figures, defined as *p<0.05, **p<0.01, ***p<0.001, ****p<0.0001, #p<0.05, ##p<0.01, ###p<0.001, ####p<0.0001, and $p<0.05. Data are reported as mean ±SEM (standard error of the mean). Overview and representative figures were designed using *Biorender.com*.

3 Results

The following sections report the data and data analysis of all performed *in vivo* (see section 3.1 and section 3.2) and *in vitro* (see section 3.3) experiments.

3.1 The role of TRβ and TRα1 in thermoregulation

The different contributions of TRβ and TRα1 signaling to body temperature regulation and homeostasis remain enigmatic. Interestingly, TRα1+m mice have a lower core body temperature at room temperature (Warner et al., 2013), while TRβ KO animals do not show any body temperature alterations at 22°C in comparison to wildtype animals (Forrest and Vennström, 2000). Whether the body temperature phenotype in TRα1+m mice is a peripheral defect or whether defective central TRα1 signaling contributes to a lower body temperature phenotype is currently unknown.

3.1.1 Experimental design: What are the contributions of a TRβ KO or mutated TRα1 to whole-body thermoregulation?

To dissect the contributions of TRβ and TRα1 signaling to body temperature regulation at different ambient temperatures, radiotelemetry transmitters were implanted into the abdominal cavity of wildtype mice, TRβ KO mice, and TRα1+m mutants to continuously record body temperature in a touch-free experimental set-up. All animals were subsequently treated with T3 (0.5 mg/L) via the drinking water for 12 days to reactivate the mutant TRα1.

To test whether thermoneutral housing conditions would reverse tail heat loss and thus the defective body temperature of TRa1+m mice that occurs at room temperature (Warner et al., 2013), mice were housed at 30°C (Figure 6). Furthermore, at room temperature, mice are constantly exposed to a mild cold challenge that requires sympathetic signaling and BAT action. In contrast, humans developed protection against minor cold challenges by wearing clothes and therefore lowered their thermoneutral comfort zone to room temperature (Ganeshan and Chawla, 2017). Thus, to create translational relevance, mice were also placed at 30°C ambient temperature for the duration of T3 treatment to study the contributions of TRβ and TRα1 signaling to body temperature regulation and homeostasis during systemic hyperthyroidism. Infrared pictures were taken at the end of each baseline recording and during T3 treatment. At the end of the experiment, animals were sacrificed and organs and tissues (liver, heart, kidney, hypothalamus, iBAT, iWAT, and eWAT), as well as serum, were harvested for further molecular analysis.

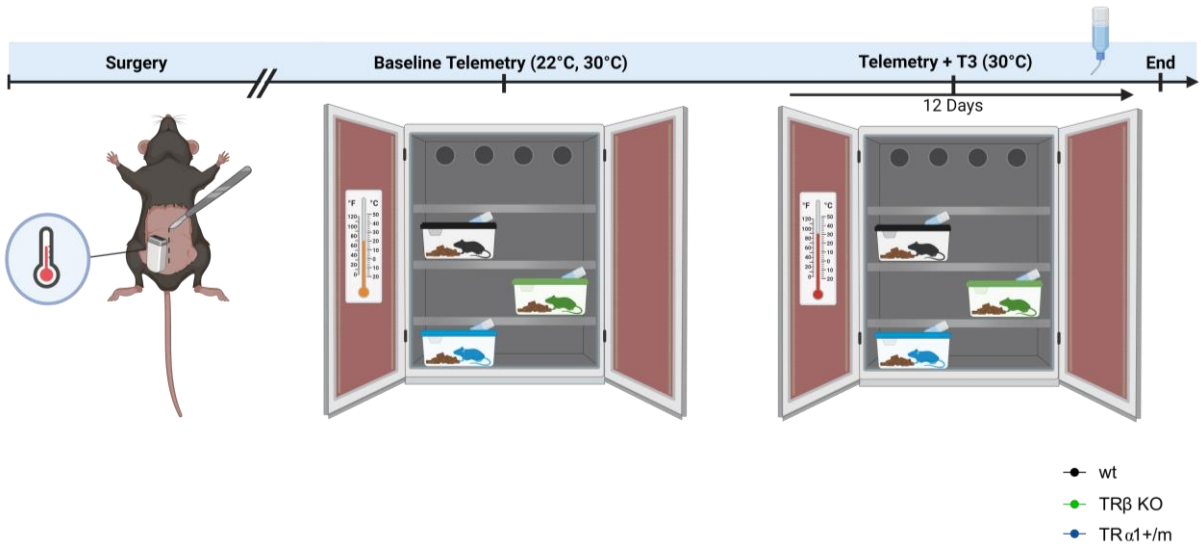

Figure 6: Experimental in vivo study design to investigate the effects of mutant TRα1 and a TRβ KO in mice on body temperature regulation and homeostasis in comparison to wildtype (wt) animals. The overview figure was adapted from Sentis et al., 2023 in press.

3.1.2 Body temperature phenotypes of wildtype animals, TRβ KO, and TRα1+m mutants

At the beginning of the experiment, wildtype controls, TRβ KO mice, and TRα1+m mutants were housed at 22°C to record body temperature baseline profiles. At 22°C ambient temperature, TRα1+m mice displayed significantly lower body temperature by 1.5°C compared to wildtype controls, whereas TRβ KO displayed normal body temperature (Figure 7A). When housed at thermoneutrality, to circumvent the excessive tail heat loss of TRα1+m mutants (Warner et al., 2013), body temperature of TRα1+m mice remained lower by 1.2°C, but exclusively restricted to the inactive light phase (Figure 7B). The reactivation of the mutated TRα1 by oral T3 treatment normalized the defective body temperature phenotype of TRα1+m mutants (Figure 7C), suggesting that the central control of body temperature regulation might be impaired in TRα1+m mutants. Thermoneutral housing conditions or T3 treatment did not lead to any changes in body temperature of TRβ KO animals compared to wildtype controls (Figure 7B+C).

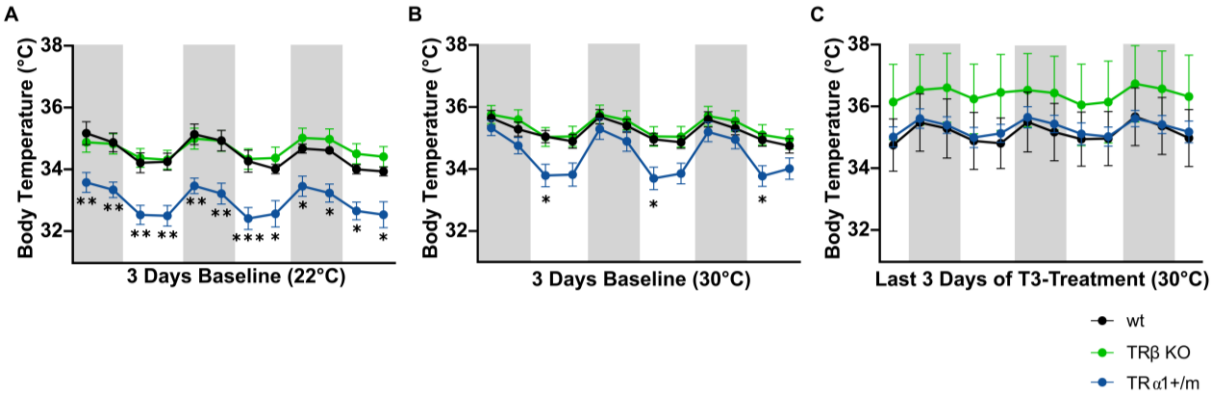

*Figure 7: Body temperature profiles of wildtype (wt) animals, TRß KO animals, and TRα1+m mutants at different ambient temperatures. Gray areas indicate nighttime. A) Body temperature profiles at 22°C ambient temperature (wt, n=9; TRα1+m, n=7; TRß KO, n= 12). B) Body temperature profiles at 30°C ambient temperature (wt, n=9; TRα1+m, n=7; TRß KO, n= 12). C) Body temperature profiles at 30°C ambient temperature during the last 3 days of oral T3 treatment (0.5 mg/L) (wt, n=4; TRα1+m, n=7; TRß KO, n= 4). Data are reported as ±SEM. 2-way ANOVA, post hoc: Dunnett's multiple comparison. *p<0.05, **p<0.01, ***p<0.001. Information on statistical tests and post hoc tests can be found in Supplementary Table 1. Parts of the data have been submitted to a peer-reviewed journal due to priority reasons (Sentis et al., 2023 in press).*

A touch-free experimental paradigm to continuously record body temperature was chosen to exclude any anxiety-induced thermogenic responses of TRα1+m mutants to touch, handling, and experimental interventions (Venero et al., 2005). Upon entry into the animal facility, body temperature of TRα1+m mice immediately started to increase (Figure 8A) and was further elevated after saline injection in both TRα1+m mutants and TRβ KO animals (Figure 8B).

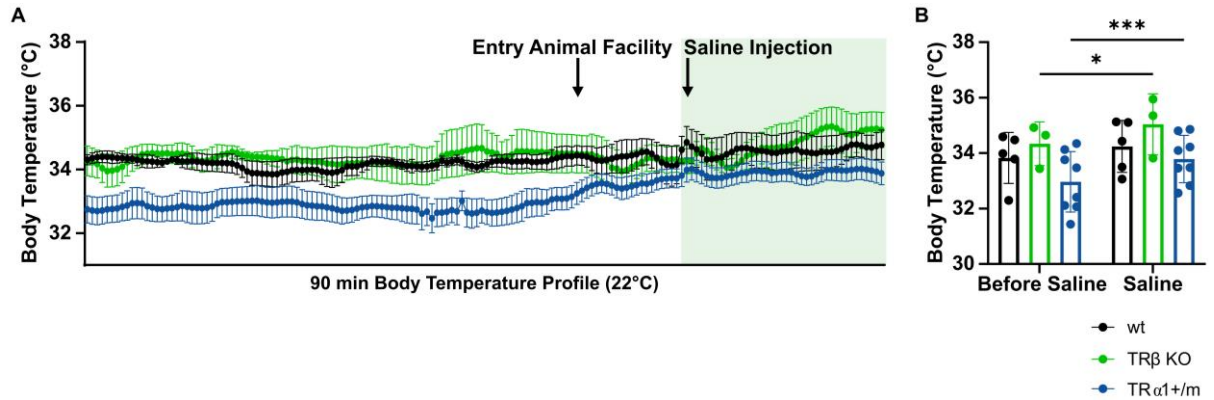

*Figure 8: Anxiety induced thermogenesis of TRα1+m mutants. A) 90 min body temperature profile of wildtype (wt) animals (n=5), TRß KO animals (n=3), and TRα1+m mutants (n=8) at 22°C. Entry into the animal facility and exact time point of saline injections (i.p.) are marked in the figure by arrows. B) Mean body temperature (30 min) of wildtype animals (n=5), TRß KO animals (n=3), and TRα1+m mutants (n=8) before and after saline injection (i.p.). Data are reported as ±SEM. 2-way ANOVA, post hoc: Šídák's multiple comparison. *p<0.05, ***p<0.001. Information on statistical tests and post hoc tests can be found in Supplementary Table 1. Parts of the data have been submitted to a peer-reviewed journal due to priority reasons (Sentis et al., 2023 in press).*

As expected, tail temperature of TRα1+m mice was significantly increased by 1°C compared to wildtype control animals (Figure 9A) at 22°C (Warner et al., 2013). However, at thermoneutrality, tail heat loss of TRα1+m mutants could be reversed (Figure 9B+C). Upon T3 treatment, tail temperature of wildtype and TRα1+m mice significantly increased by the end of T3 treatment (Figure 9C), whereas BAT temperature of TRα1+m mutants decreased by the end of T3 treatment (Figure 9D). In contrast, tail and BAT temperature of TRβ KO animals were unchanged after T3 treatment (Figure 9C+D).

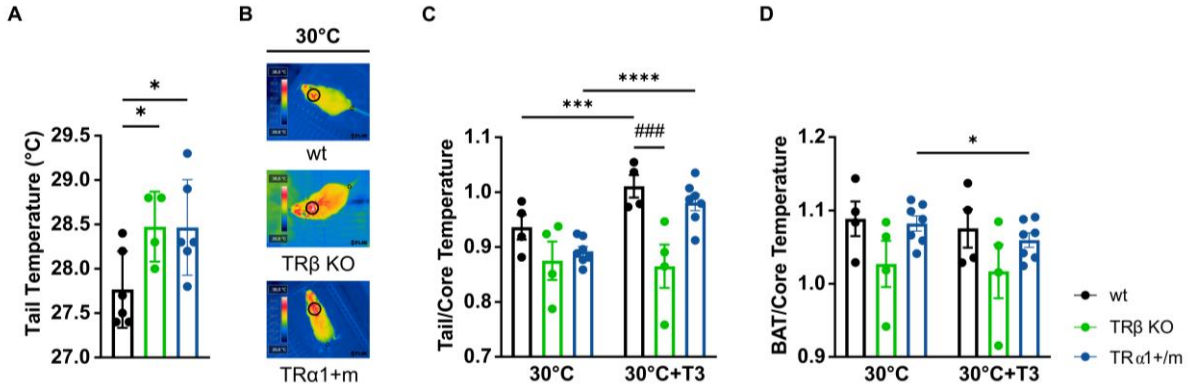

*Figure 9: Tail and BAT temperature at different ambient temperatures. A) Tail temperature at 22°C ambient temperature of wildtype (wt) animals (n=6), TRβ KO animals (n=4), and TRα1+m mutants (n=6). B) Exemplarily: Infrared thermography pictures at 30°C. C) Tail temperature at 30°C and on the last day of oral T3 treatment (0.5 mg/L) (wt, n=4; TRα1+m, n=7; TRβ KO, n= 4). D) BAT temperature at 30°C and on the last day of oral T3 treatment (0.5 mg/L) (wt, n=4; TRα1+m, n=7; TRβ KO, n= 4). Data are reported as ±SEM. For A: Unpaired Student's t-test. For C+D: 2-way ANOVA, post hoc: Bonferroni's multiple comparison. *p<0.05, ***p<0.001, ****p<0.0001, ###p<0.001. Information on statistical tests and post hoc tests can be found in Supplementary Table 1. Parts of the data have been submitted to a peer-reviewed journal due to priority reasons (Sentis et al., 2023 in press).*

Food intake of control animals and TRα1+m mice gradually increased with prolonged T3 treatment at 30°C but remained unaltered in TRβ KO mice (Figure 10A+B). The water intake remained unchanged during T3 treatment for all genotypes (Figure 10C+D). Despite the higher food intake of TRβ KO animals at the beginning of T3 treatment, the body weight increase of TRβ KO mice at the end of T3 treatment did not differ in comparison to wildtype controls (Figure 10E). Although TRα1+m mutants did not consume more food compared to wildtype animals, the body weight increase at the end of T3 treatment was higher compared to controls, albeit not reaching significance (p=0.07; Figure 10E+F).

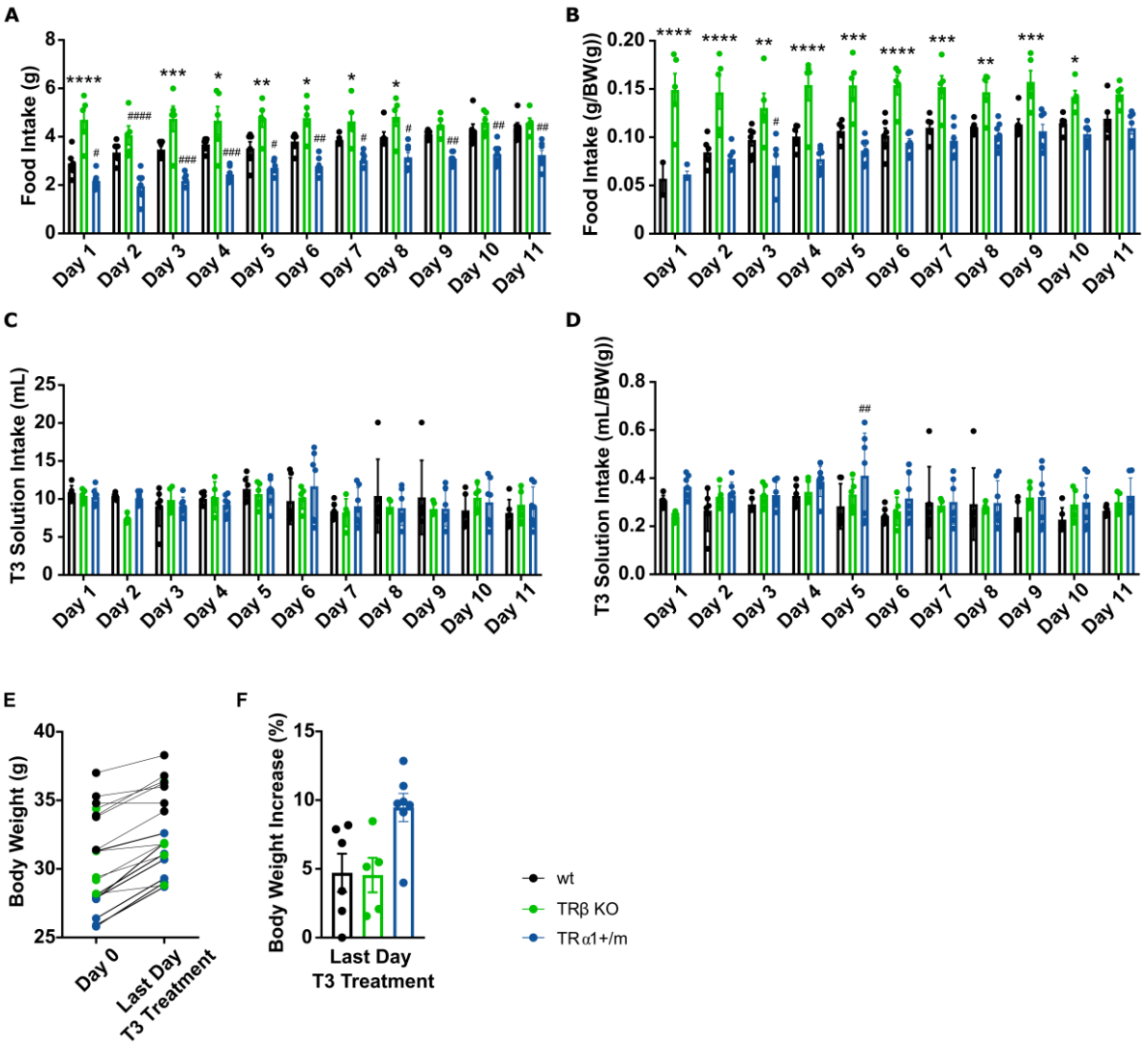

*Figure 10: Food and water intake during oral T3 treatment (0.5 mg/L) at 30°C ambient temperature of wildtype (wt) animals (n=6), TRβ KO animals (n=5), and TRα1+m mutants (n=7). A) Food intake (g). B) Normalized food intake. C) T3 solution intake (mL). D) Normalized T3 solution intake. E) Single animal body weight increase (g): comparison of start of T3 treatment vs. the last day of T3 treatment. F) Body weight increase in % on the last day of oral T3 treatment. Data are reported as ±SEM. For A-D: - 2-way ANOVA, post hoc: Dunnett's multiple comparison. For F: Unpaired Student´s t-test. *p<0.05, **p<0.01, ***p<0.001, ****p<0.0001, #p<0.05, ##p<0.01, ###p<0.001, ####p<0.0001. Information on statistical tests and post hoc tests can be found in Supplementary Table 1. Parts of the data have been submitted to a peer-reviewed journal due to priority reasons (Sentis et al., 2023 in press).*

Taken together, housing temperatures at thermoneutrality and additional T3 treatment only led to negligible body temperature changes in TRβ KO mice in comparison to control animals, whereas TRα1+m mutant mice still displayed a lower core body temperature phenotype even at 30°C, suggesting a central resetting.

3.1.3 Molecular phenotyping of wildtype animals, TRβ KO animals, and TRα1+m mutants

In addition to the physiological mouse data during T3 treatment, subsequent qPCR analysis was performed to detect molecular changes on the expression level after T3 treatment at 30°C of TRα1+m mutants and TRβ KO animals. Genes of interest in fat tissue were thermoregulatory genes and TH-responsive genes (Lee et al., 2022; Pilkington et al., 2021).

In iBAT, TH-responsive and thermoregulatory genes such as *Ucp1*, *Dio2*, and *Adrb3* were upregulated in TRβ KO mice, whereas *Ucp1* and *Dio2* expression were downregulated and *Adrb3* and *Pargc1a* (peroxisome proliferator-activated receptor gamma coactivator 1-alpha) expression were increased in TRα1+m mice (Figure 11A). eWAT and iWAT expression was unaltered upon oral T3 treatment in both TRβ KO animals and TRα1+m mice (Figure 11B+C).

As the hypothalamus is greatly involved in thermoregulation (Gans et al., 2021; Laperrousaz et al., 2017; Werneck De Castro et al., 2015), expression analyses of direct and indirect TH target genes in hypothalami of TRβ KO and TRα1+m mice were performed. *Lpl* (lipoprotein lipase), *Dio2*, and *Adrb2* (ß2-adrenergic receptor) gene expression were increased in TRβ KO animals, whereas *Klf9* (krueppel-like factor 9) and *Dio3* (iodothyronine deiodinase type III) expression were significantly decreased in TRα1+m mutants after T3 treatment (Figure 11D). However, the satiety and hunger regulating genes (Timper and Brüning, 2017) *Npy* (neuropeptide Y) and *Pomc* (poopiomelanocortin) did not respond to T3 treatment with altered expression pattern in the hypothalamus of TRβ KO and TRα1+m mice. Interestingly, *Hcrt* encoding the hypocretin neuropeptide precursor protein was downregulated in TRβ KO mice after T3 treatment (Figure 11D).

As expected from previously published work on TRβ KO animals (Lopez-Alcantara et al., 2023), expression of TH target genes such as *Dio2*, *Thrsp* (thyroid hormone responsive gene spot14), and *Cd5l* (CD5 molecule like) were non-responsive to T3 treatment in the liver of TRβ KO animals (Figure 11E). However, metabolism-related genes, such as *Gk* (glycerol kinase), *Pck1* (Phosphoenolpyruvate carboxykinase 1), *Gys* (glycogen synthase 1), and *Fasn* (fatty acid synthase) were upregulated upon T3 treatment in TRβ KO animals. The expression of the same set of genes was unaltered in TRα1+m mice after T3 treatment (Figure 11E).

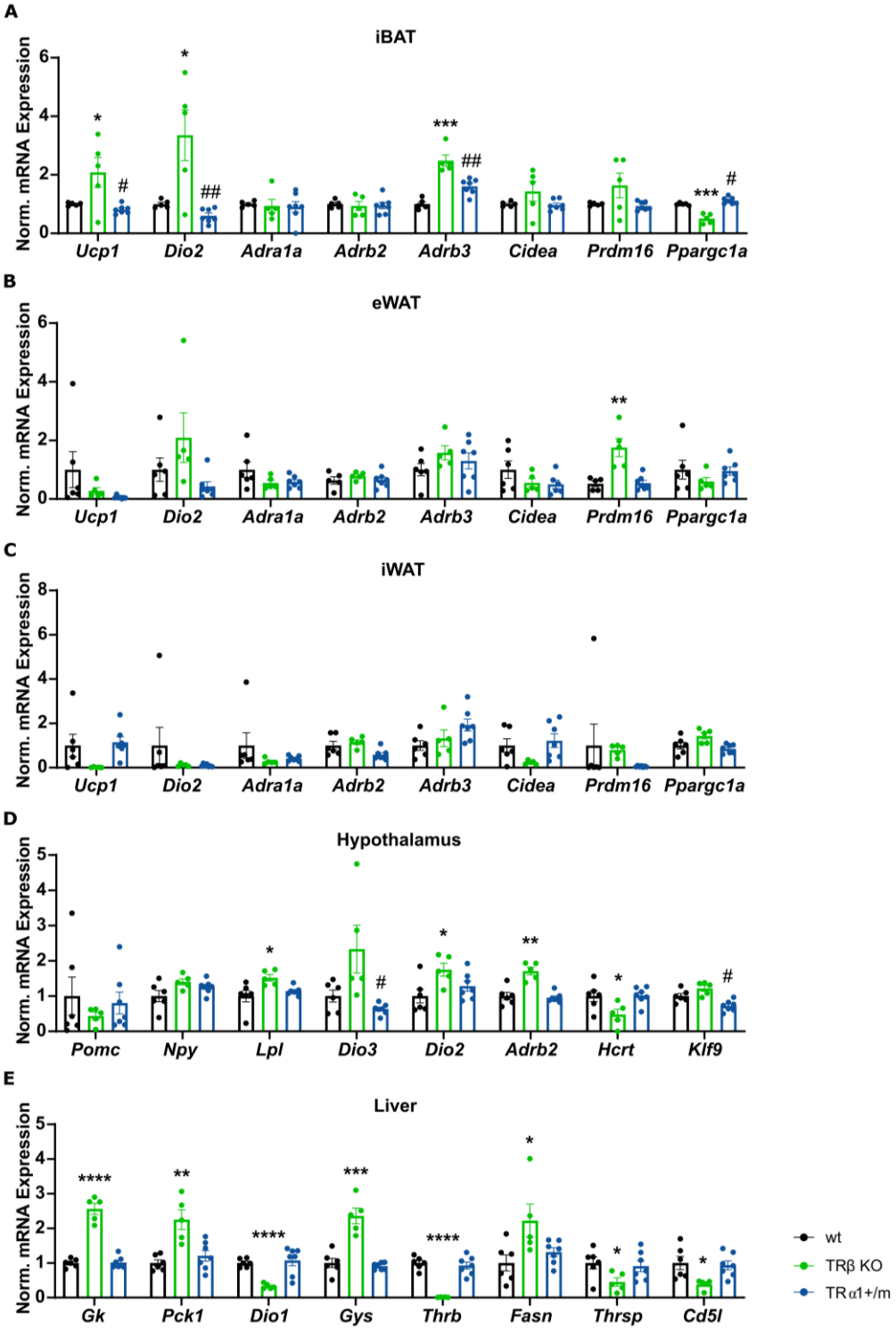

*Figure 11: qPCR analysis of fat tissues, hypothalami, and liver in wildtype (wt) controls (n=6), TRß KO animals (n=5), and TRα1+m mutants (n=7) after oral T3 treatment (0.5 mg/L). A) Normalized mRNA expression in iBAT. B) Normalized mRNA expression in eWAT. C) Normalized mRNA expression in iWAT. D) Normalized mRNA expression in the hypothalamus. E) Normalized mRNA expression in the liver. Data are reported as ±SEM. Unpaired Student´s t-test. *p<0.05, **p<0.01, ***p<0.001, ****p<0.0001, #p<0.05, ##p<0.01. Information on statistical tests and post hoc tests can be found in Supplementary Table 1. Parts of the data have been submitted to a peer-reviewed journal due to priority reasons (Sentis et al., 2023 in press).*

To investigate molecular changes on the protein level in TRα1+m mutants and TRβ KO animals upon T3 treatment at 30°C, Western Blot analysis of iBAT was performed. The Western Blot membranes were stained for UCP1 (Jastroch, 2012) and the five OXPHOS complexes and were normalized to a calibrator sample and whole protein content (Figure 12A).

However, neither *Ucp1* upregulation in TRβ KO mice nor *Ucp1* downregulation in TRα1+m mutants led to any changes in UCP1 protein content after T3 treatment (Figure 12B). Although relative UCP1 protein content was unchanged in TRα1+m mutants and TRβ KO animals after T3 treatment (Figure 12B), differences in relative protein content of the respiratory chain complexes that build the electron transport chain (I-IV) at the inner mitochondrial membrane (Xu et al., 2020) could be detected (Figure 12C). The relative protein content of the OXPHOS-complexes I, II, and IV was significantly increased in TRβ KO animals. In contrast, the protein content of complex I was increased in TRα1+m animals, whereas protein content of complex III was significantly decreased. Despite higher complex V (ATP synthase) protein content in TRα1+m mice, values did not reach significance (p=0.09).

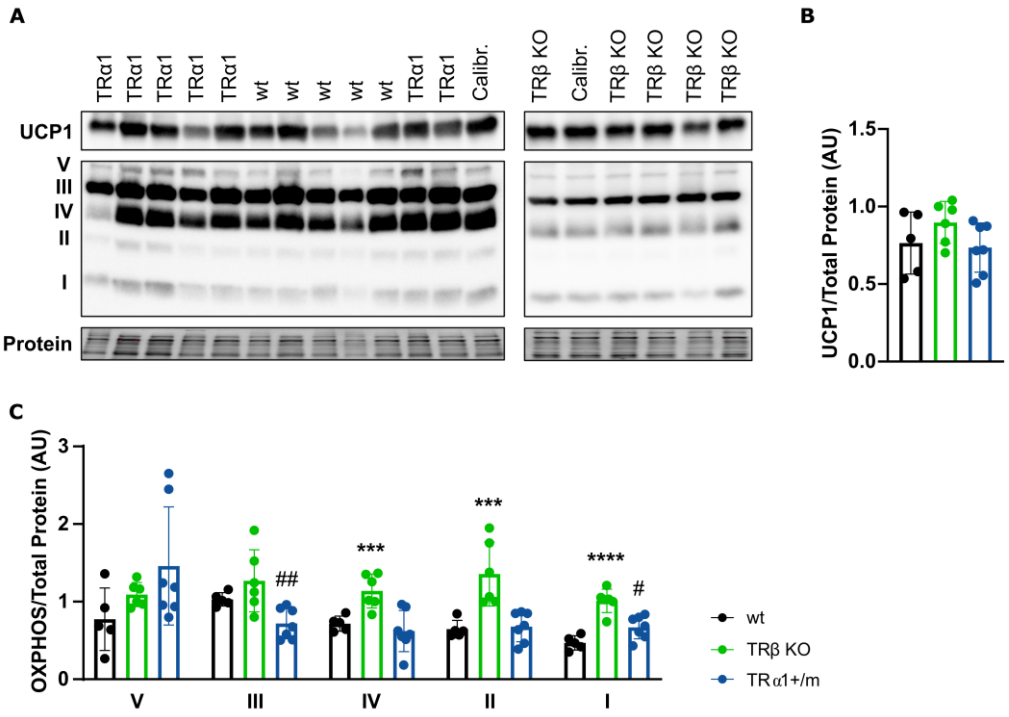

*Figure 12: Western Blot analysis of iBAT of wildtype (wt) controls (n=5), TRα1+m mutants (n=7), and TRβ KO animals (n=6) after T3 treatment (0.5 mg/L). A) Western Blots stained for UCP1 and the five OXPHOS complexes. B) Protein quantification of UCP1. C) Protein quantification of the five OXPHOS complexes. Data are reported as ±SEM. Unpaired Student´s t-test. ***p<0.001, ****p<0.0001, #p<0.05, ##p<0.01. Information on statistical tests and post hoc tests can be found in Supplementary Table 1.*

In addition to the mRNA expression data, glycogen content in the liver was increased following T3 treatment in TRβ KO mice but not in TRα1+m mutants (Figure 13).

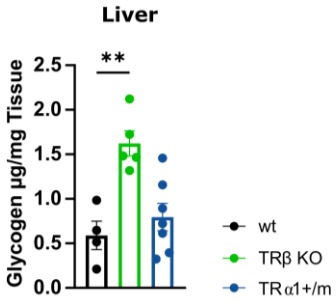

*Figure 13: Glycogen content in the liver of wildtype (wt) animals (n=4), TRβ KO animals (n=5), and TRα1+m mutants (n=7) after T3 treatment (0.5 mg/L). Data are reported as ±SEM. Unpaired Student´s t-test. **p<0.01. Information on statistical tests and post hoc tests can be found in Supplementary Table 1.*

Taken together, the molecular data on the regulation of TH-responsive genes in various tissues and organs suggest that prolonged T3 treatment in TRβ KO animals and TRα1+m mutants influences TH target gene expression.

3.2 The role of hypothalamic TRα1 in thermoregulation

Given that the defective body temperature phenotype of TRα1+m mice could only partially be rescued at 30°C, a role for central TRα1 signaling in the regulation of the body temperature set-point is hypothesized.

3.2.1 Experimental design: Does TRα1 in the hypothalamus regulate core body temperature?

To further investigate the role of TRα1 signaling in the brain on temperature regulation, AAV vectors carrying either dominant-negative TRα1 or a control vector were injected into the hypothalamus of wildtype mice, as this region is a known regulator of body temperature homeostasis (Contreras et al., 2017, 2016; Warner and Mittag, 2012). This aimed at locally inhibiting TRα1 signaling in cells of the hypothalamus. Simultaneously, radiotelemetry transmitters were implanted into the abdominal cavity to continuously record body temperature (Figure 14). Mice were given a recovery period of two weeks to ensure sufficient expression of dominant-negative TRα1 or control GFP. Next, mice were transferred into an open respiratory system to measure oxygen consumption and carbon dioxide exchange rates, as well as energy expenditure at different ambient temperatures (Figure 14). Infrared pictures of BAT and tails were taken at 22°C before and after the indirect calorimetry measurements.

Before sacrifice, the ECG of freely moving animals was recorded. At the end of the experiment, animals were sacrificed and organs and tissues (liver, heart, kidney, gastrocnemius muscle, soleus muscle, iBAT, iWAT, and eWAT), as well as serum, were harvested for further molecular analysis.

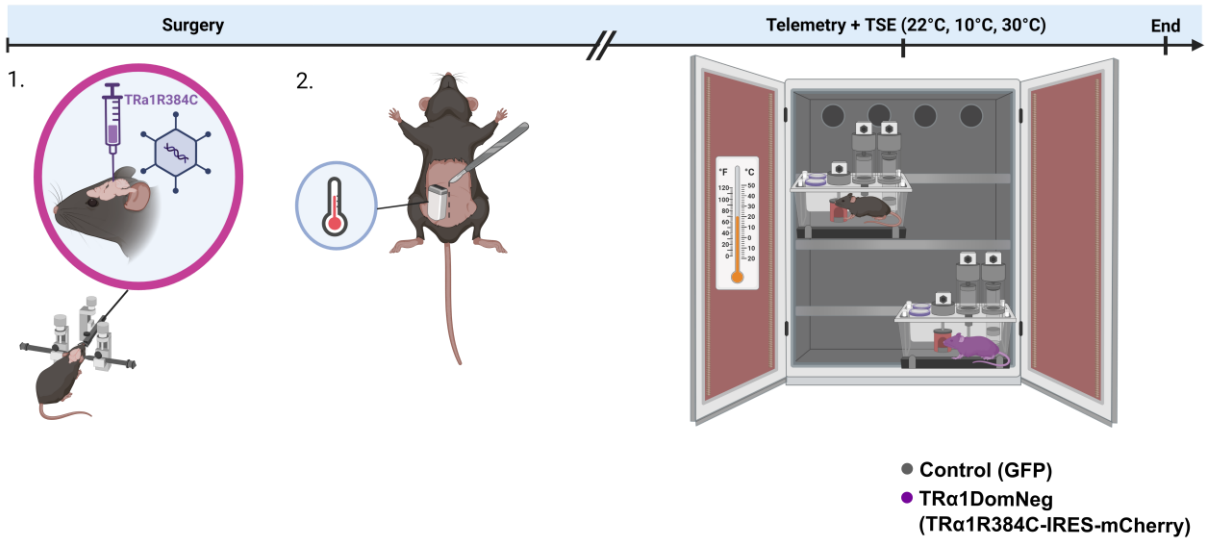

Figure 14: Experimental in vivo study design to investigate the temperature-dependent effects of defective TRα1 in the hypothalamus on body temperature regulation and energy metabolism. The overview figure was adapted from Sentis et al., 2023 in press.

3.2.2 Hypothalamic dominant-negative TRα1 promotes slower body weight gain

To demonstrate that dominant-negative TRα1 or control GFP was expressed in the hypothalamic target region, brain sections were stained for either mCherry or GFP. Strong expression of mCherry (TRα1R384C construct) and GFP (control construct) could be detected in regions near the 3rd ventricle and close to the paraventricular nucleus (PVN) of the hypothalamus (Figure 15A). Only animals with validated expression of mCherry (n=5) and GFP (n=8) were included for further analysis of physiological and molecular data.

Given that the dominant-negative TRα1 expression was also detected near the PVN, an area involved in regulating the HPT axis (Kondo et al., 2021), total serum T3 and T4 levels, as well as fT4 levels were determined. However, neither T3, nor T4, or fT4 serum levels were changed in comparison to control animals, suggesting that the HPT axis was not influenced by the expression of dominant-negative TRα1 in the hypothalamus (Figure 15B).

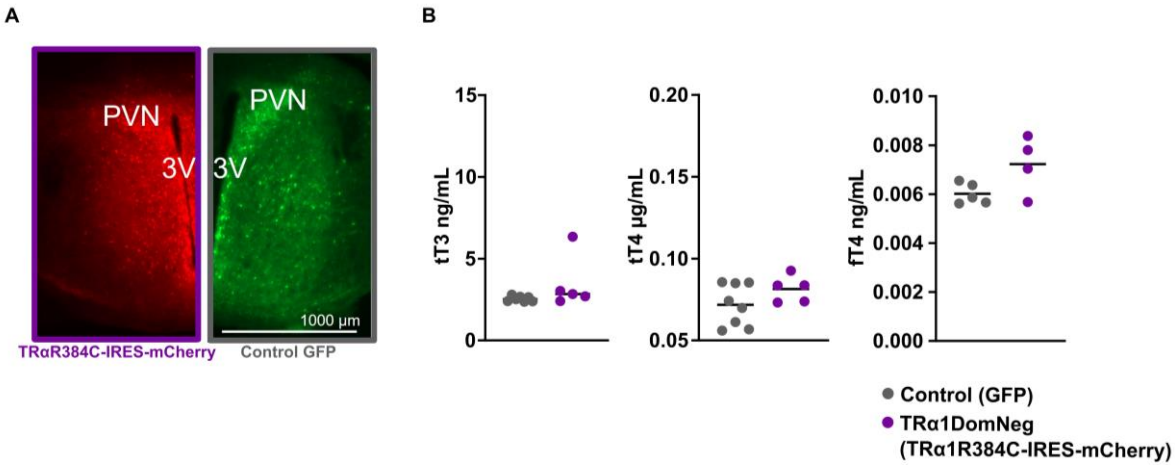

Figure 15: Proof of concept: Expression of dominant-negative TRα1 and control GFP in the hypothalamic target region. A) Exemplary immunofluorescence staining of brains sections of animals that received dominant-negative TRα1 (TRα1R384C construct) or control virus (control construct with GFP). B) Determination of total T3 (TRα1DomNeg, n=5; control, n=8), total T4 (TRα1DomNeg, n=5; control, n=8), and free T4 (TRα1DomNeg, n=4; control, n=5) serum levels. Unpaired Student´s t-test. Information on statistical tests and post hoc tests can be found in Supplementary Table 1. Parts of the data have been submitted to a peer-reviewed journal due to priority reasons (Sentis et al., 2023 in press).

Body weight gain, food intake, and water intake, as well as body temperature of all animals, were monitored until the end of the experiment. Starting one week after the stereotaxic delivery of the AAV vectors, animals who received dominant-negative TRα1 stopped gaining weight and failed to increase their post-surgery weight until the end of the experiment (Figure 16A). In comparison, control animals gradually increased their weight by 2.2 g (1-week post-surgery vs. 6-weeks post-surgery) until the end of the experiment. Additionally, dominant-negative TRα1 expressing animals reduced their

mean food intake by 0.6 g/day on average compared to control animals (Figure 16B+C), which, however, did not reach significance. Water intake was not different between the two groups (Figure 16B+C).

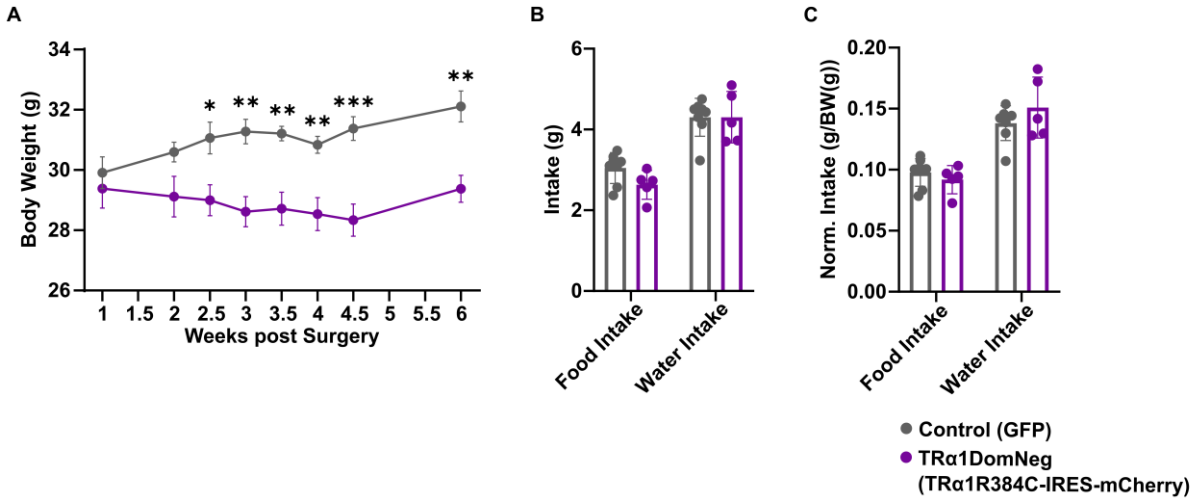

*Figure 16: Body weight gain and food and water intake after AAV-delivery of mutant TRα1 or control AAV (TRα1DomNeg, n=5; control, n=8). A) Increasing body weight (g) after stereotaxic surgery. B) Food and water intake (g). C) Normalized food and water intake. Data are reported as ±SEM. For A: 2-way ANOVA, post hoc: Bonferroni's multiple comparison. For B+C: Unpaired Student´s t-test. *p<0.05, **p<0.01, ***p<0.001. Information on statistical tests and post hoc tests can be found in Supplementary Table 1. Parts of the data have been submitted to a peer-reviewed journal due to priority reasons (Sentis et al., 2023 in press).*

To investigate the slower body weight gain of dominant-negative hypothalamic TRα1 expressing mice in further detail, all animals were placed into an indirect calorimetry system to assess possible changes in energy expenditure and the RQ. At 22°C ambient temperature, the RQ profile over two days did not display any obvious alterations (Figure 17A) and no differences in the RQ during the inactive phase compared to the active phase could be detected (Figure 17B). Although dominant-negative TRα1 expressing animals had a significantly lower RMR compared to controls (Figure 17C), the RMR, however, correlated with increasing body weight in both mutant TRα1 expressing animals and controls (Figure 17D). Additionally, oxygen consumption during the day and during the night was unchanged in both groups (Figure 17E+F). The analysis of covariance (ANCOVA) of the energy expenditure during the day (Figure 17G) and during the night (Figure 17H) revealed that oxygen consumption and thus energy expenditure in kJ are also body weight dependent in both, dominant-negative TRα1 expressing animals and controls. Therefore, all animals, independent of group affiliation, had appropriate energy expenditure with regard to their body weight (Figure 17G+H). In line with unaltered oxygen consumption, mean energy expenditure during the day and night was also unaltered in both groups (Figure 17I).

To determine the BMR at rest of dominant-negative TRα1 expressing animals and controls, all

animals were placed at 30°C. Oxygen consumption gradually decreased at 30°C until reaching a plateau (Figure 17J), but no differences in oxygen consumption between the two groups could be detected (Figure 17K). After a recovery period of 24h, animals were exposed to a cold challenge at 10°C to test for defects in facultative thermogenesis by determining the RMR during cold exposure. At 10°C, oxygen consumption gradually increased until reaching a plateau (Figure 17L). However, also during cold exposure, no differences in the RMR between the two groups could be detected (Figure 17M).

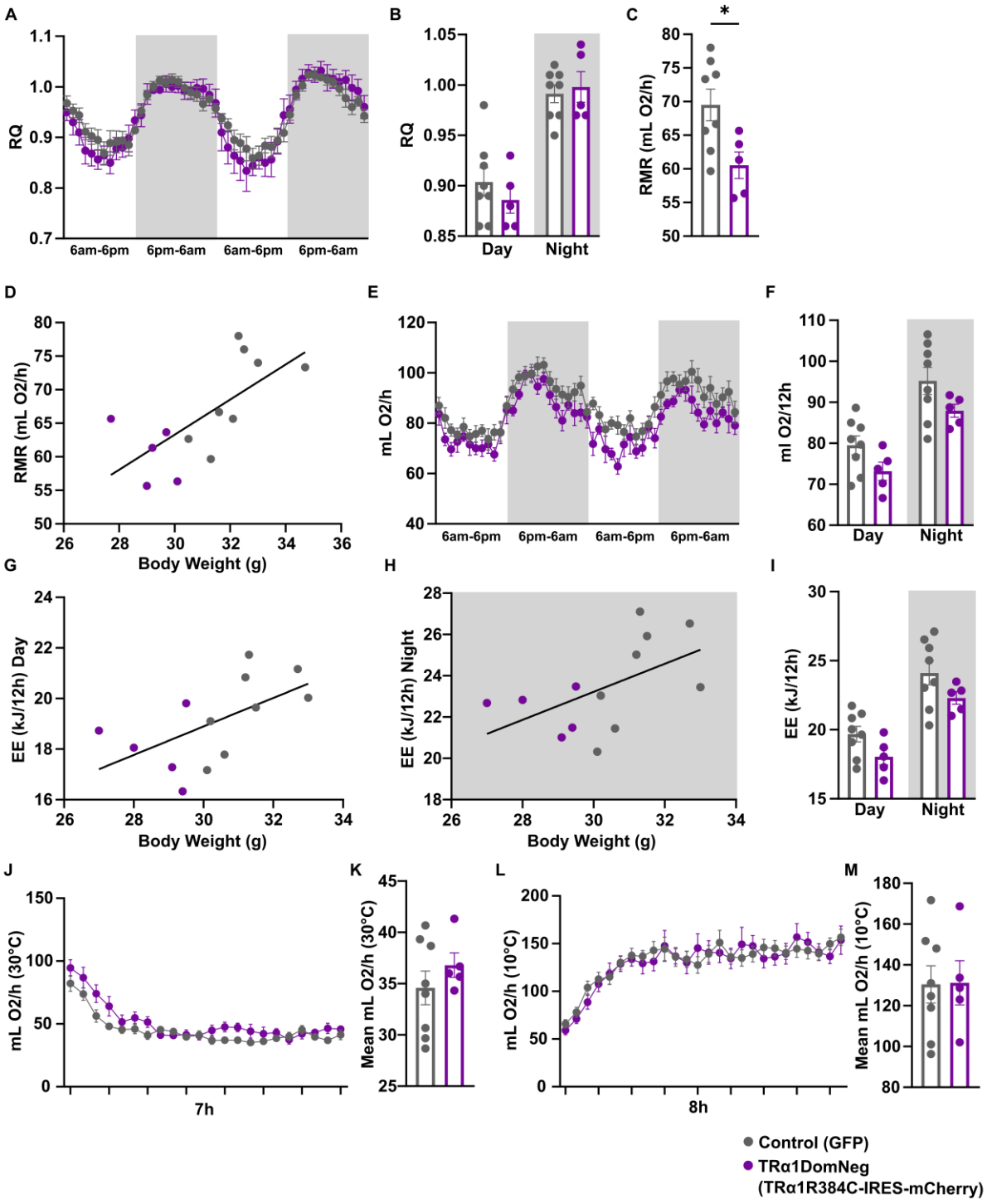

*Figure 17: Indirect calorimetry of animals that received dominant-negative TRα1 or control GFP (TRα1DomNeg, n=5; control, n=8). Gray areas indicate nighttime. A) Respiratory quotient (RQ) over 2 days. B) Mean RQ over 2 days. C) Resting metabolic rate (RMR). D) RMR plotted against body weight. E) Oxygen consumption over 2 days. F) Mean oxygen consumption during the day and during the night. G) Energy expenditure (EE) during the day plotted against body weight. H) EE during the night plotted against body weight. I) Mean EE during the day and during the night. J) Oxygen consumption at 30°C. K) Mean oxygen consumption at 30°C. L) Oxygen consumption at 10°C. M) Mean oxygen consumption at 10°C. Data are reported as ±SEM. For B+C+F+I+K+M: Unpaired Student's t-test. For D+G+H: Simple linear regression. For J+L: 2-way ANOVA, post hoc: Šídák's multiple comparison. *p<0.05. Data were analyzed with the help of Dr. Rebecca Oelkrug. Information on statistical tests and post hoc tests can be found in Supplementary Table 1. Parts of the data have been submitted to a peer-reviewed journal due to priority reasons (Sentis et al., 2023 in press).*

Taken together, the indirect calorimetry data revealed only minor changes and decreases in energy metabolism that are likely caused by the reduced body weight of the mice expressing the dominant-negative TRα1 in the hypothalamus.

3.2.3 Hypothalamic dominant-negative TRα1 lowers core body temperature

To investigate whether body temperature regulation was affected by the mutant TRα1 in the hypothalamus, animals were placed at different environmental temperatures to continuously record body temperature via implanted radiotelemetry transmitters.

At 22°C, the body temperature of animals expressing dominant-negative TRα1 in the hypothalamus was significantly lower during the active and inactive phases compared to GFP-expressing controls (Figure 18A). Locomotor activity did also not differ between the two groups at 22°C, except on the first day which can be attributed to the new environment in the climate chamber (Figure 18B). When placing the animals at thermoneutrality (30°C), the body temperature of animals expressing mutant TRα1 still remained significantly lower compared to the control animals (Figure 18C). Although, body temperature of dominant-negative TRα1 expressing animals was reduced by 0.6°C at 10°C ambient temperature (Figure 18C), values, however, did not reach significance ($p=0.1$). Interestingly, normalized BAT temperature was significantly increased upon expression of dominant-negative TRα1 in the hypothalamus, whereas tail temperature remained unchanged at 22°C (Figure 18D+E).

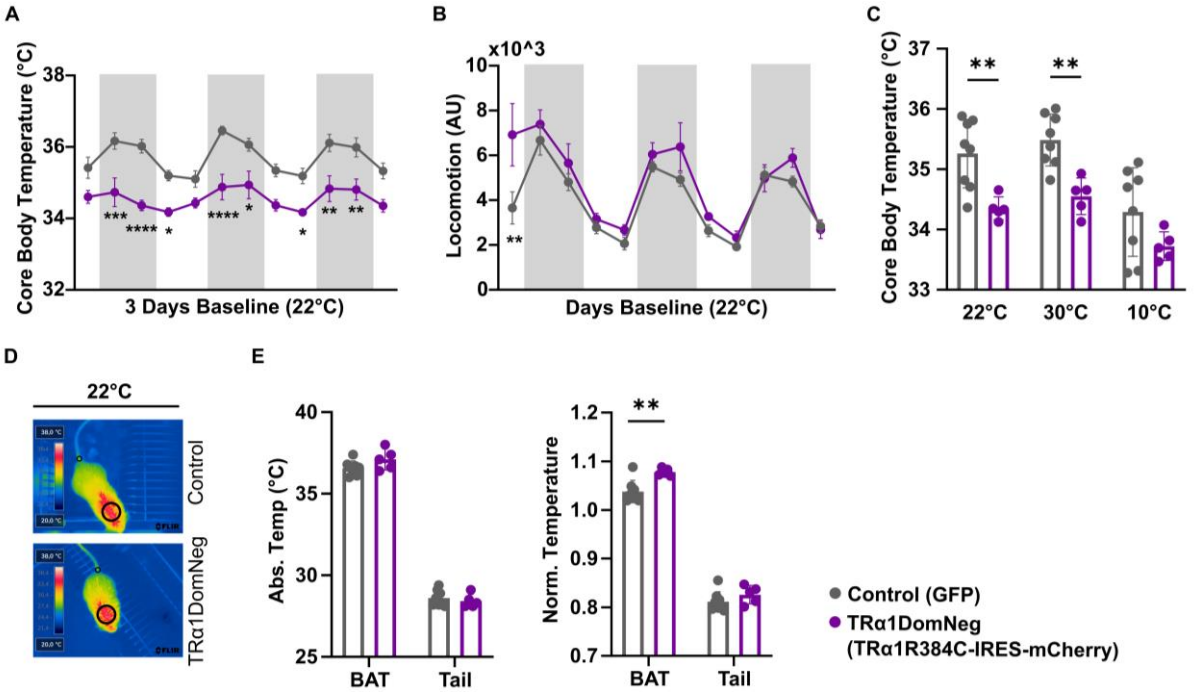

*Figure 18: Body temperature phenotype of mice expressing dominant-negative TRα1 in the hypothalamus (n=5) and control animals (n=8). Grey areas indicate nighttime. A) Body temperature profile at 22°C. B) Locomotor activity at 22°C. C) Mean body temperature at different ambient temperatures. D) Exemplarily: Infrared thermography pictures at 22°C. E) Absolute and normalized BAT and tail temperature. Data are reported as ±SEM. For A+B: 2-way ANOVA, post hoc: Šídák's multiple comparison. For C+E: Unpaired Student's t-test. *p<0.05, **p<0.01, ***p<0.001, ****p<0.0001. Information on statistical tests and post hoc tests can be found in Supplementary Table 1. Parts of the data have been submitted to a peer-reviewed journal due to priority reasons (Sentis et al., 2023 in press).*

In summary, the expression of dominant-negative TRα1 in the hypothalamus could lower body temperature at 22°C and 30°C suggesting that central TRα1 signaling is important for body temperature regulation.

3.2.4 Molecular phenotype of animals expressing dominant-negative TRα1 in the hypothalamus

Subsequent qPCR analysis was performed to detect molecular changes in the expression level of TH target genes upon expression of mutant TRα1 in the hypothalamus. In contrast to the higher relative BAT temperature of dominant-negative TRα1 expressing animals, gene expression analysis of thermogenically active iBAT did not reveal any changes in thermogenic marker expression of *Ucp1*, *Dio2*, *Adrb3*, *Prdm16* (PR domain containing 16), and *Ppargc1a* (Figure 19A). Additionally, thermogenic marker expression in eWAT and iWAT was also unaltered (Figure 19B+C). Gene expression analysis in the liver did also not reveal any major changes in fat metabolism upon the expression of mutant TRα1 in the hypothalamus. Only the expression of *Pck1* encoding the phosphoenolpyruvate carboxykinase

was increased in the liver of dominant-negative TRα1 expressing animals, whereas the expression of *Fasn* (fatty acid synthase) was decreased (Figure 19D).

Interestingly, gene expression analysis of the skeletal soleus lower limb muscle (more slow-twitch fibers) revealed significant upregulation of *Gpd2* (glycerol-3-phosphate dehydrogenase 2), *Atp2a1* (ATPase sarcoplasmic/endoplasmic reticulum Ca^{2+} transporting 1), *Atp2a2* (ATPase sarcoplasmic/endoplasmic reticulum Ca^{2+} transporting 2), and *Mstn* encoding Myostatin, a protein that slows muscle growth in skeletal muscle, upon expression of dominant-negative TRα1 (Figure 19E). However, gene expression of the same set of genes in the skeletal gastrocnemius limb muscle (more fast-twitch fibers) remained unaffected (Figure 19E).

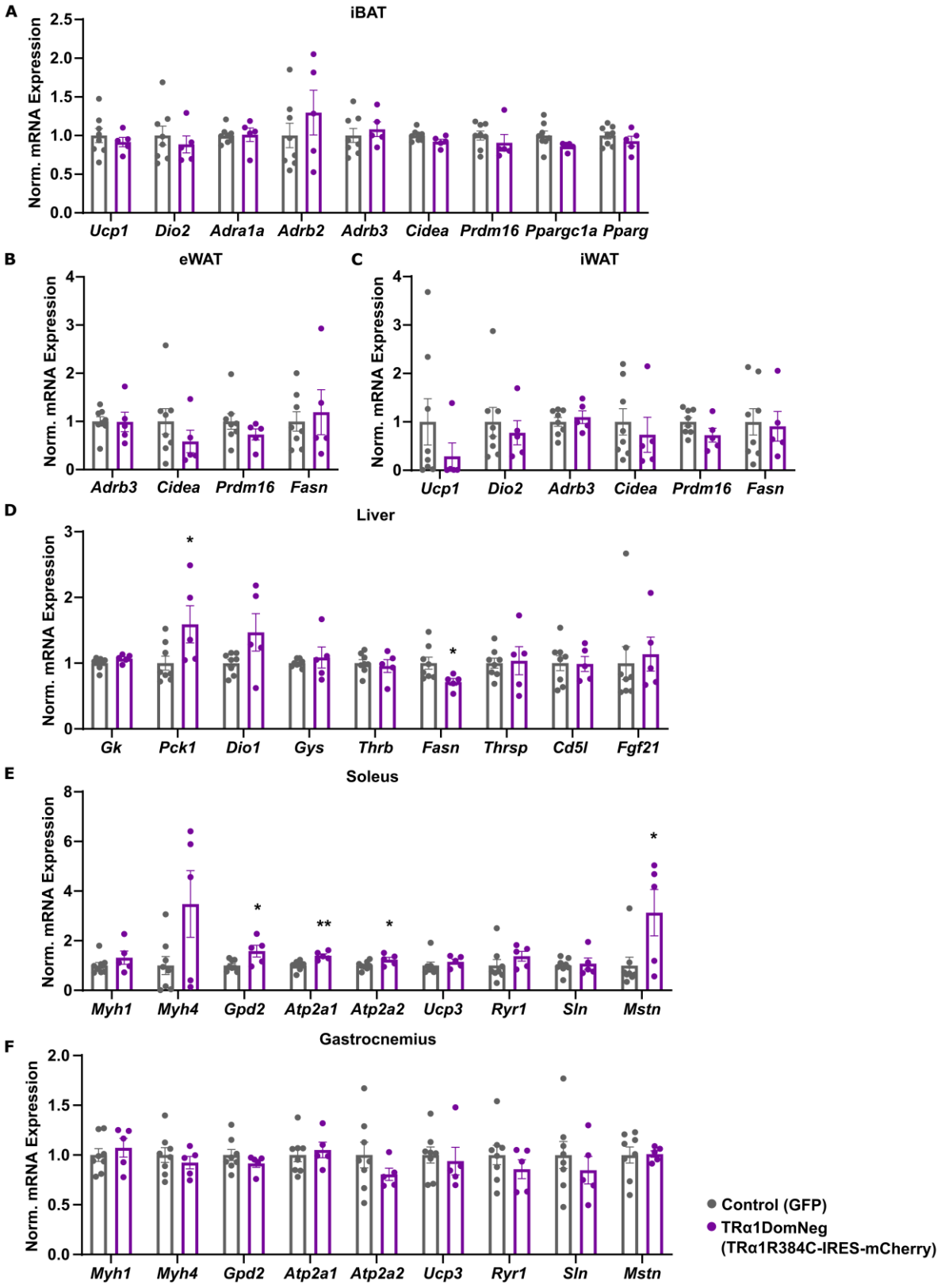

*Figure 19: Molecular phenotyping of dominant-negative TRα1 expressing mice (n=5) and control animals (n=8). A) Normalized mRNA expression in iBAT. B) Normalized mRNA expression in eWAT. C) Normalized mRNA expression in iWAT. D) Normalized mRNA expression in the liver. E) Normalized mRNA expression in gastrocnemius muscle. F) Normalized mRNA expression in soleus muscle. Data are reported as ±SEM. Unpaired Student's t-test. *p<0.05, **p<0.01. Information on statistical tests and post hoc tests can be found in Supplementary Table 1. Parts of the data have been submitted to a peer-reviewed journal due to priority reasons (Sentis et al., 2023 in press).*

In addition to the molecular data, the expression of dominant-negative TRα1 in the hypothalamus did not lead to any changes in FFA content or cAMP content in iBAT (Figure 20A+B), which is in line with no changes in thermogenic marker expression in fat tissue (Figure 19A-C). To gain further insight into glucose metabolism in dominant-negative TRα1 expressing animals, glycogen content in the liver, soleus muscle, and gastrocnemius muscle was determined, as glycogen is mostly stored in the liver and skeletal muscle (Jensen et al., 2011; Nicolaisen et al., 2020; Soon and Torbenson, 2023). Despite higher glycogen content in the liver in mutant TRα1 expressing animals (Figure 20C), values did not reach significance (p=0.06). Glycogen content in the soleus and gastrocnemius muscle was unchanged (Figure 20D+E), which is in line with no changes in gene expression upon expression of mutant TRα1 in the gastrocnemius muscle (Figure 19E).

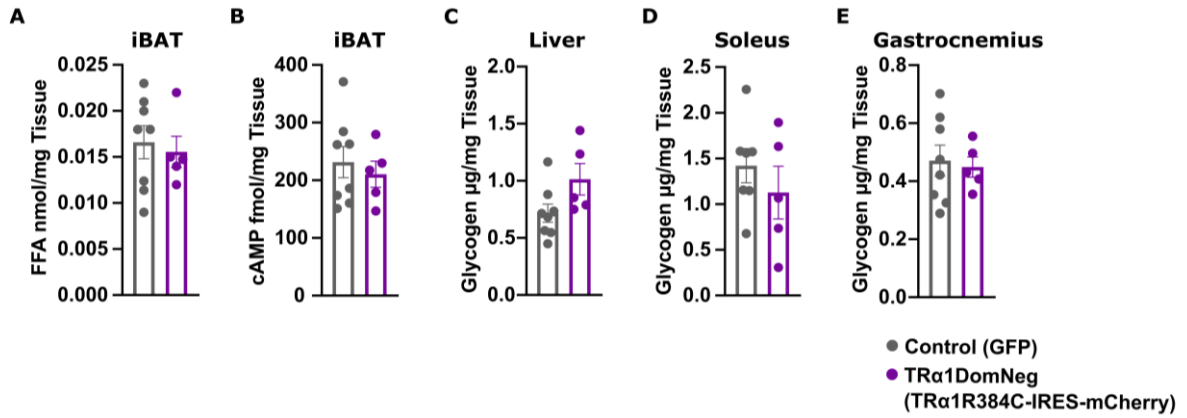

Figure 20: Free fatty acid (FFA), cyclic adenosine monophosphate (cAMP), and glycogen content in iBAT, liver, soleus muscle, and gastrocnemius muscle of animals expressing dominant-negative TRα1 in the hypothalamus (n=5) and control animals (n=8). A) FFA content in iBAT. B) cAMP content in iBAT. C) Glycogen content in the liver. D) Glycogen content in the soleus muscle. E) Glycogen content in the gastrocnemius muscle. Data are reported as ±SEM. Unpaired Student's t-test. Information on statistical tests and post hoc tests can be found in Supplementary Table 1. Parts of the data have been submitted to a peer-reviewed journal due to priority reasons (Sentis et al., 2023 in press).

Subsequently, Western Blot analysis in the soleus muscle of SERCA2 and the OXPHOS complexes were performed (Figure 21A). However, both SERCA2 and OXPHOS protein content were unaltered in comparison to control animals (Figure 21B+C).

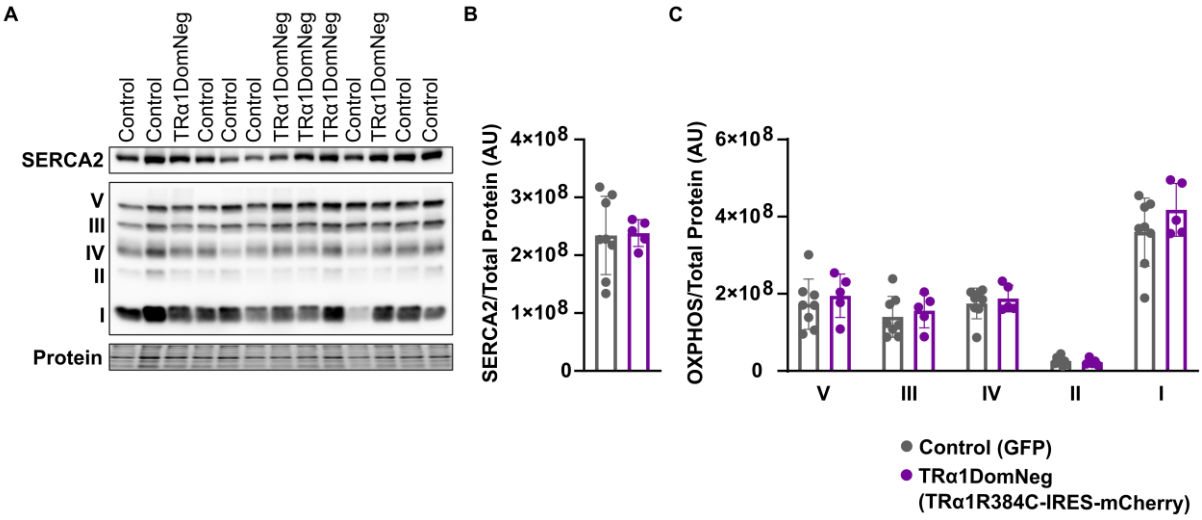

Figure 21: Western Blot analysis of soleus muscle of animals expressing dominant-negative TRα1 in the hypothalamus (n=5) and control animals (n=8). A) Western Blot stained for SERCA2 and OXPHOS. B) Protein quantification of SERCA2. C) Protein quantification of the five OXPHOS complexes. Data are reported as ±SEM. Unpaired Student's t-test. Information on statistical tests and post hoc tests can be found in Supplementary Table 1. Parts of the data have been submitted to a peer-reviewed journal due to priority reasons (Sentis et al., 2023 in press).

Due to the involvement of TRα1 in heart rate regulation via the hypothalamus (Dore et al., 2023b; Mittag, 2010; Mittag et al., 2013), cardiac parameters such as heart rate, heart rate variability, heart weight, and ECG complexes were measured by non-invasive ECG. However, all cardiac parameters were unaltered in animals expressing dominant-negative TRα1 in the hypothalamus in comparison to control animals (Figure 22A-E).

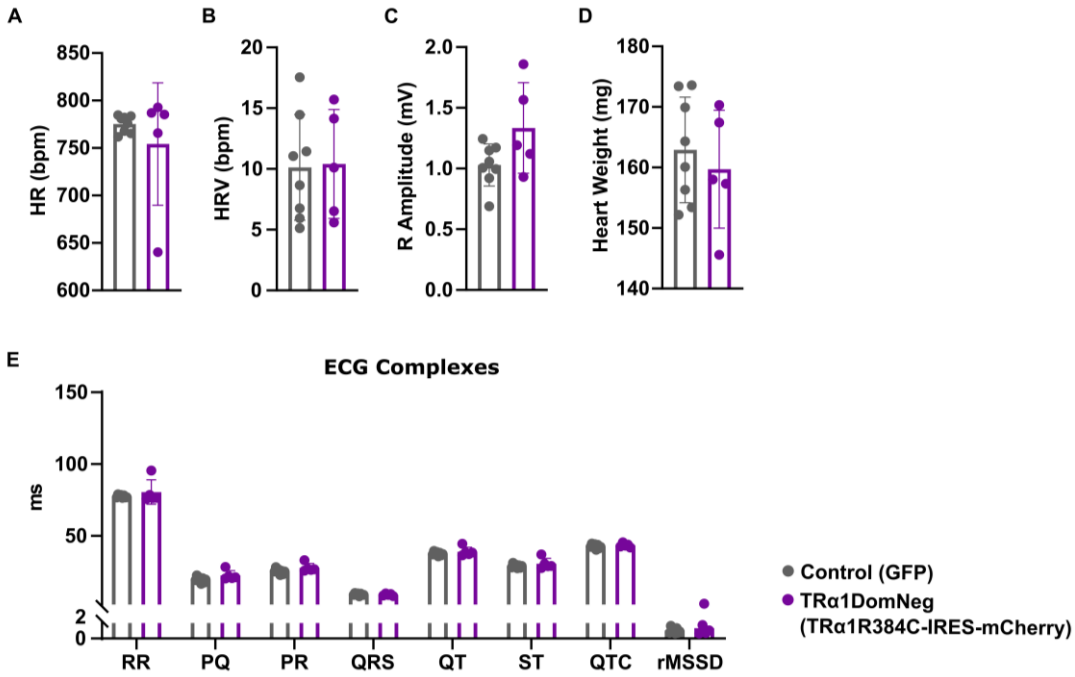

Figure 22: ECG parameters recorded from freely-moving mice and heart weight of animals expressing dominant-negative TRα1 in the hypothalamus (n=5) and control animals (n=8). A) Heart rate. B) Heart rate variability (HRV). C) R amplitude. D) Heart weight (mg). E) ECG complexes (RR, PQ, PR, QRS, QT, ST, QTC) and root mean square of successive differences between normal heartbeats (rMSSD). Data are reported as ±SEM. Unpaired Student's t-test. Information on statistical tests and post hoc tests can be found in Supplementary Table 1. Parts of the data have been submitted to a peer-reviewed journal due to priority reasons (Sentis et al., 2023 in press).

In summary, the expression of hypothalamic dominant-negative TRα1 promoted slower body weight gain and lowered body temperature of these animals at 22°C and 30°C ambient temperature, despite unchanged EE and oxygen consumption. On the molecular level, the expression of dominant-negative TRα1 in the hypothalamus did not lead to changes in thermogenic marker expression in fat tissue but influenced the expression of metabolic genes in the skeletal soleus muscle. Interestingly, these findings could not be confirmed on the protein level.

3.3 Rats vs. mice – Differences in β3-adrenergic receptor expression in adipose tissue

Systemic hyperthyroidism in mice leads to gradual weight gain accompanied by a shutdown of BAT and a downregulation of β3-adrenergic receptor expression (Johann et al., 2019). On the contrary, systemic hyperthyroidism in rats activates BAT and triggers thermogenesis (Abelenda and Puerta, 1992; Rial-Pensado et al., 2022). On the molecular level, it remains unclear whether β3-adrenergic receptor expression in rats and mice in response to TH is differentially regulated.

3.3.1 *In vivo*: *Adrb3* expression is increased upon T4 treatment in rats

To investigate the underlying mechanism at which β3-adrenergic receptor expression in iBAT of rats and mice is regulated, iBAT samples from rats (received from Prof. Miguel Lopez, University of Santiago de Compostela, Spain) that were orally treated with T4 for 14 days at room temperature were used for Western Blot analysis. Subsequent gene expression analysis was performed and compared to published mouse data (Capelli et al., 2021; Johann et al., 2019).

However, UCP1 protein content did not increase upon T4 treatment in rats, which is in line with data from T4-treated mice (Johann et al., 2019; Figure 23A+B). T4 treatment in rats led to a significant increase in complex V (ATP synthase) protein content of the oxidative phosphorylation complexes (Figure 23C). Interestingly and in contrast to mice treated with T4 (Johann et al., 2019), qPCR analysis of iBAT of the T4-treated rats revealed a significant upregulation of *Adrb3*, with no changes in *Ucp1* and *Dio2* expression (Figure 23D). Additionally, infrared thermography detected that iBAT of T4-treated rats was highly activated in response to T4 treatment (Rial-Pensado et al., 2022), whereas iBAT temperature of T4-treated mice was reduced compared to controls (Johann et al., 2019).

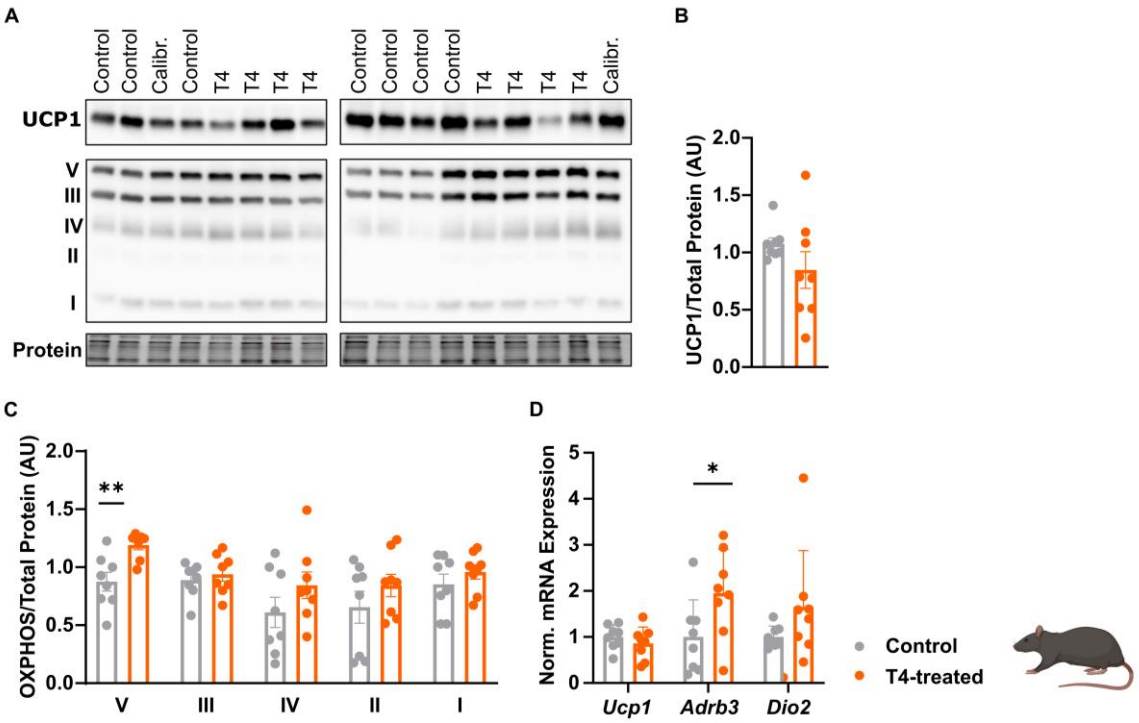

*Figure 23: Western Blot analysis and gene expression analysis of iBAT of T4-treated rats (n=8) vs. control animals (n=8). A) Western Blot stained for UCP1 and OXPHOS. B) Protein quantification of UCP1. C) Protein quantification of the five OXPHOS complexes. D) Normalized mRNA expression in iBAT. Data are reported as ±SEM. Unpaired Student's t-test. *p<0.05, **p<0.01. Information on statistical tests and post hoc tests can be found in Supplementary Table 1.*

Taken together, *in vivo* β3-adrenergic receptor expression in iBAT seems so be differentially regulated in mice and rats in response to T4 treatment, which may contribute to the activation of iBAT in rats in response to TH treatment and a shutdown of iBAT in mice.

3.3.2 Experimental design: Is *Adrb3* expression in brown and white adipocytes dependent on thyroid hormone concentration?

To further investigate the TH dependent expression of TH target genes and particularly the regulation of β3-adrenergic receptor expression in iBAT and iWAT of rats and mice, preadipocytes from rats and mice were isolated and cultured (Figure 24).

After reaching confluency, the differentiation of preadipocytes to mature brown or white adipocytes was initiated (Figure 24). As TH is a crucial driver of differentiation of brown adipocytes (Obregon, 2008), primary iBAT cells were T3-starved for two days starting on day four after the induction of differentiation until the beginning of the experiment to exclude confounding effects of T3 media supplementation. Cells were treated for 24 h with different concentrations of T3 (1 nM, 10 nM, 50 nM) in the presence of 100 µM CL 316243 (b-Cl), a β3-adrenergic receptor agonist. Subsequently,

cells were harvested and the supernatant and cells for RNA isolation were stored at -80°C until further analysis.

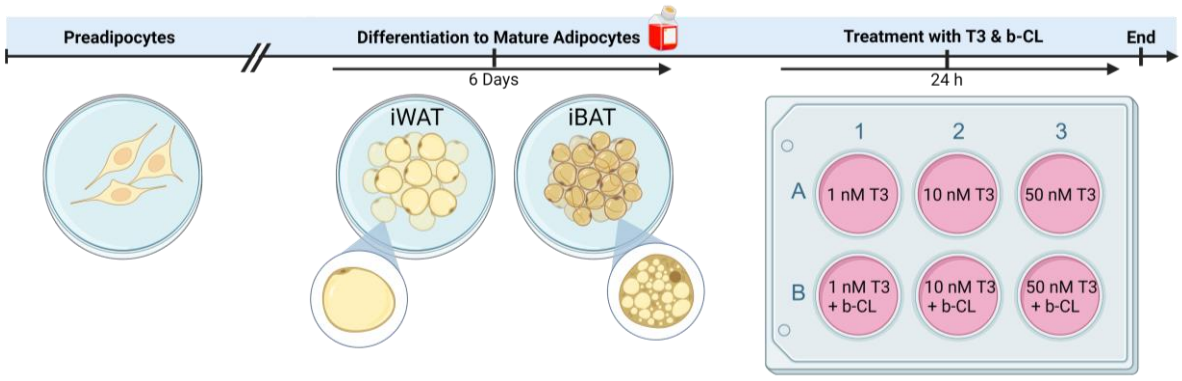

Figure 24: Experimental in vitro study design to investigate thermogenic marker expression changes in differentiated mature brown and white adipocytes isolated from either rats or mice upon CL 316243 (b-CL) treatment (100 µM) in the presence of high and low concentrations (1 nM, 10 nM, 50 nM) of T3.

3.3.3 *In vitro*: Thyroid hormone treatment of primary rat and mouse adipocytes does not lead to changes in *Adrb3* expression

Based on the *in vivo* findings, primary cell culture experiments were conducted to investigate the differences of *Adrb3* expression in rats and mice upon TH treatment *in vitro*. First, primary preadipocytes isolated from mice and rats were differentiated according to existing differentiation protocols (Engelhard et al., 2022; Galmozzi et al., 2021) for preadipocytes (Figure 25).

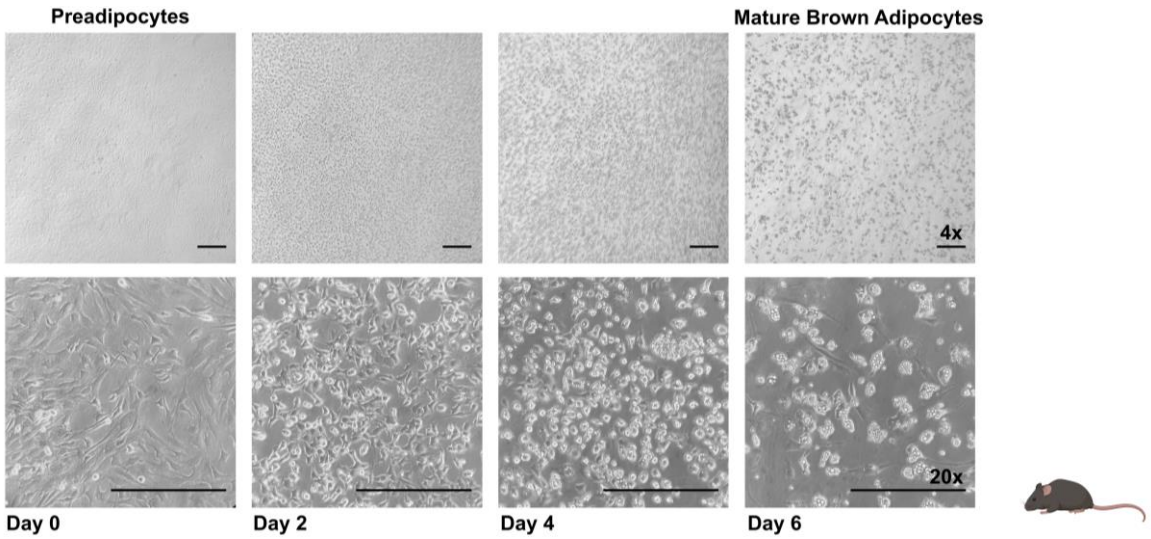

Figure 25: Exemplarily: Differentiation of isolated mouse preadipocytes to mature brown adipocytes. Differentiation took place over six days in the presence of differentiation media. Information on the differentiation protocol can be found in section 2.2.2.2. Microscope pictures were taken by Berenike Soehl, M.Sc.

Due to the adaption of the differentiation protocol of mouse preadipocytes for rat preadipocytes, the differentiation process was documented and verified via light microscopy (Figure 26). Mature mouse adipocytes, as well as mature adipocytes isolated from rats accumulated lipid droplets (Himms-Hagen et al., 2000; Shinde et al., 2021) upon induction of differentiation. Once the differentiation process was concluded and the accumulation of lipid droplets was confirmed, experimental interventions were performed.

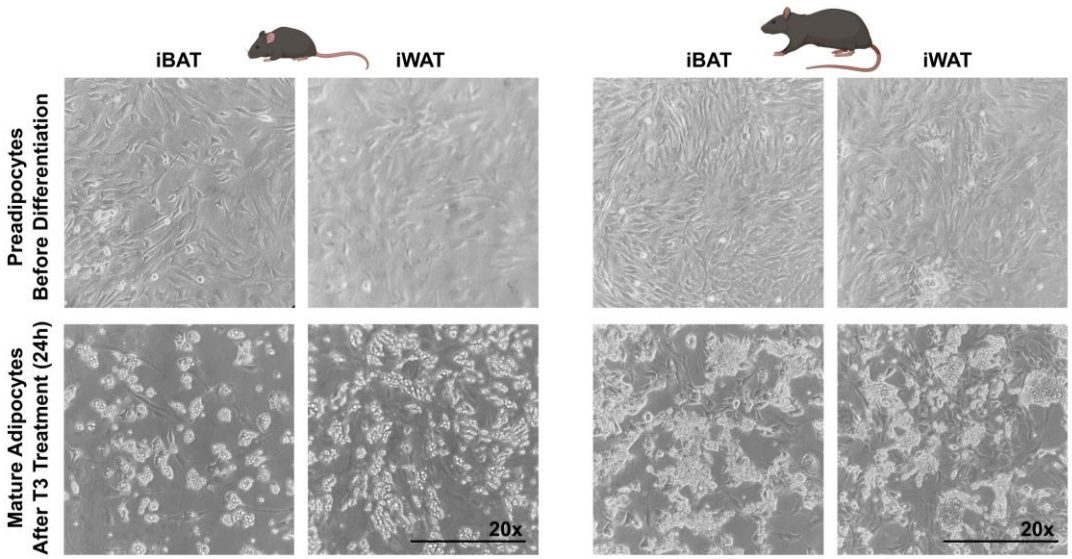

Figure 26: Differentiation of mouse and rat preadipocytes to mature adipocytes isolated from iBAT and iWAT depots. Differentiation took place over six days in the presence of differentiation media. Information on the differentiation protocol can be found in section 2.2.2.2. Microscope pictures were taken by Berenike Soehl, M.Sc.

Following differentiation, matured primary brown and white adipocytes were treated with different doses of T3 (1 nM, 10 nM, 50 nM) in the presence and absence of b-CL (100 µM). Subsequent gene expression analysis was performed to detect differences in *Adrb3* expression and in other thermogenic markers. In contrast to the *in vivo* data, the expression of *Adrb3* did not respond to increasing T3 treatment concentrations in matured primary brown rat adipocytes (Figure 27A). However, the additional presence of b-CL led to an overall significant effect when comparing no b-CL treatment to b-CL treatment ($p=0.0036$). Gene expression of *Adra1a* was non-responsive to T3 treatment and b-CL treatment (Figure 27B). Other thermogenic markers, such as *Dio2*, responded to increasing T3 treatment concentrations as a dose-effect ($p=0.03$) could be observed (Figure 27C). However, *Ucp1* expression, a classical thermogenic marker, did not respond to increasing T3 treatment concentrations (Figure 27D); only additional b-CL treatment led to an overall significant effect when comparing no b-CL treatment to b-CL treatment ($p=0.0019$).

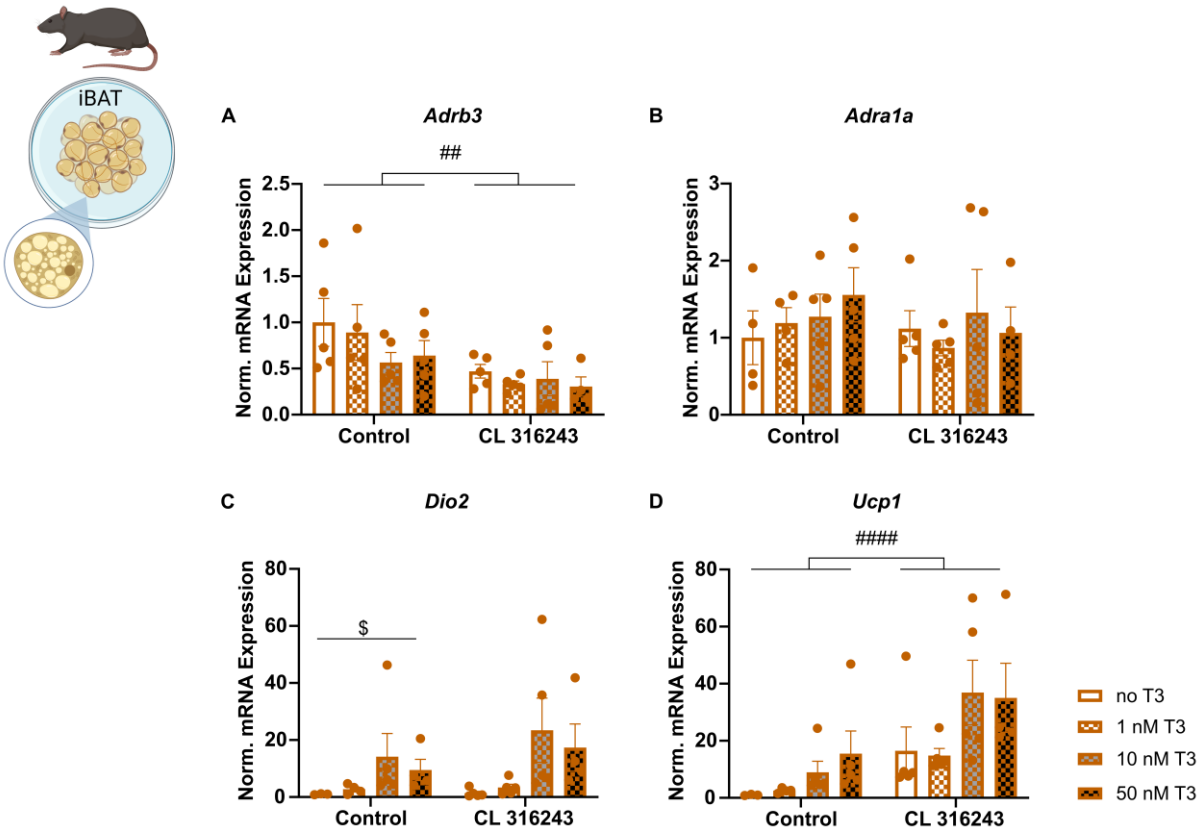

Figure 27: Matured primary rat brown adipocytes treated with increasing concentrations of T3 (1 nM, 10 nM, 50 nM) in the presence or absence of b-CL (100 µM) A) Normalized mRNA expression of Adrb3. B) Normalized mRNA expression of Adra1a. C) Normalized mRNA expression of Dio2. D) Normalized mRNA expression of Ucp1. Data are reported as ±SEM. 2-way ANOVA, post hoc: Tukey's multiple comparison. ##p<0.01, $p<0.05. Information on statistical tests and post hoc tests can be found in Supplementary Table 1. Parts of the experiments were performed by Berenike Soehl, M.Sc.

As TH is also a crucial driver of browning of white adipocytes (Johann et al., 2019; Petrovic et al., 2010; Weiner et al., 2016), gene expression analysis in matured primary rat white adipocytes was performed for the same set of genes as in brown adipocytes. Similar to brown adipocytes, *Adrb3* expression in differentiated white adipocytes from rats did not respond to increasing T3 treatment concentrations (Figure 28A). However, *Adrb3* expression was significantly reduced in the presence of b-CL for all doses, accompanied by an additional dose effect ($p<0.0001$). In line with data from brown adipocytes, *Adra1a* expression did not respond to T3 treatment or additional b-CL treatment (Figure 28B). Thermogenic marker expression of *Dio2* and *Ucp1* did not respond to T3 treatment, but additional b-CL treatment led to an overall effect when comparing no b-CL treatment vs. b-CL treatment (*Dio2*: $p=0.16$; *Ucp1*: $p=0.12$) in these genes (Figure 28C+D).

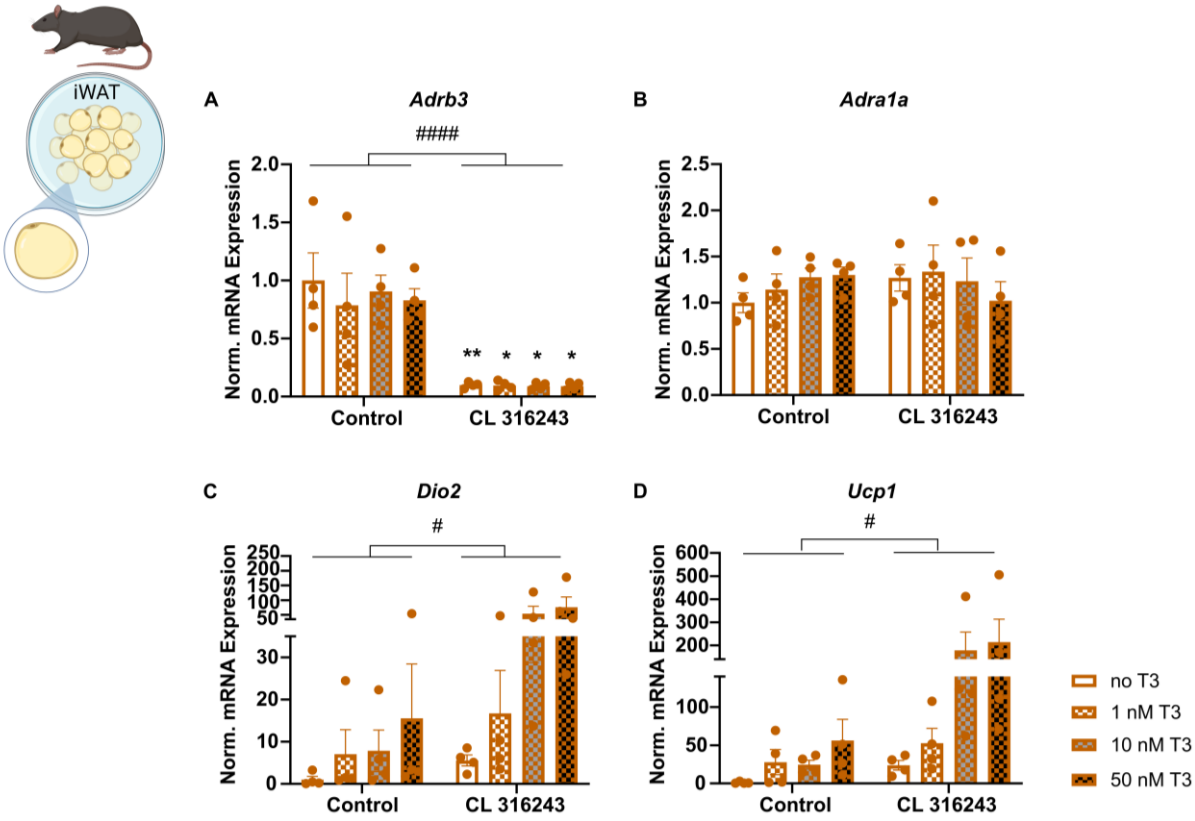

*Figure 28: Matured primary rat white adipocytes treated with increasing concentrations of T3 (1 nM, 10 nM, 50 nM) in the presence or absence of b-CL (100 µM) A) Normalized mRNA expression of Adrb3. B) Normalized mRNA expression of Adra1a. C) Normalized mRNA expression of Dio2. D) Normalized mRNA expression of Ucp1. Data are reported as ±SEM. 2-way ANOVA, post hoc: Tukey's multiple comparison. *p<0.05, **p<0.01, #p<0.05, #p<0.0001. Information on statistical tests and post hoc tests can be found in Supplementary Table 1. Parts of the experiments were performed by Berenike Soehl, M.Sc.*

To be able to compare the expression data from adipocytes isolated from rats with primary fat cells isolated from mice, expression analysis in matured mouse adipocytes after T3 and b-CL treatment was performed. Therefore, the same set of genes as in rat adipocytes was analyzed. Despite a reduction of *Adrb3* expression with increasing T3 treatment concentrations (Figure 29A), values did not reach significance (control vs. 50 nM T3: p=0.08). However, the presence of b-CL significantly reduced the expression of *Adrb3* which was accompanied by an overall effect when comparing no b-CL treatment vs. b-CL treatment (p<0.0001). In contrast to gene expression data from rat adipocytes, overall *Adra1a* expression was altered in response to b-CL treatment (p=0.03; Figure 29B). Thermogenic marker expression of *Dio2* and *Ucp1* was overall increased in response to b-CL (*Dio2*: p=0.0003; *Ucp1*: p<0.0001), but T3 treatment alone did not induce *Dio2* and *Ucp1* gene expression (Figure 29C+D).

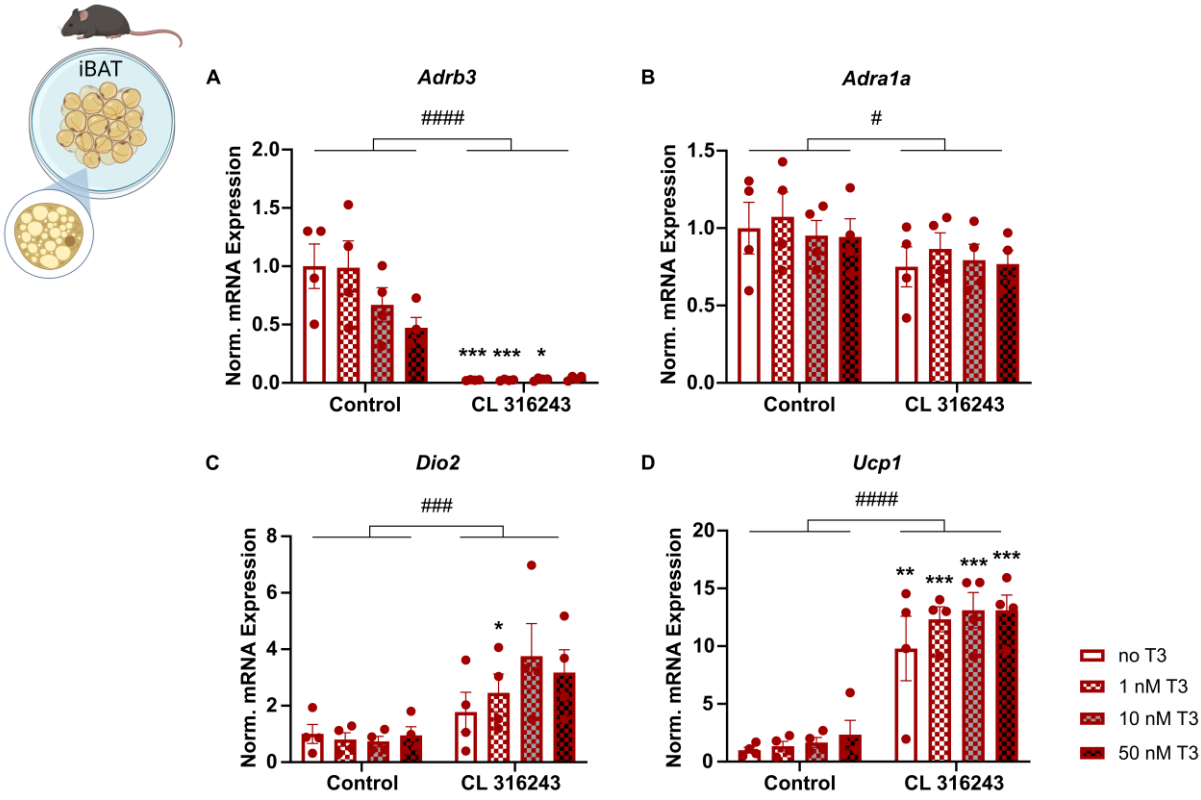

*Figure 29: Matured primary mouse brown adipocytes treated with increasing concentrations of T3 (1 nM, 10 nM, 50 nM) in the presence or absence of b-CL (100 µM) A) Normalized mRNA expression of Adrb3. B) Normalized mRNA expression of Adra1a. C) Normalized mRNA expression of Dio2. D) Normalized mRNA expression of Ucp1. Data are reported as ±SEM. 2-way ANOVA, post hoc: Tukey's multiple comparison. *p<0.05, ***p<0.001, #p<0.05, ###p<0.001, ####p<0.0001. Information on statistical tests and post hoc tests can be found in Supplementary Table 1. Parts of the experiments were performed by Berenike Soehl, M.Sc.*

To conclude the primary cell culture experiments, gene expression analysis was also performed in matured white adipocytes isolated from mice. In line with data from rat white adipocytes, *Adrb3* expression did not respond to T3 treatment (Figure 30A), but the expression was significantly reduced after b-CL treatment accompanied by an overall effect when comparing no b-CL treatment vs. b-CL treatment ($p<0.0001$). Similar to *Adra1a* expression in rat white adipocytes, *Adra1a* did not respond to T3 or b-CL treatment in white mouse adipocytes (Figure 30B). The thermogenic marker *Dio2* responded to increasing T3 treatment concentrations ($p=0.28$), but no effect on *Dio2* expression upon b-CL treatment could be observed (Figure 30C). However, *Ucp1* expression, as a classical thermogenic marker, did not respond to increasing T3 treatment concentrations (Figure 30D) and additional b-CL treatment led to an overall significant effect when comparing no b-CL treatment to b-CL treatment ($p=0.003$).

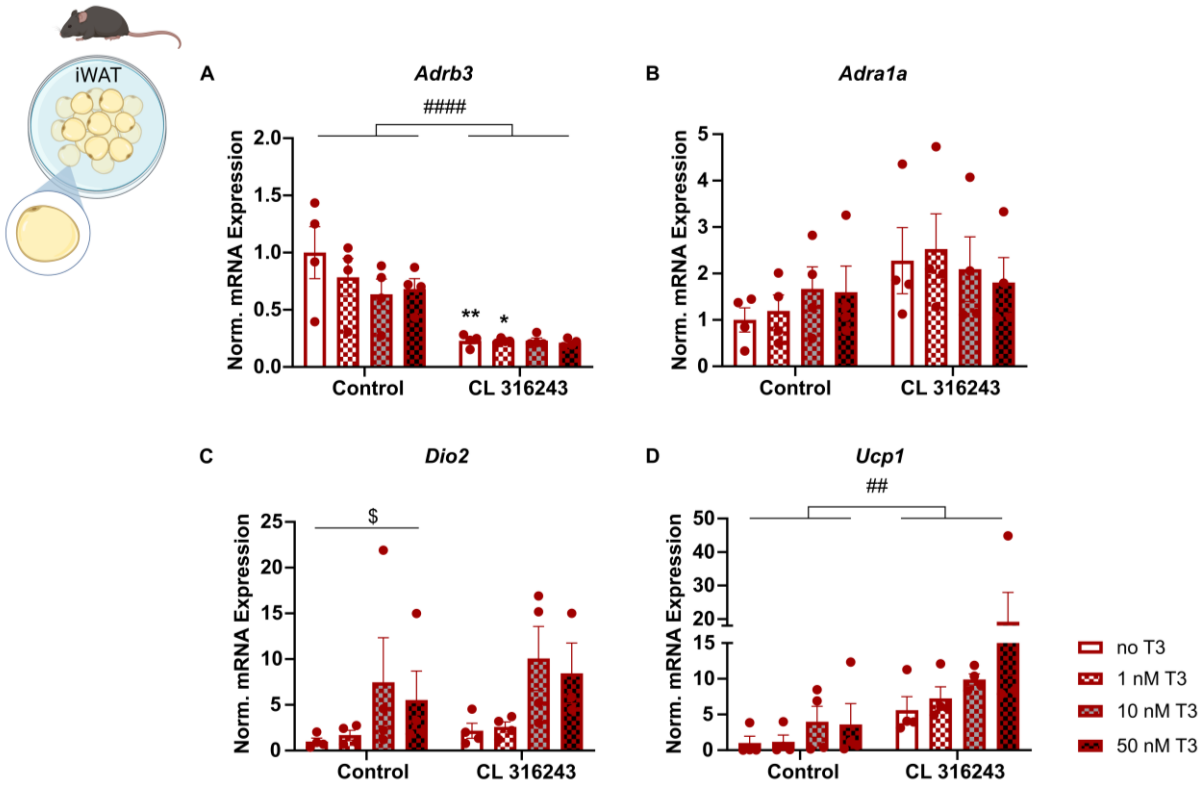

*Figure 30: Matured primary mouse white adipocytes treated with increasing concentrations of T3 (1 nM, 10 nM, 50 nM) in the presence or absence of b-CL (100 µM) A) Normalized mRNA expression of Adrb3. B) Normalized mRNA expression of Adra1a. C) Normalized mRNA expression of Dio2. D) Normalized mRNA expression of Ucp1. Data are reported as ±SEM. 2-way ANOVA, post hoc: Tukey's multiple comparison. *p<0.05, **p<0.01, ##p<0.01, ###p<0.001, $p<0.05. Information on statistical tests and post hoc tests can be found in Supplementary Table 1. Parts of the experiments were performed by Berenike Soehl, M.Sc.*

Taken together, despite a significantly increased expression of *Adrb3* in rats treated with T4, *Adrb3* gene expression in matured brown adipocytes isolated from rats did not respond to T3 treatment *in vitro*. Interestingly, *Adrb3* gene expression of matured brown adipocytes isolated from mice did also not respond to increasing T3 treatment concentrations. *Adrb3* expression in white mouse and rat adipocytes did also not respond to T3 treatment.

In conclusion, the direct effects of TH on *Adrb3* expression are negligible and only the simultaneous treatment of TH and b-CL mimicking SNS signaling provokes changes in *Adrb3* expression *in vitro*.

4 Discussion

Despite extensive research on TH and TR action in the brain and peripheral target organs and tissues, the individual contributions of TRα1 and TRβ signaling to body temperature homeostasis and regulation are not entirely understood (Sentis et al., 2021). This thesis aimed at investigating and understanding the role of peripheral TRα1 and TRβ and hypothalamic TRα1 in body temperature regulation, with special interest in brown fat thermogenesis.

For this, TRα1+m mutants and TRβ KO mice were housed at room temperature, as well as thermoneutrality where BAT innervation is minimized (Cui et al., 2016). Numerous studies that employ rodent models to investigate the fundamental mechanisms of body temperature control typically use room temperature as an experimental housing condition (Fischer et al., 2019; Škop et al., 2020a). Unlike humans, mice constantly face a mild cold challenge at room temperature, which leads to permanent SNS signaling and BAT activation (Škop et al., 2020a). Consequently, recent research suggests that employing thermoneutral housing conditions (30°C) during experiments may have greater translational relevance (Fischer et al., 2019; Ganeshan and Chawla, 2017). Subsequently, all animals were treated with T3 via the drinking water at 30°C to study the effects and consequences of systemic hyperthyroidism at thermoneutrality in mouse models with either a mutant TRα1 or TRβ KO (Dore et al., 2023b, 2023a). Touch-free body temperature profiles were acquired with the help of implanted radiotelemetry transmitters to reduce anxiety-induced hyperthermia in TRα1+m mice (Venero et al., 2005). Finally, to investigate the contributions of hypothalamic TRα1 in the control of the central body temperature set-point, AAVs carrying dominant-negative TRα1 were delivered into the hypothalamus. Especially, the preoptic area (POA) of the hypothalamus is known to be greatly involved in whole-body temperature regulation (Contreras et al., 2017, 2016), rendering the hypothalamus an interesting target to test the thermoregulatory consequences of defective TRα1 action in the brain.

Furthermore, previous *in vivo* studies could show that systemic hyperthyroidism in rats leads to BAT activation (Abelenda and Puerta, 1992; Rial-Pensado et al., 2022), whereas TH treatment in mice leads to reduced BAT activity and a downregulation of β3-adrenergic receptor expression (Johann et al., 2019). Thus, this work also aimed at dissecting the underlying TH-dependent *in vitro* mechanisms at which *Adrb3* expression is regulated in mice compared to rats. For that, primary matured brown and white adipocytes isolated from rats and mice, were treated with T3 and the β3-agonist, b-CL, to dissect the differences in TH-induced thermogenic marker expression in rats and mice.

4.1 The role of TRβ in body temperature regulation

Previous studies on TR action in peripheral organs suggest that TRβ mediates the direct action of THs in brown fat leading to an increased thermogenic potential of BAT by inducing thermogenesis-relevant target gene expression (Ribeiro et al., 2010, 2001; Villicev et al., 2007). Although the TRβ KO mice used in this study have significantly increased T3 and T4 serum levels at 22°C (Dore et al., 2023a; Forrest et al., 1996; Table 13), the endogenous hyperthyroidism of these animals did not elevate body temperature at 22°C (Forrest et al., 1996; Forrest and Vennström, 2000). This could be attributed to either the comparatively mild hyperthyroidism with a 1.6-fold increase of circulating TH levels in this TRβ KO strain (Dore et al., 2023a; Johann et al., 2019), or due to a compensatory adaptation considering that the TRβ KO is already established during embryonal development (Forrest et al., 1996). In comparison, a 2-fold increase in circulating T3 levels only results in a minor elevation of body temperature in wildtype animals (Herrmann et al., 2020). Due to the findings on body temperature during hyperthyroidism in wildtype mice, the endogenous mild hyperthyroidism of TRβ KO mice (Table 13) might not be sufficient to elevate their body temperature at 22°C in comparison to control animals.

Table 13: Total T3 (tT3) and T4 (tT4) serum levels of TRß KO and TRα1+m animals at different ambient temperatures (22°C or 30°C) and treated with T3 (0.5 mg/L) for 12 days at 30°C. The table was adapted from Sentis et al., 2023 in press.

Temperature	**22°C**		**30°C**		**30°C + T3-Treatment (0.5 mg/L)**	
Serum T4/T3	tT4	tT3	tT4	tT3	tT4	tT3
TRβ KO	~1.7-fold[1] ⬆ (Dore et al., 2023a; Johann et al. 2019)	~1.6-fold[1] ⬆ (Dore et al., 2023a; Johann et al. 2019)	= [2] Dore et al., 2023a	= [2] Dore et al., 2023a	~6-fold[3] ⬇ Dore et al., 2023a	~7.8-fold[3] ⬆ Dore et al., 2023a
TRα1+m	= [1] Tinnikov et al., 2002; Sjögren et al., 2007	= [1] Sjögren et al., 2007	= [2] Sjögren et al., 2007	= [2] Sjögren et al., 2007	~3.6-fold[3] ⬇ Dore et al., 2023b	~5.6-fold[3] ⬆ Dore et al., 2023b
	[1]Serum T3/T4 level were compared to wildtype controls housed at 22°C		[2]Serum T3/T4 level were compared to wildtype controls housed at 30°C		[3]Serum T3/T4 level were compared to untreated wildtype controls housed at 30°C	

The tissue-specific TRβ actions in BAT to induce thermogenesis are interestingly independent of whole-body temperature homeostasis, as a global TRβ KO did not lead to an altered body temperature phenotype at 22°C or 30°C (Dore et al., 2023a; Forrest and Vennström, 2000; Johann et al., 2019). Furthermore, it was recently shown that serum T3 and T4 levels of TRβ KO animals at thermoneutral housing conditions are in a normal range and thus significantly lower in comparison to serum TH levels of TRβ KO mice housed at 22°C (Dore et al., 2023a; Lopez-Alcantara et al., 2023; Table 13). Most importantly, the normalized TH serum levels in TRβ KO mice at 30°C allow to study the consequences of defective TRβ signaling in absence of the confounding endogenous hyperthyroidism that occurs in TRβ KO animals housed at room temperature. Therefore, it is no surprise that body

temperature of TRβ KO animals was not higher in comparison to wildtype animals at 30°C.

In response to oral T3 treatment at 30°C, the body temperature phenotype of TRβ KO mice was comparable to the body temperature phenotype of T3-treated wildtype animals. Interestingly, after oral T3 treatment, TRβ KO animals had significantly higher T3 and T4 serum levels in comparison to controls (Dore et al., 2023a), despite no differences in daily T3 solution intake. This difference might be due to a defective suppression of the HPT-axis in TRβ KO animals. The used T3 treatment dosage to induce systemic hyperthyroidism led to an overall 6-8-fold increase of T3 serum levels (Dore et al., 2023a) and very little circulating T4 levels in TRβ KO animals (Table 13). Due to the involvement of TRβ signaling in the regulation of the HPT-axis (Costa-e-Sousa and Hollenberg, 2012; Ortiga-Carvalho et al., 2014, 2005), the negative feedback mechanism is impaired in TRβ KO mice, likely leading to a continuous release of T4 and T3 by the thyroid gland which further elevates T3 and T4 serum levels during TH treatment. In comparison, the endogenous production of TH in wildtypes is entirely abolished by the oral T3 treatment (Dore et al., 2023a; Johann et al., 2019).

Although impaired TRβ signaling did not lead to body temperature phenotype alterations, tail temperature of TRβ KO mice did not increase in response to oral T3 treatment in comparison to wildtype controls. Therefore, heat stress triggered by T3 treatment induced heat dissipation mechanisms in wildtype mice but not in TRβ KO animals, implying a partial resistance to TH in the context of heat dissipation mechanisms. A previous study postulated that the direct actions of T3 in BAT are predominantly mediated by TRβ signaling (Ribeiro et al., 2010, 2001). However, T3 treatment induced thermogenic marker expression in BAT at 30°C in TRβ KO mice despite the absence of TRβ signaling, proposing a compensatory role for TRα1 signaling in BAT by inducing the expression of TH target genes. Although *Ucp1* expression was induced by T3 treatment in TRβ KO mice, UCP1 protein content was not elevated in BAT. This can partially be explained by the thermoneutral housing conditions as BAT is naturally denervated and inactivated at 30°C (Cui et al., 2016). Only the synergistic interplay of SNS signaling, T3 signaling, and *Ucp1* expression can activate BAT thermogenesis in response to cold (Abelenda and Puerta, 1992; Nedergaard et al., 1997; Yau and Yen, 2020). Furthermore, previous studies showed that cold exposure rapidly increases *Ucp1* mRNA, but only prolonged cold exposure leads to an increase of UCP1 protein content (Nedergaard and Cannon, 2013). Therefore, the sole increase of *Ucp1* mRNA does not automatically translate to UCP1 activity and thus the thermogenic capacity of brown fat (Li and Fromme, 2022; Nedergaard and Cannon, 2013).

In summary, this current study implies that the impact of TRβ signaling on whole-body temperature homeostasis appears to be restricted to minor defects in heat dissipation. Furthermore, the thermoregulatory phenotype of TRβ KO mice is primarily influenced by the degree of their endogenous hyperthyroidism. Lastly, the induction of thermogenesis related TH target genes in BAT of TRβ KO animals upon T3 treatment demonstrates a role for TRα1 signaling in body temperature control.

4.2 The role of TRβ in energy homeostasis

Studies utilizing the TRβ-specific agonist GC-1 propose a pivotal role for TRβ signaling in energy expenditure and the regulation of energy homeostasis (Chiellini et al., 1998; Saponaro et al., 2020; Villicev et al., 2007).

Interestingly, food intake of TRβ KO animals housed at 30°C was significantly increased compared to wildtype controls but T3 treatment did not lead to a further increase in food intake. As the whole-body TRβ KO is already present during embryonic development, TRβ KO animals grew up under hyperthyroid conditions that resulted in increased energy expenditure and higher food intake to accommodate the higher energy demands (Forrest et al., 1996; Oppenheimer and Schwartz, 1980). Despite normalized serum T3 and T4 levels in TRβ KO mice at 30°C (Dore et al., 2023a; Lopez-Alcantara et al., 2023; Table 13), food intake remained higher, suggesting that the food intake set-point is not immediately adjusted in response to changes in ambient temperature and resulting changes in TH serum levels. More than 40 years ago, it was already shown that rats treated with T3, immediately increase energy expenditure but not food intake (Mariash et al., 1980; Oppenheimer and Schwartz, 1980), suggesting that the food effect is a secondary adaptation. This is also supported by the slow increase of food intake of wildtype animals in response to T3 treatment in this current study. Furthermore, the involvement of central TRβ signaling in metabolism and energy homeostasis has recently been proposed in a study that selectively knocked-down TRβ in the VMH (Hameed et al., 2017). The VMH is greatly involved in energy homeostasis and satiety and expresses TRβ as the predominant isoform (Cook et al., 1992). Upon knockdown of TRβ signaling in the VMH, mice significantly gain weight and become obese, due to reduced energy expenditure (Hameed et al., 2017).

Additionally, the great involvement of TRβ signaling in metabolism has long been proposed with regard to the actions of TH in the liver (Lopez-Alcantara et al., 2023; Piantanida et al., 2020; Sinha et al., 2018; Weiss et al., 1998). Due to the lack of functioning TRβ signaling in TRβ KO animals, the T3 treatment cannot induce target gene expression in tissues predominantly expressing TRβ, such as the liver. As expected, and in line with previous studies, TH target genes in the liver such as *Dio1* and *Thrsp* are significantly downregulated (Lopez-Alcantara et al., 2023). Additionally, glycogen content in the liver is increased in TRβ KO mice as a result of local hypothyroidism (Lopez-Alcantara et al., 2023; Rehman et al., 2023).

In summary, the endogenous hyperthyroidism of TRβ KO at 22°C led to increased food intake to accommodate the higher energy demands triggered by the higher TH serum levels that even persisted at 30°C despite normalized TH serum levels. These findings underline the important role of TRβ signaling in whole-body energy homeostasis.

4.3 The role of TRα1 in body temperature regulation

TRα1 signaling has long been proposed to promote energy expenditure in skeletal muscle and to regulate heat dissipation in mice via the tail (Mullur et al., 2014; Nicolaisen et al., 2020; Warner et al., 2013). As for the latter, a previous publication showed that mice heterozygous for a R384C mutation in TRα1 (Tinnikov et al., 2002) have significantly lower body temperature at 22°C, accompanied by increased BAT activity (Warner et al., 2013). These TRα1+m mutants suffer from defective vasoconstriction in their tails, while BAT is highly active to compensate for the tail heat loss (Warner et al., 2013). Vascular contractility and thus heat dissipation via the tail in mice is greatly dependent on functioning TRα1, emphasizing the role of TRα1 in whole-body thermoregulation and temperature homeostasis.

However, the excess heat loss via the tail of TRα1+m mice should be reversed at thermoneutral housing conditions, as no heat dissipation or heat conserving mechanisms are needed at 30°C (Fischer et al., 2019). When placing the TRα1+m mice at thermoneutrality, heat loss via the tail was indeed reversed, and the lower core body temperature phenotype could partially be rescued. Surprisingly, during the inactive light phase of mice, TRα1+m mutants still had a significantly lower body temperature phenotype at 30°C compared to wildtype controls, suggesting that also the TRα1-dependent central control of body temperature is relevant for whole-body temperature homeostasis in these animals. During the inactive phase, only little additional heat from locomotor activity contributes to thermogenesis in the resting TRα1+m mutants. This implies a potential metabolic defect in the resting skeletal muscle, a tissue recognized for its elevated expression of TRα1 in mice (Nicolaisen et al., 2020; Yen, 2001).

Interestingly, upon oral T3 treatment that led to 6-fold increase of circulating T3 levels (Dore et al., 2023b; Table 13), body temperature in TRα1+m mutants could be fully rescued due to the reactivation of the mutant TRα1 (Tinnikov et al., 2002). However, T3 treatment surprisingly lowered BAT temperature in TRα1 animals, which was accompanied by decreased protein content of OXPHOS complex III, suggesting that the central response to a lower body temperature was indeed impaired in TRα1 animals. In turn, tail temperature increased upon T3 treatment, which is in line with a tail temperature increase in wildtype controls, indicating that the reactivation of TRα1 signaling stopped uncontrolled tail heat dissipation (Warner et al., 2013).

On the molecular level, T3 treatment in TRα1+m animals led to a decrease in *Ucp1* and *Dio2* expression and an increase in *Adrb3* expression in BAT at 30°C. A decreased expression of thermogenesis-related TH-responsive genes in TRα1+m mice indicates that intact TRβ signaling in BAT may temperature-dependently downregulate target gene expression. The opposite is observable in TRβ KO mice, suggesting that intact TRα1 signaling induces TH target gene expression independent of ambient temperature. Furthermore, thermogenic marker expression in iWAT of TRα1+m animals was

not induced upon T3 treatment, which is in line with a previous study that showed that browning of iWAT is dependent on the TRβ isoform (Johann et al., 2019). In contrast to findings in TRβ KO animals (Feng et al., 2000; Lopez-Alcantara et al., 2023; Piantanida et al., 2020; Sinha et al., 2018), TH target gene expression in the liver of TRα1+m animals did not differ in comparison to wildtype animals upon T3 treatment (Vujovic et al., 2009).

In conclusion, the defective body temperature phenotype of TRα1+m mutants could only partially be restored at 30°C, indicating that the central temperature set-point is shifted as BAT temperature is lowered in TRα1+m mice. Only oral T3 treatment at 30°C and thus the reactivation of mutant TRα1 could fully normalize the defective body temperature phenotype of TRα1+m mice. This demonstrates that intact TRα1 signaling is highly required for body temperature regulation and temperature homeostasis. Although the mutant TRα1 is already present during development in the TRα1+m mice, the acute reactivation of TRα1 and subsequent normalization of body temperature implies that no permanent thermoregulatory developmental defect persists in these animals, which, however, was recently observed for cardiovascular function (Dore et al., 2023b; Nappi et al., 2022).

4.4 The role of hypothalamic TRα1 in body temperature regulation

The hypothalamus is a central key regulator of energy uptake and expenditure, thus whole-body energy homeostasis (Hameed et al., 2017; López et al., 2016). The most important regulator of appetite, food intake, and energy expenditure in the hypothalamus is the arcuate nucleus (ARC) (Timper and Brüning, 2017). However, also other hypothalamic nuclei, like the lateral hypothalamus (LH) or the VMH, have been proven to play a critical role in the central regulation of appetite and satiety (Rossi, 2023; Timper and Brüning, 2017, 2017). Besides that, the hypothalamus also participates in the regulation of body temperature and body temperature homeostasis (Contreras et al., 2017, 2016; Sentis et al., 2021; Warner and Mittag, 2012). Furthermore, studies from López et al. proposed a role for centrally acting TH in the regulation of BAT thermogenesis and energy metabolism (López et al., 2010). However, the exact contributions of the different TR isoforms in the hypothalamus to TH-dependently regulate body temperature homeostasis remain unknown. Due to the observed defective body temperature phenotype of TRα1+m mutants at room temperature (Warner et al., 2013) and 30°C, which can only be rescued upon the reactivation of the mutant TRα1, this study aimed at testing whether central TRα1 signaling mediates fine-tuning of the central body temperature set-point as in anapyrexia (Cannon and Nedergaard, 2010).

To investigate the contributions of hypothalamic TRα1 signaling to the control of whole-body temperature homeostasis, AAVs carrying CMV-driven dominant-negative TRα1 were delivered into the hypothalamus to impair TRα1 signaling. Strong expression of mCherry was confirmed via fluorescence microscopy. A thorough analysis of the injection site revealed that the POA and the anterior hypothalamic area (AHA) of the hypothalamus were the main area of dominant-negative TRα1 expression (Table 14), suggesting that most phenotypical alterations in transgenic mice are due to defective TRα1 signaling in the POA and AHA (Paxinos and Franklin, 2019). Due to strong expression of mCherry close to the PVN, an area that greatly influences the HPT-axis (Duntas, 2016; Kondo et al., 2021) and that also induces thermogenesis in BAT (Mota et al., 2023; Zhang and Bi, 2015), serum T3 and T4 levels were determined in transgenic mice revealing that hypothalamic mutant TRα1 did not influence the HPT-axis. Thus, any phenotypical alterations in transgenic dominant-negative expressing TRα1 mice are not due to imbalances of the HPT-axis.

Table 14: Hypothalamic areas with no (O), weak (+), or strong (++) expression of mCherry upon injection of CMV-driven TRα1R384C-mCherry. The table was adapted from Sentis et al., 2023 in press.

Hypothalamic Area	
MPOM (Medial Preoptic Nucleus, medial)	++
MPOL (Medial Preoptic Nucleus, lateral)	++
PVN (Paraventricular Nucleus)	+
AHA (Anterior Hypothalamic Area)	++
LA (Lateroanterior Hypothalamus)	+
LH (Lateral Hypothalamus)	●
MPA (Medial Preoptic Area)	++
AHC (Anterior Hypothalamic Area, central)	++
LPO (Lateral Preoptic Area)	+
AC (Anterior Commissure Nucleus)	++
ARC (Arcuate Nucleus)	+

Interestingly, the expression of hypothalamic dominant-negative TRα1 indeed led to alterations of the body temperature phenotype. The expression of mutant TRα1 in the hypothalamus significantly lowered body temperature at 22°C and at thermoneutrality. However, during cold exposure, reduced body temperature values of dominant-negative TRα1 did not reach significance. Consequently, during cold exposure, other thermoregulatory mechanisms in thermogenic tissues might be activated such as muscle tissue or BAT thermogenesis to counteract the cold stress. Additionally, the skeletal soleus muscle seems to be activated at room temperature as seen in the upregulation of *Atp2a2* and *Gpd2*. Furthermore, the expression of hypothalamic dominant-negative TRα1 led to higher BAT temperatures at room temperature as compared to controls. It is known that impaired TRα1 signaling can regulate downstream BAT thermogenesis (López et al., 2010), however, whether hypothalamic dominant-negative TRα1 drives BAT action in the transgenic animals or whether additional peripheral mechanisms contribute to BAT thermogenesis remains unknown.

Interestingly, the findings of this current study contrast with a recent study showing that neuronal mutant TRα1 and a simultaneous neuronal TRβ KO do not cause a reduced body temperature phenotype (Rial-Pensado et al., 2023). However, considering the elevated anxiety levels in TRα1+m mice (Venero et al., 2005; Wallis et al., 2008), even minor disruptions such as opening the cage induce immediate stress-induced hyperthermia. Therefore, it is plausible that the rectal probing used to measure body temperature in the neuronal mutant TRα1 and neuronal TRβ KO mice (Rial-Pensado et al., 2023) might not have accurately captured baseline reductions in body temperature.

Furthermore, the same study found that neuronal TRα1 mutants with a simultaneous neuronal TRβ KO have lower energy expenditure on chow diet and are prone to diet-induced obesity (Rial-Pensado et al., 2023). However, the expression of hypothalamic dominant-negative TRα1 did not lead to changes in energy expenditure in the transgenic animals, despite their inability to gain weight due to a yet undiscovered mechanism. Although food intake of dominant-negative TRα1 expressing animals was indeed lower, albeit not significant, the observation period of the experimental time frame was not sufficient to detect minor statistically significant changes in food intake. However, already small changes in food intake may induce changes in the lean mass or the fat mass and thus body weight, which may also be accompanied by minor and non-significant changes in energy expenditure (Tschöp et al., 2012). Additionally, the expression of mutant TRα1 in the hypothalamus was also confirmed in regions near the ARC that controls food intake (Timper and Brüning, 2017) and even myostatin expression in brown fat (Steculorum et al., 2016), which was, however, found to be altered in the soleus muscle of mutant TRα1 expressing animals.

Several differences exist between the study that utilized neuronal TRα1 mutants with a simultaneous neuronal TRβ KO (Rial-Pensado et al., 2023) and the hypothalamic mutant TRα1 approach used in this present study that may explain the confounding results: Firstly, the neuronal mutant TRα1 and TRβ KO impacts the entire brain, potentially influencing metabolic rate through other regions like the brainstem (Roh et al., 2016). Secondly, the previous study on neuronal mutant TRα1 and TRβ KO (Rial-Pensado et al., 2023) investigated the actions of both receptor isoforms in the brain on energy homeostasis and thermogenesis simultaneously. Consequently, the specific TRα1 and TRβ actions in the brain cannot be distinguished. Thus, changes in energy expenditure can be attributed to the TRβ knockout, as TRβ is known to greatly influence energy expenditure via actions in the VMH (Hameed et al., 2017). Lastly, and most importantly, the neuronal model utilized a $Cre3^{tg/+}$ mouse model (Banares et al., 2005) and thus a Cre/loxP approach to introduce the mutant TRα1 and TRβ KO in neurons of the central but also peripheral nervous system already during early embryonic development, whereas in this current study, mutant TRα1 was expressed in the adult hypothalamus.

However, the expression of hypothalamic dominant-negative TRα1 in this study is not restricted to neurons only. The expression of dominant-negative TRα1 exclusively in the hypothalamus allows a more distinct assessment of the hypothalamic regions that control body temperature homeostasis. Nevertheless, the approach to express mutant TRα1 under a CMV promoter does not allow conclusion to be made about distinct cellular populations that TRα1-dependently influence thermogenesis. In detail, the used AAV serotypes, AAV1 and AAV2, delivering dominant-negative TRα1 into the hypothalamus target neuronal cell types, as well as astrocytes, and oligodendrocytes (Hadaczek et al., 2016; Haery et al., 2019; Wang et al., 2019). Likewise, the CMV promoter drives highly specific expression in neurons, but also in astrocytes (Bäck et al., 2019; Yaguchi et al., 2013). Thus, any

body temperature phenotype alterations upon the expression of hypothalamic dominant-negative TRα1 likely result from actions of multiple TRα1 expressing cell types in different hypothalamic areas (Alkemade et al., 2005; Sreenivasan et al., 2023). One cell type that could be affected by defective TRα1 signaling are GABAergic neurons in the POA which were recently identified as thermoresponsive in response to ambient thermal challenges (Zhao et al., 2017). Finally, to narrow down regions and cell types that TRα1 dependently regulate body temperature and the central body temperature set-point, further experiments are required targeting, e.g., the POA or lateral hypothalamus exclusively.

In summary, impaired TRα1 in the hypothalamus induces a lower body temperature phenotype as in anapyrexia, which is accompanied by slower body weight gain (Dittner et al., 2019; Johann et al., 2019). However, during acute cold exposure, other unknown peripheral and/or central thermoregulatory mechanisms seem to be at play defending a normal body temperature.

4.5 Differences in *Adrb3* expression in primary rat and mouse adipocytes after thyroid hormone treatment

Hypothyroidism is associated with weight gain and a slower metabolic rate in humans, but also in rats (Chaker et al., 2022; Herwig et al., 2014). Interestingly, the opposite findings were made in thyroid disease mouse models. Despite reduced energy expenditure and reduced daily activity, hypothyroid mice develop a leaner body weight phenotype compared to euthyroid controls (Kaspari et al., 2020; Niedowicz et al., 2021). However, the underlying mechanisms and species-specific differences at which TH exert their peripheral actions in, e.g., BAT and skeletal muscle to boost metabolism are not entirely understood and remain enigmatic.

Interestingly, also in hyperthyroid conditions, phenotypical differences in rats and mice can be observed. While prolonged T4 treatment in rats actives BAT thermogenesis and leads to slower body weight gain compared to euthyroid controls at room temperature (López et al., 2010; Rial-Pensado et al., 2022), systemic hyperthyroidism in mice leads to weight gain and lower BAT temperature compared to controls (Dittner et al., 2019; Johann et al., 2019; Lombardi et al., 2015). The lower BAT temperature in mice in response to T4 treatment suggests that brown fat thermogenesis is shut down in response to excess TH. In addition to the lower BAT temperature, mice treated with T3 or T4 had lower *Adrb3* expression in iBAT (Johann et al., 2019), whereas this current study shows that rats treated with T4 had higher *Adrb3* expression levels in iBAT in response to systemic hyperthyroidism. However, the exact mechanisms that contribute to the phenotypical *in vivo* difference between mice and rats during hyperthyroidism remain incompletely understood. Due to the translational relevance of animal disease models, a greater understanding of disease phenotypes in rodents is anticipated (Vandamme, 2014). To further investigate the local TH effects on brown fat activation in rats and mice, cultured primary adult adipocytes were treated for 24 h with T3 and/or b-CL, a β3-adrenergic agonist (Ghorbani et al., 1997). This experimental design allowed the investigation of the direct actions of T3 in brown adipocytes, as cell cultures are denervated and therefore not influenced by SNS signaling.

Interestingly, T3 treatment alone did not lead to changes in *Adrb3* expression in matured rat and mouse brown adipocytes *in vitro*, whereas additional b-Cl treatment significantly downregulated *Adrb3* expression (Table 15A). Other thermogenic markers such as *Ucp1* and *Dio2* expression did also not respond to T3 treatment (Table 15A). These data suggest that TH alone does not mediate the *in vivo Adrb3* expression differences in rats and mice and that additional indirect mechanism are at play to induce BAT thermogenesis in rats (Rial-Pensado et al., 2022) and to shut down brown fat thermogenesis in mice following systemic hyperthyroidism (Johann et al., 2019). Despite the crucial role of TH during the differentiation of preadipocytes to brown adipocytes (Obregon, 2008), the actions of TH on target gene regulation *in vitro* in mature brown adipocytes may require additional thermogenic key players.

Table 15: Summary of gene expression changes of Adrb3, Adra1a, Dio2, and Ucp1 in cultured mature brown and white adipocytes (isolated from rats and mice) in response to 24 h T3 and/or b-CL treatment.

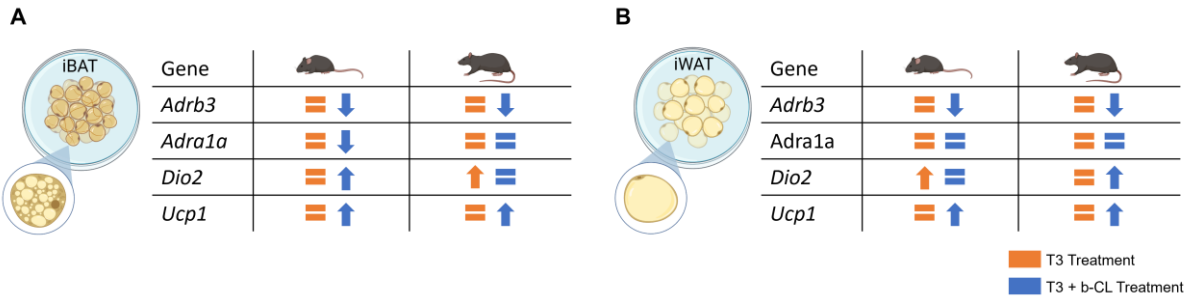

An example of additional metabolic key players that can enhance the response of BAT to TH signaling are bile acids that have been identified as signaling molecules (Bonde et al., 2014; Gupta et al., 2001; Qiao et al., 2003). A previous publication could show that bile acids indirectly enhance DIO2 activity, which in turn may mediate the conversion of intracellular T4 to T3. The metabolic effect of bile acids in brown fat are dependent on DIO2 action and induce BAT thermogenesis and increase energy expenditure when directly administered to BAT of mice (Watanabe et al., 2006). Furthermore, the treatment of brown adipocytes and myocytes with bile acids leads to increased DIO2 activity and oxygen consumption (Watanabe et al., 2006), suggesting that TH-dependent BAT thermogenesis may also be influenced and fine-tuned by bile acids (Bonde et al., 2014). Whether differences in bile acid signaling in rats and mice may contribute to differences in the thermogenic response of rats in mice during systemic hyperthyroidism remains to be investigated in future experiments.

In addition to bile acids, also well-known peptide hormones like the fibroblast growth factor 21 (FGF21; Angelin et al., 2012) may play a role in the fine-tuning of TH-induced brown fat thermogenesis in rats and mice. A publication that investigated the interplay of TH and FGF21 serum levels and its effects on liver metabolism and BAT could show that TH regulates FGF21 expression in liver and adipose tissue (Domouzoglou et al., 2014). However, FGF21 administration also influences TH serum levels in hypothyroid mice, suggesting that TH and FGF21 both influence the availability and tissue-specific actions of each other (Angelin et al., 2012; Domouzoglou et al., 2014). Conclusively, the *in vivo* effects of TH on target gene expression in BAT are likely accompanied and mediated by other mechanisms that could include bile acid signaling and the regulation of TH by FGF21 that could not be investigated by the *in vitro* experiments of this current study. Thus, future experiments aiming at dissecting the direct effects of TH in mature rat and mouse brown adipocytes on, e.g., *Adrb3* target gene expression should also include investigating the effects of additional TH regulators.

Additionally, and in line with other studies, T3 treatment and simultaneous b-CL treatment led to the induction of thermogenic marker expression (Table 15B) in mature white adipocytes isolated

and cultured from rats and mice (Klaus et al., 2001; Liu et al., 2022; Martínez-Sánchez et al., 2017a; Volke and Krause, 2021; Weiner et al., 2016). In line with literature, these data implies that SNS signaling is required for browning of white adipocytes and thus an increase of the thermogenic potential of white fat cells (Collins et al., 2014).

In summary, the direct effects of TH on *Adrb3* expression *in vitro* differ from *Adrb3* expression patterns *in vivo* in response to systemic hyperthyroidism, indicating that additional mechanisms are at play governing and influencing the *in vivo* effects and consequences of TH treatment in BAT in rats and in mice. Although a recent study proposed that the paradoxical lean phenotype of hypothyroid mice compared to hypothyroid rats is the results of skeletal muscle mediated adaptive thermogenesis (Kaspari et al., 2020), the different phenotypes of hyperthyroid rats and mice are likely due to differences in brown fat activation (Johann et al., 2019; Rial-Pensado et al., 2022).

5 Conclusion and Outlook

Taken together the results of this thesis demonstrate the importance of TH signaling in thermogenesis and whole-body temperature homeostasis in mice (Figure 31A). Furthermore, this study showed for the first time that hypothalamic TRα1 signaling regulates body temperature by lowering the body temperature set-point emphasizing that the interplay between centrally (Figure 31B) and peripherally (Figure 31C) acting TH is of great importance for body temperature homeostasis. This topic has not been thoroughly explored before, making the presented study a significant and valuable contribution to the current research in this field.

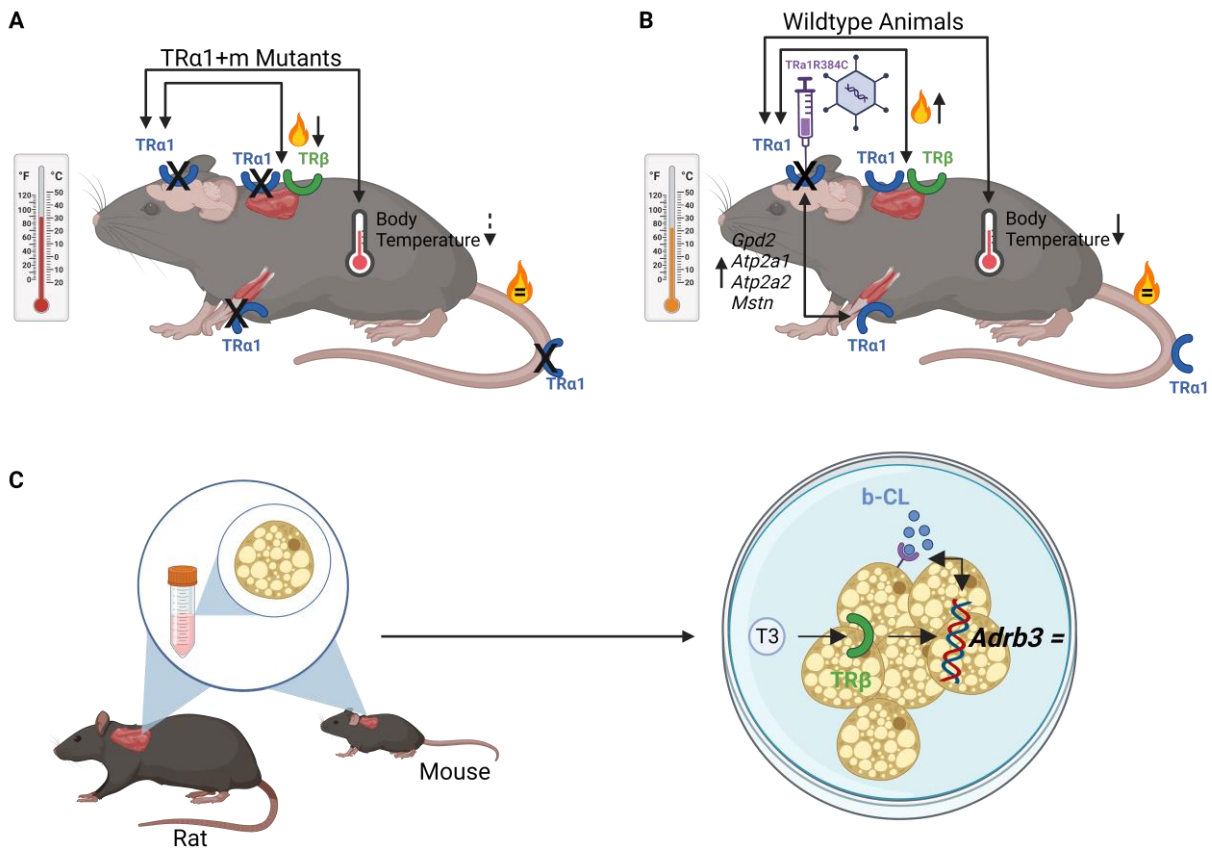

Figure 31: The role of TRα1 signaling in whole-body temperature regulation. A) TRα1+m mutants only partially normalize their defective body temperature phenotype at 30°C during the active phase, while heat loss via the tail is normalized. These data suggest that their body temperature set-point is lower due to defective TRα1 signaling. B) Hypothalamic mutant TRα1 lowers the body temperature set-point. C) The actions of TH on BAT thermogenesis and Adrb3 expression in rats and mice are likely indirect as TH treatment in in vitro does not up- or downregulate Adrb3 expression.

However, the precise mechanisms at which TRα1 regulates whole-body temperature homeostasis are not entirely resolved by this study as hypothalamic TRα1 action did not induce BAT thermogenesis or heat dissipation via the tail. Furthermore, the exact mechanisms at which the interplay of centrally and peripherally acting TH is mediated remains enigmatic (Cannon and

Nedergaard, 2010; Sentis et al., 2021; Zhang et al., 2018) as defects in central TH signaling seemingly lead to a lowering of the body temperature set-point, whereas the *in vitro* experiments of this study could show that the effects of TH on *Adrb3* expression in brown fat are likely indirect. Further studies targeting specific hypothalamic nuclei that control whole-body thermoregulation are required to understand the different actions of TH signaling in different neuronal subpopulations of the hypothalamus.

To date, the consequences of central and particularly hypothalamic TH signaling on whole-body temperature regulation are still poorly understood and require further research to dissect the underlying cause and origin of symptoms that manifest in clinical hypo- or hyperthyroidism (Cannon and Nedergaard, 2010). Nevertheless, by demonstrating that impaired central TRα1 action can lead to a reduced body temperature phenotype in mice, this study suggests a novel pathway through which hypothalamic control influences the regulation of whole-body temperature. This pathway may be of relevance to clinical disorders in humans such as hyperthyroidism, mental illnesses, and conditions like multiple sclerosis, where altered temperature sensations manifest as a symptom (Christogianni et al., 2022, 2018; Epstein et al., 1997; Lõhmus, 2018; Marcocci and Cetani, 2018; Sulman et al., 1975).

6 References

Abelenda, M., Puerta, M., 1992. Brown Adipose Tissue Thermogenesis in T3-Treated Rats. Horm. Metab. Res. 24, 60–62. https://doi.org/10.1055/s-2007-1003256

Alkemade, A., Vuijst, C.L., Unmehopa, U.A., Bakker, O., Vennström, B., Wiersinga, W.M., Swaab, D.F., Fliers, E., 2005. Thyroid Hormone Receptor Expression in the Human Hypothalamus and Anterior Pituitary. J. Clin. Endocrinol. Metab. 90, 904–912. https://doi.org/10.1210/jc.2004-0474

Alvarez-Crespo, M., Csikasz, R.I., Martínez-Sánchez, N., Diéguez, C., Cannon, B., Nedergaard, J., López, M., 2016. Essential role of UCP1 modulating the central effects of thyroid hormones on energy balance. Mol. Metab. 5, 271–282. https://doi.org/10.1016/j.molmet.2016.01.008

Andersen, C.L., Jensen, J.L., Ørntoft, T.F., 2004. Normalization of Real-Time Quantitative Reverse Transcription-PCR Data: A Model-Based Variance Estimation Approach to Identify Genes Suited for Normalization, Applied to Bladder and Colon Cancer Data Sets. Cancer Res. 64, 5245–5250. https://doi.org/10.1158/0008-5472.CAN-04-0496

Angelin, B., Larsson, T.E., Rudling, M., 2012. Circulating Fibroblast Growth Factors as Metabolic Regulators—A Critical Appraisal. Cell Metab. 16, 693–705. https://doi.org/10.1016/j.cmet.2012.11.001

Anyetei-Anum, C.S., Roggero, V.R., Allison, L.A., 2018. Thyroid hormone receptor localization in target tissues. J. Endocrinol. 237, R19–R34. https://doi.org/10.1530/JOE-17-0708

Astapova, I., Lee, L.J., Morales, C., Tauber, S., Bilban, M., Hollenberg, A.N., 2008. The nuclear corepressor, NCoR, regulates thyroid hormone action in vivo. Proc. Natl. Acad. Sci. 105, 19544–19549. https://doi.org/10.1073/pnas.0804604105

Bäck, S., Dossat, A., Parkkinen, I., Koivula, P., Airavaara, M., Richie, C.T., Chen, Y.-H., Wang, Y., Harvey, B.K., 2019. Neuronal Activation Stimulates Cytomegalovirus Promoter-Driven Transgene Expression. Mol. Ther. - Methods Clin. Dev. 14, 180–188. https://doi.org/10.1016/j.omtm.2019.06.006

Bahouth, S.W., 1991. Thyroid hormones transcriptionally regulate the beta 1-adrenergic receptor gene in cultured ventricular myocytes. J. Biol. Chem. 266, 15863–15869. https://doi.org/10.1016/S0021-9258(18)98488-7

Banares, S., Zeh, K., Krajewska, M., Kermer, P., Baribault, H., Reed, J.C., Krajewski, S., 2005. Novel pan-neuronal Cre-transgenic line for conditional ablation of genes in the nervous system. Genesis 42, 6–16. https://doi.org/10.1002/gene.20117

Bartelt, A., Bruns, O.T., Reimer, R., Hohenberg, H., Ittrich, H., Peldschus, K., Kaul, M.G., Tromsdorf, U.I., Weller, H., Waurisch, C., Eychmüller, A., Gordts, P.L.S.M., Rinninger, F., Bruegelmann, K., Freund, B., Nielsen, P., Merkel, M., Heeren, J., 2011. Brown adipose tissue activity controls triglyceride clearance. Nat. Med. 17, 200–205. https://doi.org/10.1038/nm.2297

Bartelt, A., Heeren, J., 2014. Adipose tissue browning and metabolic health. Nat. Rev. Endocrinol. 10, 24–36. https://doi.org/10.1038/nrendo.2013.204

Bartesaghi, S., Hallen, S., Huang, L., Svensson, P.-A., Momo, R.A., Wallin, S., Carlsson, E.K., Forslöw, A., Seale, P., Peng, X.-R., 2015. Thermogenic Activity of UCP1 in Human White Fat-Derived Beige Adipocytes. Mol. Endocrinol. 29, 130–139. https://doi.org/10.1210/me.2014-1295

Bartness, T.J., Liu, Y., Shrestha, Y.B., Ryu, V., 2014. Neural innervation of white adipose tissue and the control of lipolysis. Front. Neuroendocrinol. 35, 473–493. https://doi.org/10.1016/j.yfrne.2014.04.001

Bernal, J., Morte, B., 2013. Thyroid hormone receptor activity in the absence of ligand: Physiological and developmental implications. Biochim. Biophys. Acta BBA - Gen. Subj. 1830, 3893–3899. https://doi.org/10.1016/j.bbagen.2012.04.014

Bianco, A.C., Da Conceição, R.R., 2018. The Deiodinase Trio and Thyroid Hormone Signaling, in: Plateroti, M., Samarut, J. (Eds.), Thyroid Hormone Nuclear Receptor, Methods in Molecular Biology. Springer, New York, USA, pp. 67–83. https://doi.org/10.1007/978-1-4939-7902-8_8

Bianco, A.C., Kim, B.W., 2006. Deiodinases: implications of the local control of thyroid hormone action. J. Clin. Invest. 116, 2571–2579. https://doi.org/10.1172/JCI29812

Bianco, A.C., Silva, J.E., 1988. Cold exposure rapidly induces virtual saturation of brown adipose tissue nuclear T3 receptors. Am. J. Physiol.-Endocrinol. Metab. 255, E496–E503. https://doi.org/10.1152/ajpendo.1988.255.4.E496

Bianco, A.C., Silva, J.E., 1987. Intracellular conversion of thyroxine to triiodothyronine is required for the optimal thermogenic funciton of brown adipose tissue. J. Clin. Invest. 79, 295–300. https://doi.org/10.1172/JCI112798

Blondin, D.P., Haman, F., 2018. Shivering and nonshivering thermogenesis in skeletal muscles. Handb. Clin. Neurol. 156, 153–173. https://doi.org/10.1016/B978-0-444-63912-7.00010-2

Bonde, Y., Breuer, O., Lütjohann, D., Sjöberg, S., Angelin, B., Rudling, M., 2014. Thyroid hormone reduces PCSK9 and stimulates bile acid synthesis in humans. J. Lipid Res. 55, 2408–2415. https://doi.org/10.1194/jlr.M051664

Börgeson, E., Boucher, J., Hagberg, C.E., 2022. Of mice and men: Pinpointing species differences in adipose tissue biology. Front. Cell Dev. Biol. 10, 1003118. https://doi.org/10.3389/fcell.2022.1003118

Brent, G.A., Dunn, M.K., Harney, J.W., Gulick, T., Larsen, P.R., Moore, D.D., 1989. Thyroid hormone aporeceptor represses T3-inducible promoters and blocks activity of the retinoic acid receptor. New Biol. 1, 329–336.

Cannon, B., Nedergaard, J., 2010. Thyroid hormones: igniting brown fat via the brain. Nat. Med. 16, 965–967. https://doi.org/10.1038/nm0910-965

Cannon, B., Nedergaard, J., 2004. Brown adipose tissue: function and physiological significance. Physiol. Rev. 84, 277–359. https://doi.org/10.1152/physrev.00015.2003

Capelli, V., Grijota-Martínez, C., Dragano, N.R.V., Rial-Pensado, E., Fernø, J., Nogueiras, R., Mittag, J., Diéguez, C., López, M., 2021. Orally Induced Hyperthyroidism Regulates Hypothalamic AMP-Activated Protein Kinase. Nutrients 13, 4204. https://doi.org/10.3390/nu13124204

Chaker, L., Razvi, S., Bensenor, I.M., Azizi, F., Pearce, E.N., Peeters, R.P., 2022. Hypothyroidism. Nat. Rev. Dis. Primer 8, 30. https://doi.org/10.1038/s41572-022-00357-7

Cheng, L., Wang, J., Dai, H., Duan, Y., An, Y., Shi, L., Lv, Y., Li, H., Wang, C., Ma, Q., Li, Y., Li, P., Du, H., Zhao, B., 2021. Brown and beige adipose tissue: a novel therapeutic strategy for obesity and type 2 diabetes mellitus. Adipocyte 10, 48–65. https://doi.org/10.1080/21623945.2020.1870060

Chiellini, G., Apriletti, J.W., Yoshihara, H.A., Baxter, J.D., Ribeiro, R.C.J., Scanlan, T.S., 1998. A high-affinity subtype-selective agonist ligand for the thyroid hormone receptor. Chem. Biol. 5, 299–306. https://doi.org/10.1016/S1074-5521(98)90168-5

Christogianni, A., Bibb, R., Davis, S.L., Jay, O., Barnett, M., Evangelou, N., Filingeri, D., 2018. Temperature sensitivity in multiple sclerosis: An overview of its impact on sensory and cognitive symptoms. Temperature 5, 208–223. https://doi.org/10.1080/23328940.2018.1475831

Christogianni, A., O'Garro, J., Bibb, R., Filtness, A., Filingeri, D., 2022. Heat and cold sensitivity in multiple sclerosis: A patient-centred perspective on triggers, symptoms, and thermal resilience practices. Mult. Scler. Relat. Disord. 67, 104075. https://doi.org/10.1016/j.msard.2022.104075

Collins, S., Sarzani, R., Bordicchia, M., 2014. Coordinate control of adipose 'browning' and energy expenditure by β-adrenergic and natriuretic peptide signalling. Int. J. Obes. Suppl. 4, S17–S20. https://doi.org/10.1038/ijosup.2014.6

Contreras, C., Nogueiras, R., Diéguez, C., Medina-Gómez, G., López, M., 2016. Hypothalamus and thermogenesis: Heating the BAT, browning the WAT. Mol. Cell. Endocrinol. 438, 107–115. https://doi.org/10.1016/j.mce.2016.08.002

Contreras, C., Nogueiras, R., Diéguez, C., Rahmouni, K., López, M., 2017. Traveling from the hypothalamus to the adipose tissue: The thermogenic pathway. Redox Biol. 12, 854–863. https://doi.org/10.1016/j.redox.2017.04.019

Cook, C.B., Kakucska, I., Lechan, R.M., Koenig, R.J., 1992. Expression of thyroid hormone receptor beta 2 in rat hypothalamus. Endocrinology 130, 1077–1079. https://doi.org/10.1210/endo.130.2.1733708

Costa-e-Sousa, R.H., Hollenberg, A.N., 2012. Minireview: The Neural Regulation of the Hypothalamic-Pituitary-Thyroid Axis. Endocrinology 153, 4128–4135. https://doi.org/10.1210/en.2012-1467

Cui, X., Nguyen, N.L.T., Zarebidaki, E., Cao, Q., Li, F., Zha, L., Bartness, T., Shi, H., Xue, B., 2016. Thermoneutrality decreases thermogenic program and promotes adiposity in high-fat diet-fed mice. Physiol. Rep. 4, e12799. https://doi.org/10.14814/phy2.12799

Cypess, A.M., Lehman, S., Williams, G., Tal, I., Rodman, D., Goldfine, A.B., Kuo, F.C., Palmer, E.L., Tseng, Y.-H., Doria, A., Kolodny, G.M., Kahn, C.R., 2009. Identification and importance of brown adipose tissue in adult humans. N. Engl. J. Med. 360, 1509–1517. https://doi.org/10.1056/NEJMoa0810780

De Leo, S., Lee, S.Y., Braverman, L.E., 2016. Hyperthyroidism. The Lancet 388, 906–918. https://doi.org/10.1016/S0140-6736(16)00278-6

de Meis, L., Bianconi, M.L., Suzano, V.A., 1997. Control of energy fluxes by the sarcoplasmic reticulum Ca2+-ATPase: ATP hydrolysis, ATP synthesis and heat production. FEBS Lett. 406, 201–204. https://doi.org/10.1016/s0014-5793(97)00244-5

Demine, S., Renard, P., Arnould, T., 2019. Mitochondrial Uncoupling: A Key Controller of Biological Processes in Physiology and Diseases. Cells 8, 795. https://doi.org/10.3390/cells8080795

Dittner, C., Lindsund, E., Cannon, B., Nedergaard, J., 2019. At thermoneutrality, acute thyroxine-induced thermogenesis and pyrexia are independent of UCP1. Mol. Metab. 25, 20–34. https://doi.org/10.1016/j.molmet.2019.05.005

Divakaruni, A.S., Humphrey, D.M., Brand, M.D., 2012. Fatty Acids Change the Conformation of Uncoupling Protein 1 (UCP1). J. Biol. Chem. 287, 36845–36853. https://doi.org/10.1074/jbc.M112.381780

Domouzoglou, E.M., Fisher, F.M., Astapova, I., Fox, E.C., Kharitonenkov, A., Flier, J.S., Hollenberg, A.N., Maratos-Flier, E., 2014. Fibroblast Growth Factor 21 and Thyroid Hormone Show Mutual Regulatory Dependency but Have Independent Actions In Vivo. Endocrinology 155, 2031–2040. https://doi.org/10.1210/en.2013-1902

Dore, R., Sentis, S.C., Johann, K., Lopez-Alcantara, N., Resch, J., Moeller, L.C., Fuehrer, D., Obermayer, B., Opitz, R., Mittag, J., 2023a. Partial resistance to thyroid hormone-induced tachycardia and cardiac hypertrophy in mice lacking thyroid hormone receptor β (preprint). https://doi.org/10.1101/2023.11.21.567193

Dore, R., Watson, L., Hollidge, S., Krause, C., Sentis, S.C., Oelkrug, R., Geißler, C., Johann, K., Pedaran, M., Lyons, G., Lopez-Alcantara, N., Resch, J., Sayk, F., Iwen, K.A., Franke, A., Boysen, T.J., Dalley, J.W., Lorenz, K., Moran, C., Rennie, K.L., Arner, A., Kirchner, H., Chatterjee, K., Mittag, J., 2023b. Resistance to thyroid hormone induced tachycardia in RTHα syndrome. Nat. Commun. 14, 3312. https://doi.org/10.1038/s41467-023-38960-1

Dunn, J., Grider, M.H., 2023. Physiology, Adenosine Triphosphate, in: StatPearls. StatPearls Publishing, Treasure Island, USA.

Duntas, L., 2016. New Insights into the Hypothalamic-Pituitary-Thyroid Axis. Acta Endocrinol. Buchar. 12, 125–129. https://doi.org/10.4183/aeb.2016.125

Engelhard, C.A., Huang, C., Khani, S., Kasparek, P., Prochazka, J., Rozman, J., Reguera, D.P., Sedlacek, R., Kornfeld, J.-W., 2022. Comprehensive Transcriptional Profiling and Mouse Phenotyping Reveals Dispensable Role for Adipose Tissue Selective Long Noncoding RNA Gm15551. Non-Coding RNA 8, 32. https://doi.org/10.3390/ncrna8030032

Epstein, Y., Albukrek, D., Kalmovitc, B., Mora, D.S., Shapiro, Y., 1997. Heat Intolerance Induced by Antidepressants. Ann. N. Y. Acad. Sci. 813, 553–558. https://doi.org/10.1111/j.1749-6632.1997.tb51746.x

Fedorenko, A., Lishko, P.V., Kirichok, Y., 2012. Mechanism of fatty-acid-dependent UCP1 uncoupling in brown fat mitochondria. Cell 151, 400–413. https://doi.org/10.1016/j.cell.2012.09.010

Feng, X., Jiang, Y., Meltzer, P., Yen, P.M., 2000. Thyroid Hormone Regulation of Hepatic Genes in Vivo Detected by Complementary DNA Microarray. Mol. Endocrinol. 14, 947–955. https://doi.org/10.1210/mend.14.7.0470

Fischer, A.W., Cannon, B., Nedergaard, J., 2019. The answer to the question “What is the best housing temperature to translate mouse experiments to humans?” is: thermoneutrality. Mol. Metab. 26, 1–3. https://doi.org/10.1016/j.molmet.2019.05.006

Fisher, F.M., Kleiner, S., Douris, N., Fox, E.C., Mepani, R.J., Verdeguer, F., Wu, J., Kharitonenkov, A., Flier, J.S., Maratos-Flier, E., Spiegelman, B.M., 2012. FGF21 regulates PGC-1α and browning of white adipose tissues in adaptive thermogenesis. Genes Dev. 26, 271–281. https://doi.org/10.1101/gad.177857.111

Flamant, F., Cheng, S.-Y., Hollenberg, A.N., Moeller, L.C., Samarut, J., Wondisford, F.E., Yen, P.M., Refetoff, S., 2017. Thyroid Hormone Signaling Pathways: Time for a More Precise Nomenclature. Endocrinology 158, 2052–2057. https://doi.org/10.1210/en.2017-00250

Forrest, D., Hanebuth, E., Smeyne, R.J., Everds, N., Stewart, C.L., Wehner, J.M., Curran, T., 1996. Recessive resistance to thyroid hormone in mice lacking thyroid hormone receptor ß: evidence for tissue-specific modulation of receptor function. EMBO J. 15, 3006–3015.

Forrest, D., Vennström, B., 2000. Functions of Thyroid Hormone Receptors in Mice. Thyroid 10, 41–52. https://doi.org/10.1089/thy.2000.10.41

Fristoe, T.S., Burger, J.R., Balk, M.A., Khaliq, I., Hof, C., Brown, J.H., 2015. Metabolic heat production and thermal conductance are mass-independent adaptations to thermal environment in birds and mammals. Proc. Natl. Acad. Sci. 112, 15934–15939. https://doi.org/10.1073/pnas.1521662112

Galmozzi, A., Kok, B.P., Saez, E., 2021. Isolation and Differentiation of Primary White and Brown Preadipocytes from Newborn Mice. J Vis Exp. 25, e62005. https://doi.org/oi: 10.3791/62005

Ganeshan, K., Chawla, A., 2017. Warming the mouse to model human diseases. Nat. Rev. Endocrinol. 13, 458–465. https://doi.org/10.1038/nrendo.2017.48

Gans, I.M., Grendler, J., Babich, R., Jayasundara, N., Coffman, J.A., 2021. Glucocorticoid-Responsive Transcription Factor Krüppel-Like Factor 9 Regulates fkbp5 and Metabolism. Front. Cell Dev. Biol. 9, 727037. https://doi.org/10.3389/fcell.2021.727037

Gaspar, R.C., Pauli, J.R., Shulman, G.I., Muñoz, V.R., 2021. An update on brown adipose tissue biology: a discussion of recent findings. Am. J. Physiol.-Endocrinol. Metab. 320, E488–E495. https://doi.org/10.1152/ajpendo.00310.2020

Ghorbani, M., Claus, T.H., Himms-Hagen, J., 1997. Hypertrophy of brown adipocytes in brown and white adipose tissues and reversal of diet-induced obesity in rats treated with a β3-adrenoceptor agonist. Biochem. Pharmacol. 54, 121–131. https://doi.org/10.1016/S0006-2952(97)00162-7

Gordon, C.J., 2012. Thermal physiology of laboratory mice: Defining thermoneutrality. J. Therm. Biol. 37, 654–685. https://doi.org/10.1016/j.jtherbio.2012.08.004

Gothe, S., Wang, Z., Ng, L., Kindblom, J.M., Barros, A.C., Ohlsson, C., Vennstrom, B., Forrest, D., 1999. Mice devoid of all known thyroid hormone receptors are viable but exhibit disorders of the pituitary-thyroid axis, growth, and bone maturation. Genes Dev. 13, 1329–1341. https://doi.org/10.1101/gad.13.10.1329

Groeneweg, S., Van Geest, F.S., Peeters, R.P., Heuer, H., Visser, W.E., 2020. Thyroid Hormone Transporters. Endocr. Rev. 41, 146–201. https://doi.org/10.1210/endrev/bnz008

Grujic, D., Susulic, V.S., Harper, M.-E., Himms-Hagen, J., Cunningham, B.A., Corkey, B.E., Lowell, B.B., 1997. β3-Adrenergic Receptors on White and Brown Adipocytes Mediate β3-Selective Agonist-induced Effects on Energy Expenditure, Insulin Secretion, and Food Intake. J. Biol. Chem. 272, 17686–17693. https://doi.org/10.1074/jbc.272.28.17686

Guilherme, A., Yenilmez, B., Bedard, A.H., Henriques, F., Liu, D., Lee, A., Goldstein, L., Kelly, M., Nicoloro, S.M., Chen, M., Weinstein, L., Collins, S., Czech, M.P., 2020. Control of Adipocyte Thermogenesis and Lipogenesis through β3-Adrenergic and Thyroid Hormone Signal Integration. Cell Rep. 31, 107598. https://doi.org/10.1016/j.celrep.2020.107598

Gupta, S., Stravitz, R.T., Dent, P., Hylemon, P.B., 2001. Down-regulation of Cholesterol 7α-Hydroxylase (CYP7A1) Gene Expression by Bile Acids in Primary Rat Hepatocytes Is Mediated by the c-Jun N-terminal Kinase Pathway. J. Biol. Chem. 276, 15816–15822. https://doi.org/10.1074/jbc.M010878200

Hadaczek, P., Stanek, L., Ciesielska, A., Sudhakar, V., Samaranch, L., Pivirotto, P., Bringas, J., O'Riordan, C., Mastis, B., San Sebastian, W., Forsayeth, J., Cheng, S.H., Bankiewicz, K.S., Shihabuddin, L.S., 2016. Widespread AAV1- and AAV2-mediated transgene expression in the nonhuman primate brain: implications for Huntington's disease. Mol. Ther. - Methods Clin. Dev. 3, 16037. https://doi.org/10.1038/mtm.2016.37

Haery, L., Deverman, B.E., Matho, K.S., Cetin, A., Woodard, K., Cepko, C., Guerin, K.I., Rego, M.A., Ersing, I., Bachle, S.M., Kamens, J., Fan, M., 2019. Adeno-Associated Virus Technologies and Methods for Targeted Neuronal Manipulation. Front. Neuroanat. 13, 93. https://doi.org/10.3389/fnana.2019.00093

Haman, F., Blondin, D.P., 2017. Shivering thermogenesis in humans: Origin, contribution and metabolic requirement. Temperature 4, 217–226. https://doi.org/10.1080/23328940.2017.1328999

Hameed, S., Patterson, M., Dhillo, W.S., Rahman, S.A., Ma, Y., Holton, C., Gogakos, A., Yeo, G.S.H., Lam, B.Y.H., Polex-Wolf, J., Fenske, W., Bell, J., Anastasovska, J., Samarut, J., Bloom, S.R., Bassett, J.H.D., Williams, G.R., Gardiner, J.V., 2017. Thyroid Hormone Receptor Beta in the Ventromedial Hypothalamus Is Essential for the Physiological Regulation of Food Intake and Body Weight. Cell Rep. 19, 2202–2209. https://doi.org/10.1016/j.celrep.2017.05.066

Heldmaier, G., 1975. Metabolic and thermoregulatory responses to heat and cold in the Djungarian hamster, Phodopus sungorus. J. Comp. Physiol. 102, 115–122. https://doi.org/10.1007/BF00691297

Hernández, A., Obregón, M.-J., 1996. Presence and mRNA expression of T3 receptors in differentiating rat brown adipocytes. Mol. Cell. Endocrinol. 121, 37–46. https://doi.org/10.1016/0303-7207(96)03849-X

Hernandez, A., Stohn, J., 2018. The Type 3 Deiodinase: Epigenetic Control of Brain Thyroid Hormone Action and Neurological Function. Int. J. Mol. Sci. 19, 1804. https://doi.org/10.3390/ijms19061804

Herrmann, B., Harder, L., Oelkrug, R., Chen, J., Gachkar, S., Nock, S., Resch, J., Korkowski, M., Heuer, H., Mittag, J., 2020. Central Hypothyroidism Impairs Heart Rate Stability and Prevents Thyroid Hormone-Induced Cardiac Hypertrophy and Pyrexia. Thyroid 30, 1205–1216. https://doi.org/10.1089/thy.2019.0705

Herwig, A., Campbell, G., Mayer, C.-D., Boelen, A., Anderson, R.A., Ross, A.W., Mercer, J.G., Barrett, P., 2014. A Thyroid Hormone Challenge in Hypothyroid Rats Identifies T3 Regulated Genes in the Hypothalamus and in Models with Altered Energy Balance and Glucose Homeostasis. Thyroid 24, 1575–1593. https://doi.org/10.1089/thy.2014.0169

Himms-Hagen, J., Melnyk, A., Zingaretti, M.C., Ceresi, E., Barbatelli, G., Cinti, S., 2000. Multilocular fat cells in WAT of CL-316243-treated rats derive directly from white adipocytes. Am. J. Physiol.-Cell Physiol. 279, C670–C681. https://doi.org/10.1152/ajpcell.2000.279.3.C670

Ikeda, K., Yamada, T., 2020. UCP1 Dependent and Independent Thermogenesis in Brown and Beige Adipocytes. Front. Endocrinol. 11, 498. https://doi.org/10.3389/fendo.2020.00498

Ishibashi, J., Seale, P., 2010. Beige can be slimming. Science 328, 1113–1114. https://doi.org/10.1126/science.1190816

Jacobsson, A., Stadler, U., Glotzer, M.A., Kozak, L.P., 1985. Mitochondrial uncoupling protein from mouse brown fat. Molecular cloning, genetic mapping, and mRNA expression. J. Biol. Chem. 260, 16250–16254.

Jastroch, M., 2012. Expression of Uncoupling Proteins in a Mammalian Cell Culture System (HEK293) and Assessment of Their Protein Function, in: Palmeira, C.M., Moreno, A.J. (Eds.), Mitochondrial Bioenergetics, Methods in Molecular Biology. Humana Press, Totowa, NJ, pp. 153–164. https://doi.org/10.1007/978-1-61779-382-0_10

Jensen, J., Rustad, P.I., Kolnes, A.J., Lai, Y.-C., 2011. The Role of Skeletal Muscle Glycogen Breakdown for Regulation of Insulin Sensitivity by Exercise. Front. Physiol. 2. https://doi.org/10.3389/fphys.2011.00112

Johann, K., Cremer, A.L., Fischer, A.W., Heine, M., Pensado, E.R., Resch, J., Nock, S., Virtue, S., Harder, L., Oelkrug, R., Astiz, M., Brabant, G., Warner, A., Vidal-Puig, A., Oster, H., Boelen, A., López, M., Heeren, J., Dalley, J.W., Backes, H., Mittag, J., 2019. Thyroid-Hormone-Induced Browning of White Adipose Tissue Does Not Contribute to Thermogenesis and Glucose Consumption. Cell Rep. 27, 3385-3400.e3. https://doi.org/10.1016/j.celrep.2019.05.054

Kaspari, R.R., Reyna-Neyra, A., Jung, L., Torres-Manzo, A.P., Hirabara, S.M., Carrasco, N., 2020. The paradoxical lean phenotype of hypothyroid mice is marked by increased adaptive thermogenesis in the skeletal muscle. Proc. Natl. Acad. Sci. 117, 22544–22551. https://doi.org/10.1073/pnas.2008919117

Kennedy, W.R., Sakuta, M., Quick, D.C., 1984. Rodent eccrine sweat glands: A case of multiple efferent innervation. Neuroscience 11, 741–749. https://doi.org/10.1016/0306-4522(84)90057-5

Khedoe, P.P.S.J., Hoeke, G., Kooijman, S., Dijk, W., Buijs, J.T., Kersten, S., Havekes, L.M., Hiemstra, P.S., Berbée, J.F.P., Boon, M.R., Rensen, P.C.N., 2015. Brown adipose tissue takes up plasma triglycerides mostly after lipolysis. J. Lipid Res. 56, 51–59. https://doi.org/10.1194/jlr.M052746

Klaus, S., Seivert, A., Boeuf, S., 2001. Effects of the b3-adrenergic agonist Cl316,243 on functional differentiation of white and brown adipocytes in primary cell culture. Biochim. Biophys. Acta Mol. Cell Res. 1539, 85–92. https://doi.org/10.1016/s0167-4889(01)00093-3

Klieverik, L.P., Janssen, S.F., van Riel, A., Foppen, E., Bisschop, P.H., Serlie, M.J., Boelen, A., Ackermans, M.T., Sauerwein, H.P., Fliers, E., Kalsbeek, A., 2009. Thyroid hormone modulates glucose production via a sympathetic pathway from the hypothalamic paraventricular nucleus to the liver. Proc. Natl. Acad. Sci. 106, 5966–5971. https://doi.org/10.1073/pnas.0805355106

Koenig, R.J., 1998. Thyroid Hormone Receptor Coactivators and Corepressors. Thyroid 8, 703–713. https://doi.org/10.1089/thy.1998.8.703

Kondo, Y., Ozawa, A., Kohno, D., Saito, K., Buyandalai, B., Yamada, S., Horiguchi, K., Nakajima, Y., Shibusawa, N., Harada, A., Yokoo, H., Akiyama, H., Sasaki, T., Kitamura, T., Yamada, M., 2021. The Hypothalamic Paraventricular Nucleus Is the Center of the Hypothalamic–Pituitary–Thyroid Axis for Regulating Thyroid Hormone Levels. Thyroid 32, 105–114. https://doi.org/10.1089/thy.2021.0444

Kozak, L.P., Britton, J.H., Kozak, U.C., Wells, J.M., 1988. The mitochondrial uncoupling protein gene. Correlation of exon structure to transmembrane domains. J. Biol. Chem. 263, 12274–12277. https://doi.org/10.1016/S0021-9258(18)37751-2

Lahesmaa, M., Orava, J., Schalin-Jäntti, C., Soinio, M., Hannukainen, J.C., Noponen, T., Kirjavainen, A., Iida, H., Kudomi, N., Enerbäck, S., Virtanen, K.A., Nuutila, P., 2014. Hyperthyroidism Increases Brown Fat Metabolism in Humans. J. Clin. Endocrinol. Metab. 99, E28–E35. https://doi.org/10.1210/jc.2013-2312

Laperrousaz, E., Moullé, V.S., Denis, R.G., Kassis, N., Berland, C., Colsch, B., Fioramonti, X., Philippe, E., Lacombe, A., Vanacker, C., Butin, N., Bruce, K.D., Wang, H., Wang, Y., Gao, Y., Garcia-Caceres, C., Prévot, V., Tschöp, M.H., Eckel, R.H., Le Stunff, H., Luquet, S., Magnan, C., Cruciani-Guglielmacci, C., 2017. Lipoprotein lipase in hypothalamus is a key regulator of body weight gain and glucose homeostasis in mice. Diabetologia 60, 1314–1324. https://doi.org/10.1007/s00125-017-4282-7

Lee, P., Zhao, J.T., Swarbrick, M.M., Gracie, G., Bova, R., Greenfield, J.R., Freund, J., Ho, K.K.Y., 2011. High Prevalence of Brown Adipose Tissue in Adult Humans. J. Clin. Endocrinol. Metab. 96, 2450–2455. https://doi.org/10.1210/jc.2011-0487

Lee, S., Benvie, A.M., Park, H.G., Spektor, R., Harlan, B., Brenna, J.T., Berry, D.C., Soloway, P.D., 2022. Remodeling of gene regulatory networks underlying thermogenic stimuli-induced adipose beiging. Commun. Biol. 5, 584. https://doi.org/10.1038/s42003-022-03531-5

Li, Y., Fromme, T., 2022. Uncoupling Protein 1 Does Not Produce Heat without Activation. Int. J. Mol. Sci. 23, 2406. https://doi.org/10.3390/ijms23052406

Lidell, M.E., 2018. Brown Adipose Tissue in Human Infants, in: Pfeifer, A., Klingenspor, M., Herzig, S. (Eds.), Brown Adipose Tissue, Handbook of Experimental Pharmacology. Springer International Publishing, Basel, SUI, pp. 107–123. https://doi.org/10.1007/164_2018_118

Liu, S., Shen, S., Yan, Y., Sun, C., Lu, Z., Feng, H., Ma, Y., Tang, Z., Yu, J., Wu, Y., Gereben, B., Mohácsik, P., Fekete, C., Feng, X., Yuan, F., Guo, F., Hu, C., Shao, M., Gao, X., Zhao, L., Li, Y., Jiang, J., Ying, H., 2022. Triiodothyronine (T3) promotes brown fat hyperplasia via thyroid hormone receptor α mediated adipocyte progenitor cell proliferation. Nat. Commun. 13, 3394. https://doi.org/10.1038/s41467-022-31154-1

Livak, K.J., Schmittgen, T.D., 2001. Analysis of Relative Gene Expression Data Using Real-Time Quantitative PCR and the 2−ΔΔCT Method. Methods 25, 402–408. https://doi.org/10.1006/meth.2001.1262

Lõhmus, M., 2018. Possible Biological Mechanisms Linking Mental Health and Heat—A Contemplative Review. Int. J. Environ. Res. Public. Health 15, 1515. https://doi.org/10.3390/ijerph15071515

Lombardi, A., Senese, R., De Matteis, R., Busiello, R.A., Cioffi, F., Goglia, F., Lanni, A., 2015. 3,5-Diiodo-L-thyronine activates brown adipose tissue thermogenesis in hypothyroid rats. PloS One 10, e0116498. https://doi.org/10.1371/journal.pone.0116498

López, M., Alvarez, C. V., Nogueiras, R., Diéguez, C., 2013. Energy balance regulation by thyroid hormones at central level. Trends Mol. Med. 19, 418–427. https://doi.org/10.1016/j.molmed.2013.04.004

López, M., Nogueiras, R., Tena-Sempere, M., Diéguez, C., 2016. Hypothalamic AMPK: a canonical regulator of whole-body energy balance. Nat. Rev. Endocrinol. 12, 421–432. https://doi.org/10.1038/nrendo.2016.67

López, M., Varela, L., Vázquez, M.J., Rodríguez-Cuenca, S., González, C.R., Velagapudi, V.R., Morgan, D.A., Schoenmakers, E., Agassandian, K., Lage, R., De Morentin, P.B.M., Tovar, S., Nogueiras, R., Carling, D., Lelliott, C., Gallego, R., Orešič, M., Chatterjee, K., Saha, A.K., Rahmouni, K., Diéguez, C., Vidal-Puig, A., 2010. Hypothalamic AMPK and fatty acid metabolism mediate thyroid regulation of energy balance. Nat. Med. 16, 1001–1008. https://doi.org/10.1038/nm.2207

Lopez-Alcantara, N., Oelkrug, R., Sentis, S.C., Kirchner, H., Mittag, J., 2023. Lack of thyroid hormone receptor beta is not detrimental for non-alcoholic steatohepatitis progression. iScience 26, 108064. https://doi.org/10.1016/j.isci.2023.108064

Marcocci, C., Cetani, F., 2018. Thyrotoxicosis; Systemic Manifestations, in: Encyclopedia of Endocrine Diseases. Elsevier, pp. 665–672. https://doi.org/10.1016/B978-0-12-801238-3.96034-3

Mariash, C.N., Kaiser, F.E., Oppenheimer, J.H., 1980. Comparison of the Response Characteristics of Four Lipogenic Enzymes to 3,5,3′-Triiodothyronine Administration: Evidence for Variable Degrees of Amplification of the Nuclear 3,5,3′-Triiodothyronine Signal. Endocrinology 106, 22–27. https://doi.org/10.1210/endo-106-1-22

Marrif, H., Schifman, A., Stepanyan, Z., Gillis, M.-A., Calderone, A., Weiss, R.E., Samarut, J., Silva, J.E., 2005. Temperature Homeostasis in Transgenic Mice Lacking Thyroid Hormone Receptor-α Gene Products. Endocrinology 146, 2872–2884. https://doi.org/10.1210/en.2004-1544

Martínez-Sánchez, N., Moreno-Navarrete, J.M., Contreras, C., Rial-Pensado, E., Fernø, J., Nogueiras, R., Diéguez, C., Fernández-Real, J.-M., López, M., 2017a. Thyroid hormones induce browning of white fat. J. Endocrinol. 232, 351–362. https://doi.org/10.1530/JOE-16-0425

Martínez-Sánchez, N., Seoane-Collazo, P., Contreras, C., Varela, L., Villarroya, J., Rial-Pensado, E., Buqué, X., Aurrekoetxea, I., Delgado, T.C., Vázquez-Martínez, R., González-García, I., Roa, J., Whittle, A.J., Gomez-Santos, B., Velagapudi, V., Tung, Y.C.L., Morgan, D.A., Voshol, P.J., Martínez De Morentin, P.B., López-González, T., Liñares-Pose, L., Gonzalez, F., Chatterjee, K., Sobrino, T., Medina-Gómez, G., Davis, R.J., Casals, N., Orešič, M., Coll, A.P., Vidal-Puig, A., Mittag, J., Tena-Sempere, M., Malagón, M.M., Diéguez, C., Martínez-Chantar, M.L., Aspichueta, P., Rahmouni, K., Nogueiras, R., Sabio, G., Villarroya, F., López, M., 2017b. Hypothalamic AMPK-ER Stress-JNK1 Axis Mediates the Central Actions of Thyroid Hormones on Energy Balance. Cell Metab. 26, 212-229.e12. https://doi.org/10.1016/j.cmet.2017.06.014

Mittag, J., 2010. Cardiovascular Consequences of a Mutant Thyroid Hormone Receptor α1. Eur. Endocrinol. 6, 51–54. https://doi.org/10.17925/EE.2010.06.02.51

Mittag, J., Lyons, D.J., Sällström, J., Vujovic, M., Dudazy-Gralla, S., Warner, A., Wallis, K., Alkemade, A., Nordström, K., Monyer, H., Broberger, C., Arner, A., Vennström, B., 2013. Thyroid hormone is required for hypothalamic neurons regulating cardiovascular functions. J. Clin. Invest. 123, 509–516. https://doi.org/10.1172/JCI65252

Mota, C.M.D., Siler, D.A., Burchiel, K.J., Madden, C.J., 2023. Acute deep brain stimulation of the paraventricular nucleus of the hypothalamus increases brown adipose tissue thermogenesis in rats. Neurosci. Lett. 799, 137130. https://doi.org/10.1016/j.neulet.2023.137130

Mota-Rojas, D., Titto, C.G., Orihuela, A., Martínez-Burnes, J., Gómez-Prado, J., Torres-Bernal, F., Flores-Padilla, K., Carvajal-de la Fuente, V., Wang, D., 2021. Physiological and Behavioral Mechanisms of Thermoregulation in Mammals. Animals 11, 1733. https://doi.org/10.3390/ani11061733

Mullur, R., Liu, Y.-Y., Brent, G.A., 2014. Thyroid Hormone Regulation of Metabolism. Physiol. Rev. 94, 355–382. https://doi.org/10.1152/physrev.00030.2013

Nakamura, K., Morrison, S.F., 2011. Central efferent pathways for cold-defensive and febrile shivering. J. Physiol. 589, 3641–3658. https://doi.org/10.1113/jphysiol.2011.210047

Nappi, A., Murolo, M., Cicatiello, A.G., Sagliocchi, S., Di Cicco, E., Raia, M., Stornaiuolo, M., Dentice, M., Miro, C., 2022. Thyroid Hormone Receptor Isoforms Alpha and Beta Play Convergent Roles in Muscle Physiology and Metabolic Regulation. Metabolites 12, 405. https://doi.org/10.3390/metabo12050405

Nedergaard, J., Cannon, B., 2013. UCP1 mRNA does not produce heat. Biochim. Biophys. Acta BBA - Mol. Cell Biol. Lipids 1831, 943–949. https://doi.org/10.1016/j.bbalip.2013.01.009

Nedergaard, J., Dicker, A., Cannon, B., 1997. The Interaction between Thyroid and Brown-Fat Thermogenesis: Central or Peripheral Effects? Ann. N. Y. Acad. Sci. 813, 712–717. https://doi.org/10.1111/j.1749-6632.1997.tb51772.x

Nelson, D.L., Cox, M.M., 2001. Lehninger Biochemie, Springer-Lehrbuch. Springer Berlin Heidelberg, GER. https://doi.org/10.1007/978-3-662-08289-8

Ng, L., Rüsch, A., Amma, L.L., Nordström, K., Erway, L.C., Vennström, B., Forrest, D., 2001. Suppression of the deafness and thyroid dysfunction in Thrb-null mice by an independent mutation in the Thra thyroid hormone receptor α gene. Hum. Mol. Genet. 10, 701–2708. https://doi.org/10.1093/hmg/10.23.2701

Nicolaisen, T.S., Klein, A.B., Dmytriyeva, O., Lund, J., Ingerslev, L.R., Fritzen, A.M., Carl, C.S., Lundsgaard, A., Frost, M., Ma, T., Schjerling, P., Gerhart-Hines, Z., Flamant, F., Gauthier, K., Larsen, S., Richter, E.A., Kiens, B., Clemmensen, C., 2020. Thyroid hormone receptor α in skeletal muscle is essential for T3-mediated increase in energy expenditure. FASEB J. 34, 15480–15491. https://doi.org/10.1096/fj.202001258RR

Niedowicz, D.M., Wang, W.-X., Price, D.A., Nelson, P.T., 2021. Modulating Thyroid Hormone Levels in Adult Mice: Impact on Behavior and Compensatory Brain Changes. J. Thyroid Res. 2021, 1–13. https://doi.org/10.1155/2021/9960188

Obregon, M.-J., 2008. Thyroid Hormone and Adipocyte Differentiation. Thyroid 18, 185–195. https://doi.org/10.1089/thy.2007.0254

Oelkrug, R., Mittag, J., 2021. An improved method for the precise unravelment of non-shivering brown fat thermokinetics. Sci. Rep. 11, 4799. https://doi.org/10.1038/s41598-021-84200-1

Oppenheimer, J.H., Schwartz, H.L., 1980. Factors Determining the Level of Activity of 3,5,3-Triiodothyronine-Responsive Hepatic Enzymes in the Starved Rat. Endocrinology 107, 1460–1468. https://doi.org/10.1210/endo-107-5-1460

Ortiga-Carvalho, T.M., Shibusawa, N., Nikrodhanond, A., Oliveira, K.J., Machado, D.S., Liao, X.-H., Cohen, R.N., Refetoff, S., Wondisford, F.E., 2005. Negative regulation by thyroid hormone receptor requires an intact coactivator-binding surface. J. Clin. Invest. 115, 2517–2523. https://doi.org/10.1172/JCI24109

Ortiga-Carvalho, T.M., Sidhaye, A.R., Wondisford, F.E., 2014. Thyroid hormone receptors and resistance to thyroid hormone disorders. Nat. Rev. Endocrinol. 10, 582–591. https://doi.org/10.1038/nrendo.2014.143

Pallubinsky, H., Schellen, L., Van Marken Lichtenbelt, W.D., 2019. Exploring the human thermoneutral zone – A dynamic approach. J. Therm. Biol. 79, 199–208. https://doi.org/10.1016/j.jtherbio.2018.12.014

Paquette, M.A., Atlas, E., Wade, M.G., Yauk, C.L., 2014. Thyroid Hormone Response Element Half-Site Organization and Its Effect on Thyroid Hormone Mediated Transcription. PLoS ONE 9, e101155. https://doi.org/10.1371/journal.pone.0101155

Paxinos, G., Franklin, K.B.J., 2019. Paxinos and Franklin's: The mouse brain in stereotaxic coordinates, Fifth edition. ed. Elsevier, Academic Press, London San Diego Cambridge; MA Kidlington, Oxford.

Peterson, M.E., Daniel, R.M., Danson, M.J., Eisenthal, R., 2007. The dependence of enzyme activity on temperature: determination and validation of parameters. Biochem. J. 402, 331–337. https://doi.org/10.1042/BJ20061143

Petrovic, N., Walden, T.B., Shabalina, I.G., Timmons, J.A., Cannon, B., Nedergaard, J., 2010. Chronic peroxisome proliferator-activated receptor gamma (PPARgamma) activation of epididymally derived white adipocyte cultures reveals a population of thermogenically competent, UCP1-containing adipocytes molecularly distinct from classic brown adipocytes. J. Biol. Chem. 285, 7153–7164. https://doi.org/10.1074/jbc.M109.053942

Pfaffl, M.W., Tichopad, A., Prgomet, C., Neuvians, T.P., 2004. Determination of stable housekeeping genes, differentially regulated target genes and sample integrity: BestKeeper – Excel-based tool using pair-wise correlations. Biotechnol. Lett. 26, 509–515. https://doi.org/10.1023/B:BILE.0000019559.84305.47

Piantanida, E., Ippolito, S., Gallo, D., Masiello, E., Premoli, P., Cusini, C., Rosetti, S., Sabatino, J., Segato, S., Trimarchi, F., Bartalena, L., Tanda, M.L., 2020. The interplay between thyroid and liver: implications for clinical practice. J. Endocrinol. Invest. 43, 885–899. https://doi.org/10.1007/s40618-020-01208-6

Pilkington, A.-C., Paz, H.A., Wankhade, U.D., 2021. Beige Adipose Tissue Identification and Marker Specificity—Overview. Front. Endocrinol. 12, 599134. https://doi.org/10.3389/fendo.2021.599134

Qiao, L., Han, S.I., Fang, Y., Park, J.S., Gupta, S., Gilfor, D., Amorino, G., Valerie, K., Sealy, L., Engelhardt, J.F., Grant, S., Hylemon, P.B., Dent, P., 2003. Bile Acid Regulation of C/EBPβ, CREB, and c-Jun Function, via the Extracellular Signal-Regulated Kinase and c-Jun NH_2 -Terminal Kinase Pathways, Modulates the Apoptotic Response of Hepatocytes. Mol. Cell. Biol. 23, 3052–3066. https://doi.org/10.1128/MCB.23.9.3052-3066.2003

Rabelo, R., Schifman, A., Rubio, A., Sheng, X., Silva, J.E., 1995. Delineation of thyroid hormone-responsive sequences within a critical enhancer in the rat uncoupling protein gene. Endocrinology 136, 1003–1013. https://doi.org/10.1210/endo.136.3.7867554

Rayner, D.V., 2001. The sympathetic nervous system in white adipose tissue regulation. Proc. Nutr. Soc. 60, 357–364. https://doi.org/10.1079/PNS2001101

Rehman, G., Kumari, N., Bano, F., Tyagi, R.K., 2023. Thyroid hormone receptor beta: Relevance in human health and diseases. Endocr. Metab. Sci. 13, 100144. https://doi.org/10.1016/j.endmts.2023.100144

Rehnmark, S., Bianco, A.C., Kieffer, J.D., Silva, J.E., 1992. Transcriptional and posttranscriptional mechanisms in uncoupling protein mRNA response to cold. Am. J. Physiol. - Endocrinol. Metab. 262. https://doi.org/10.1152/ajpendo.1992.262.1.e58

Rial-Pensado, E., Canaple, L., Guyot, R., Clemmensen, C., Wiersema, J., Wu, S., Richard, S., Boelen, A., Müller, T.D., López, M., Flamant, F., Gauthier, K., 2023. Neuronal Blockade of Thyroid Hormone Signaling Increases Sensitivity to Diet-Induced Obesity in Adult Male Mice. Endocrinology 164, bqad034. https://doi.org/10.1210/endocr/bqad034

Rial-Pensado, E., Rivas-Limeres, V., Grijota-Martínez, C., Rodríguez-Díaz, A., Capelli, V., Barca-Mayo, O., Nogueiras, R., Mittag, J., Diéguez, C., López, M., 2022. Temperature modulates systemic and central actions of thyroid hormones on BAT thermogenesis. Front. Physiol. 13, 1017381. https://doi.org/10.3389/fphys.2022.1017381

Ribeiro, M.O., Bianco, S.D.C., Kaneshige, M., Schultz, J.J., Cheng, S., Bianco, A.C., Brent, G.A., 2010. Expression of Uncoupling Protein 1 in Mouse Brown Adipose Tissue Is Thyroid Hormone Receptor-β Isoform Specific and Required for Adaptive Thermogenesis. Endocrinology 151, 432–440. https://doi.org/10.1210/en.2009-0667

Ribeiro, M.O., Carvalho, S.D., Schultz, J.J., Chiellini, G., Scanlan, T.S., Bianco, A.C., Brent, G.A., 2001. Thyroid hormone–sympathetic interaction and adaptive thermogenesis are thyroid hormone receptor isoform–specific. J. Clin. Invest. 108, 97–105. https://doi.org/10.1172/JCI200112584

Ricquier, D., 2017. UCP1, the mitochondrial uncoupling protein of brown adipocyte: A personal contribution and a historical perspective. Biochimie 134, 3–8. https://doi.org/10.1016/j.biochi.2016.10.018

Ricquier, D., 2006. Fundamental mechanisms of thermogenesis. C. R. Biol. 329, 578–586. https://doi.org/10.1016/j.crvi.2005.10.010

Ricquier, D., Casteilla, L., Bouillaud, F., 1991. Molecular studies of the uncoupling protein. FASEB J. 5, 2237–2242. https://doi.org/10.1096/fasebj.5.9.1860614

Roh, E., Song, D.K., Kim, M.-S., 2016. Emerging role of the brain in the homeostatic regulation of energy and glucose metabolism. Exp. Mol. Med. 48, e216–e216. https://doi.org/10.1038/emm.2016.4

Rossi, M.A., 2023. Control of energy homeostasis by the lateral hypothalamic area. Trends Neurosci. 46, 738–749. https://doi.org/10.1016/j.tins.2023.05.010

Sabatino, L., Vassalle, C., Del Seppia, C., Iervasi, G., 2021. Deiodinases and the Three Types of Thyroid Hormone Deiodination Reactions. Endocrinol. Metab. 36, 952–964. https://doi.org/10.3803/EnM.2021.1198

Saponaro, F., Sestito, S., Runfola, M., Rapposelli, S., Chiellini, G., 2020. Selective Thyroid Hormone Receptor-Beta (TRβ) Agonists: New Perspectives for the Treatment of Metabolic and Neurodegenerative Disorders. Front. Med. 7, 331. https://doi.org/10.3389/fmed.2020.00331

Sawicka-Gutaj, N., Erampamoorthy, A., Zybek-Kocik, A., Kyriacou, A., Zgorzalewicz-Stachowiak, M., Czarnywojtek, A., Ruchała, M., 2022. The Role of Thyroid Hormones on Skeletal Muscle Thermogenesis. Metabolites 12, 336. https://doi.org/10.3390/metabo12040336

Schweizer, S., Oeckl, J., Klingenspor, M., Fromme, T., 2018. Substrate fluxes in brown adipocytes upon adrenergic stimulation and uncoupling protein 1 ablation. Life Sci. Alliance 1, e201800136. https://doi.org/10.26508/lsa.201800136

Sentis, S.C., Oelkrug, R., Mittag, J., 2021. Thyroid hormones in the regulation of brown adipose tissue thermogenesis. Endocr. Connect. 10, R106–R115. https://doi.org/10.1530/EC-20-0562

Sentis, S.C., Dore, R., Oelkrug, R., Kolms, B., Iwen, K.A., Mittag, J., 2023. Hypothalamic thyroid hormone receptor α1 signaling controls body temperature. In press.

Sepa-Kishi, D.M., Jani, S., Da Eira, D., Ceddia, R.B., 2019. Cold acclimation enhances UCP1 content, lipolysis, and triacylglycerol resynthesis, but not mitochondrial uncoupling and fat oxidation, in rat white adipocytes. Am. J. Physiol.-Cell Physiol. 316, C365–C376. https://doi.org/10.1152/ajpcell.00122.2018

Shabtai, Y., Nagaraj, N.K., Batmanov, K., Cho, Y.-W., Guan, Y., Jiang, C., Remsberg, J., Forrest, D., Lazar, M.A., 2021. A coregulator shift, rather than the canonical switch, underlies thyroid hormone action in the liver. Genes Dev. 35, 367–378. https://doi.org/10.1101/gad.345686.120

Shinde, A.B., Song, A., Wang, Q.A., 2021. Brown Adipose Tissue Heterogeneity, Energy Metabolism, and Beyond. Front. Endocrinol. 12, 651763. https://doi.org/10.3389/fendo.2021.651763

Shupnik, M.A., Chin, W.W., Habener, J.F., Ridgway, E.C., 1985. Transcriptional regulation of the thyrotropin subunit genes by thyroid hormone. J. Biol. Chem. 260, 2900–2903. https://doi.org/10.1016/S0021-9258(18)89450-9

Shupnik, M.A., Chin, W.W., Ridgway, E.C., 1989. T3 Regulation of TSH Gene Expression. Endocr. Res. 15, 579–599. https://doi.org/10.3109/07435808909036353

Silva, J.E., 2006. Thermogenic mechanisms and their hormonal regulation. Physiol. Rev. 86, 435–464. https://doi.org/10.1152/physrev.00009.2005

Silva, J.E., 2003. The thermogenic effect of thyroid hormone and its clinical implications. Ann. Intern. Med. 139, 205–213.

Silva, J.E., 2001. The multiple contributions of thyroid hormone to heat production. J. Clin. Invest. 108, 35–37. https://doi.org/10.1172/JCI13397

Silva, J.E., 1995. Thyroid hormone control of thermogenesis and energy balance. Thyroid 5, 481–492. https://doi.org/10.1089/thy.1995.5.481

Silva, J.E., Bianco, S.D.C., 2008. Thyroid–Adrenergic Interactions: Physiological and Clinical Implications. Thyroid 18, 157–165. https://doi.org/10.1089/thy.2007.0252

Silva, J.E., Larsen, P.R., 1983. Adrenergic activation of triiodothyronine production in brown adipose tissue. Nature 305, 712–713. https://doi.org/10.1038/305712a0

Sinha, R.A., Singh, B.K., Yen, P.M., 2018. Direct effects of thyroid hormones on hepatic lipid metabolism. Nat. Rev. Endocrinol. 14, 259–269. https://doi.org/10.1038/nrendo.2018.10

Sinha, S.K., Saiz, L., 2014. Determinants of protein–ligand complex formation in the thyroid hormone receptor α: A molecular dynamics simulation study. Comput. Theor. Chem. 1038, 57–66. https://doi.org/10.1016/j.comptc.2014.03.034

Sjögren, M., Alkemade, A., Mittag, J., Nordström, K., Katz, A., Rozell, B., Westerblad, H., Arner, A., Vennström, B., 2007. Hypermetabolism in mice caused by the central action of an unliganded thyroid hormone receptor α1. EMBO J. 26, 4535–4545. https://doi.org/10.1038/sj.emboj.7601882

Škop, V., Guo, J., Liu, N., Xiao, C., Hall, K.D., Gavrilova, O., Reitman, M.L., 2020a. Mouse Thermoregulation: Introducing the Concept of the Thermoneutral Point. Cell Rep. 31, 107501. https://doi.org/10.1016/j.celrep.2020.03.065

Škop, V., Liu, N., Gavrilova, O., Reitman, M., 2020b. Contribution of the mouse tail to heat dissipation. FASEB J. 34, 1–1. https://doi.org/10.1096/fasebj.2020.34.s1.03339

Smeitink, J., Van Den Heuvel, L., DiMauro, S., 2001. The genetics and pathology of oxidative phosphorylation. Nat. Rev. Genet. 2, 342–352. https://doi.org/10.1038/35072063

Soares, M.J., Müller, M.J., 2018. Resting energy expenditure and body composition: critical aspects for clinical nutrition. Eur. J. Clin. Nutr. 72, 1208–1214. https://doi.org/10.1038/s41430-018-0220-0

Soon, G.S.T., Torbenson, M., 2023. The Liver and Glycogen: In Sickness and in Health. Int. J. Mol. Sci. 24, 6133. https://doi.org/10.3390/ijms24076133

Speakman, J.R., Król, E., 2010. The Heat Dissipation Limit Theory and Evolution of Life Histories in Endotherms—Time to Dispose of the Disposable Soma Theory? Integr. Comp. Biol. 50, 793–807. https://doi.org/10.1093/icb/icq049

Sreenivasan, V.K.A., Dore, R., Resch, J., Maier, J., Dietrich, C., Henck, J., Balachandran, S., Mittag, J., Spielmann, M., 2023. Single-cell RNA-based phenotyping reveals a pivotal role of thyroid hormone receptor alpha for hypothalamic development. Development 150, dev201228. https://doi.org/10.1242/dev.201228

Steculorum, S.M., Ruud, J., Karakasilioti, I., Backes, H., Engström Ruud, L., Timper, K., Hess, M.E., Tsaousidou, E., Mauer, J., Vogt, M.C., Paeger, L., Bremser, S., Klein, A.C., Morgan, D.A., Frommolt, P., Brinkkötter, P.T., Hammerschmidt, P., Benzing, T., Rahmouni, K., Wunderlich, F.T., Kloppenburg, P., Brüning, J.C., 2016. AgRP Neurons Control Systemic Insulin Sensitivity via Myostatin Expression in Brown Adipose Tissue. Cell 165, 125–138. https://doi.org/10.1016/j.cell.2016.02.044

Sulman, F., Tal, E., Pfeifer, Y., Superstine, E., 1975. Intermittent Hyperthyreosis - a Heat Stress Syndrome. Horm. Metab. Res. 7, 424–428. https://doi.org/10.1055/s-0028-1093698

Thoonen, R., Hindle, A.G., Scherrer-Crosbie, M., 2016. Brown adipose tissue: The heat is on the heart. Am. J. Physiol.-Heart Circ. Physiol. 310, H1592–H1605. https://doi.org/10.1152/ajpheart.00698.2015

Timper, K., Brüning, J.C., 2017. Hypothalamic circuits regulating appetite and energy homeostasis: pathways to obesity. Dis. Model. Mech. 10, 679–689. https://doi.org/10.1242/dmm.026609

Tinnikov, A., Nordström, K., Thorén, P., Kindblom, J.M., Malin, S., Rozell, B., Adams, M., Rajanayagam, O., Pettersson, S., Ohlsson, C., Chatterjee, K., Vennström, B., 2002. Retardation of post-natal development caused by a negatively acting thyroid hormone receptor alpha1. EMBO J. 21, 5079–5087. https://doi.org/doi: 10.1093/emboj/cdf523

Triandafillou, J., Gwilliam, C., Himms-Hagen, J., 1982. Role of thyroid hormone in cold-induced changes in rat brown adipose tissue mitochondria. Can. J. Biochem. 60, 530–537. https://doi.org/10.1139/o82-065

Tschöp, M.H., Speakman, J.R., Arch, J.R.S., Auwerx, J., Brüning, J.C., Chan, L., Eckel, R.H., Farese, R.V., Galgani, J.E., Hambly, C., Herman, M.A., Horvath, T.L., Kahn, B.B., Kozma, S.C., Maratos-Flier, E., Müller, T.D., Münzberg, H., Pfluger, P.T., Plum, L., Reitman, M.L., Rahmouni, K., Shulman, G.I., Thomas, G., Kahn, C.R., Ravussin, E., 2012. A guide to analysis of mouse energy metabolism. Nat. Methods 9, 57–63. https://doi.org/10.1038/nmeth.1806

Van Der Meer, J., 2021. Production efficiency differences between poikilotherms and homeotherms have little to do with metabolic rate. Ecol. Lett. 24, 219–226. https://doi.org/10.1111/ele.13633

Van Marken Lichtenbelt, W.D., Schrauwen, P., 2011. Implications of nonshivering thermogenesis for energy balance regulation in humans. Am. J. Physiol.-Regul. Integr. Comp. Physiol. 301, R285–R296. https://doi.org/10.1152/ajpregu.00652.2010

Vandamme, T., 2014. Use of rodents as models of human diseases. J. Pharm. Bioallied Sci. 6, 2. https://doi.org/10.4103/0975-7406.124301

Venero, C., Guadaño-Ferraz, A., Herrero, A.I., Nordström, K., Manzano, J., De Escobar, G.M., Bernal, J., Vennström, B., 2005. Anxiety, memory impairment, and locomotor dysfunction caused by a mutant thyroid hormone receptor α1 can be ameliorated by T3 treatment. Genes Dev. 19, 2152–2163. https://doi.org/10.1101/gad.346105

Vercellino, I., Sazanov, L.A., 2022. The assembly, regulation and function of the mitochondrial respiratory chain. Nat. Rev. Mol. Cell Biol. 23, 141–161. https://doi.org/10.1038/s41580-021-00415-0

Villicev, C.M., Freitas, F.R.S., Aoki, M.S., Taffarel, C., Scanlan, T.S., Moriscot, A.S., Ribeiro, M.O., Bianco, A.C., Gouveia, C.H.A., 2007. Thyroid hormone receptor β-specific agonist GC-1 increases energy expenditure and prevents fat-mass accumulation in rats. J. Endocrinol. 193, 21–29. https://doi.org/10.1677/joe.1.07066

Virtanen, K.A., Lidell, M.E., Orava, J., Heglind, M., Westergren, R., Niemi, T., Taittonen, M., Laine, J., Savisto, N.-J., Enerbäck, S., Nuutila, P., 2009. Functional Brown Adipose Tissue in Healthy Adults. N. Engl. J. Med. 360, 1518–1525. https://doi.org/10.1056/NEJMoa0808949

Volke, L., Krause, K., 2021. Effect of Thyroid Hormones on Adipose Tissue Flexibility. Eur. Thyroid J. 1, 1–9. https://doi.org/10.1159/000508483

Vujovic, M., Nordström, K., Gauthier, K., Flamant, F., Visser, T.J., Vennström, B., Mittag, J., 2009. Interference of a Mutant Thyroid Hormone Receptor α1 with Hepatic Glucose Metabolism. Endocrinology 150, 2940–2947. https://doi.org/10.1210/en.2008-1085

Wallis, K., Sjögren, M., Van Hogerlinden, M., Silberberg, G., Fisahn, A., Nordström, K., Larsson, L., Westerblad, H., Morreale De Escobar, G., Shupliakov, O., Vennström, B., 2008. Locomotor Deficiencies and Aberrant Development of Subtype-Specific GABAergic Interneurons Caused by an Unliganded Thyroid Hormone Receptor α1. J. Neurosci. 28, 1904–1915. https://doi.org/10.1523/JNEUROSCI.5163-07.2008

Wang, D., Tai, P.W.L., Gao, G., 2019. Adeno-associated virus vector as a platform for gene therapy delivery. Nat. Rev. Drug Discov. 18, 358–378. https://doi.org/10.1038/s41573-019-0012-9

Warner, A., Mittag, J., 2012. Thyroid hormone and the central control of homeostasis. J. Mol. Endocrinol. 49, R29–R35. https://doi.org/10.1530/JME-12-0068

Warner, A., Rahman, A., Solsjö, P., Gottschling, K., Davis, B., Vennström, B., Arner, A., Mittag, J., 2013. Inappropriate heat dissipation ignites brown fat thermogenesis in mice with a mutant thyroid hormone receptor α. Proc. Natl. Acad. Sci. 110, 16241–16246. https://doi.org/doi/10.1073/pnas.1310300110

Watanabe, M., Houten, S.M., Mataki, C., Christoffolete, M.A., Kim, B.W., Sato, H., Messaddeq, N., Harney, J.W., Ezaki, O., Kodama, T., Schoonjans, K., Bianco, A.C., Auwerx, J., 2006. Bile acids induce energy expenditure by promoting intracellular thyroid hormone activation. Nature 439, 484–489. https://doi.org/10.1038/nature04330

Weiner, J., Kranz, M., Klöting, N., Kunath, A., Steinhoff, K., Rijntjes, E., Köhrle, J., Zeisig, V., Hankir, M., Gebhardt, C., Deuther-Conrad, W., Heiker, J.T., Kralisch, S., Stumvoll, M., Blüher, M., Sabri, O., Hesse, S., Brust, P., Tönjes, A., Krause, K., 2016. Thyroid hormone status defines brown adipose tissue activity and browning of white adipose tissues in mice. Sci. Rep. 6, 38124. https://doi.org/10.1038/srep38124

Weiss, R.E., Murata, Y., Cua, K., Hayashi, Y., Seo, H., Refetoff, S., 1998. Thyroid Hormone Action on Liver, Heart, and Energy Expenditure in Thyroid Hormone Receptor β-Deficient Mice. Endocrinology 139, 4945–4952. https://doi.org/10.1210/endo.139.12.6412

Werneck De Castro, J.P., Fonseca, T.L., Ueta, C.B., McAninch, E.A., Abdalla, S., Wittmann, G., Lechan, R.M., Gereben, B., Bianco, A.C., 2015. Differences in hypothalamic type 2 deiodinase ubiquitination explain localized sensitivity to thyroxine. J. Clin. Invest. 125, 769–781. https://doi.org/10.1172/JCI77588

Wicksteed, B., Dickson, L.M., 2017. PKA Differentially Regulates Adipose Depots to Control Energy Expenditure. Endocrinology 158, 464–466. https://doi.org/10.1210/en.2017-00038

Xu, Y., Xue, D., Bankhead, A., Neamati, N., 2020. Why All the Fuss about Oxidative Phosphorylation (OXPHOS)? J. Med. Chem. 63, 14276–14307. https://doi.org/10.1021/acs.jmedchem.0c01013

Yaguchi, M., Ohashi, Y., Tsubota, T., Sato, A., Koyano, K.W., Wang, N., Miyashita, Y., 2013. Characterization of the Properties of Seven Promoters in the Motor Cortex of Rats and Monkeys After Lentiviral Vector-Mediated Gene Transfer. Hum. Gene Ther. Methods 24, 333–344. https://doi.org/10.1089/hgtb.2012.238

Yau, W.W., Yen, P.M., 2020. Thermogenesis in Adipose Tissue Activated by Thyroid Hormone. Int. J. Mol. Sci. 21, 3020. https://doi.org/10.3390/ijms21083020

Yen, P.M., 2001. Physiological and Molecular Basis of Thyroid Hormone Action. Physiol. Rev. 81, 1097–1142. https://doi.org/10.1152/physrev.2001.81.3.1097

Zekri, Y., Guyot, R., Flamant, F., 2022a. An Atlas of Thyroid Hormone Receptors' Target Genes in Mouse Tissues. Int. J. Mol. Sci. 23, 11444. https://doi.org/10.3390/ijms231911444

Zekri, Y., Guyot, R., Suñer, I.G., Canaple, L., Stein, A.G., Petit, J.V., Aubert, D., Richard, S., Flamant, F., Gauthier, K., 2022b. Brown adipocytes local response to thyroid hormone is required for adaptive thermogenesis in adult male mice. eLife 11, e81996. https://doi.org/10.7554/eLife.81996

Zhang, W., Bi, S., 2015. Hypothalamic Regulation of Brown Adipose Tissue Thermogenesis and Energy Homeostasis. Front. Endocrinol. 6. https://doi.org/10.3389/fendo.2015.00136

Zhang, Z., Boelen, A., Kalsbeek, A., Fliers, E., 2018. TRH Neurons and Thyroid Hormone Coordinate the Hypothalamic Response to Cold. Eur. Thyroid J. 7, 279–288. https://doi.org/10.1159/000493976

Zhao, J., Cannon, B., Nedergaard, J., 1997. α1-Adrenergic Stimulation Potentiates the Thermogenic Action of β3-Adrenoreceptor-generated cAMP in Brown Fat Cells. J. Biol. Chem. 272, 32847–32856. https://doi.org/10.1074/jbc.272.52.32847

Zhao, Z.-D., Yang, W.Z., Gao, C., Fu, X., Zhang, W., Zhou, Q., Chen, W., Ni, X., Lin, J.-K., Yang, J., Xu, X.-H., Shen, W.L., 2017. A hypothalamic circuit that controls body temperature. Proc. Natl. Acad. Sci. 114, 2042–2047. https://doi.org/10.1073/pnas.1616255114

Appendix

Statistical analysis

Physiological data and expression data from section 3.1, 3.2, and 3.3 were analyzed using 2-way ANOVA and unpaired student's t-tests (Supplementary Table 1). The used post-hoc tests can also be found in Supplementary Table 1, whereas post hoc test results can be found in the respective figures.

Supplementary Table 1: Statistical tests and the respective p values. Post hoc test results can be found in the respective figures. Parts of the data have been submitted to a peer-reviewed journal due to priority reasons (Sentis et al., 2023 in press).

Figure	**Genotype**	**Statistical test**		
Figure 7A	TRα1+m&TRβ KO vs. wt	2-way ANOVA, post hoc: Dunnett's multiple comparison		
		Interaction	Genotype	Time
		F (22, 253) = 2.113 P=0.0032	F (2, 23) = 7.397 P=0.0033	F (11, 253) = 37.41 P<0.0001
Figure 7B	TRα1+m&TRβ KO vs. wt	2-way ANOVA, post hoc: Dunnett's multiple comparison		
		Interaction	Genotype	Time
		F (22, 253) = 5.254 P<0.0001	F (2, 23) = 2.171 P=0.1368	F (11, 253) = 76.00 P<0.0001
Figure 7C	TRα1+m&TRβ KO vs. wt	2-way ANOVA, post hoc: Dunnett's multiple comparison		
		Interaction	Genotype	Time
		F (22, 121) = 1.477 P=0.0947	F (2, 11) = 0.7020 P=0.5165	F (11, 121) = 27.53 P<0.0001
Figure 8B	TRα1+m&TRβ KO vs. wt	2-way ANOVA, post hoc: Šídák's multiple comparison		
		Interaction	Genotype	Time
		F (2, 13) = 1.297 P=0.3064	F (2, 13) = 2.330 P=0.1365	F (1, 13) = 29.06 P=0.0001
Figure 9A	TRα1+m&TRβ KO vs. wt	Unpaired Student´s t-test		
TRβ KO vs. wt		Df	t	P value
		8.00	2.622	0.030538
TRα1+m vs. wt		Df	t	P value
		10.00	2.482	0.032444

Figure	**Genotype**	**Statistical test**		
Figure 9C	TRα1+m&TRβ KO vs. wt	2-way ANOVA, post hoc: Bonferroni's multiple comparison		
		Interaction	Genotype	Time
		F (2, 12) = 16.87 P=0.0003	F (2, 12) = 5.101 P=0.0249	F (1, 12) = 47.04 P<0.0001
Figure 9D	TRα1+m&TRβ KO vs. wt	2-way ANOVA, post hoc: Bonferroni's multiple comparison		
		Interaction	Genotype	Time
		F (2, 12) = 0.5740 P=0.5780	F (2, 12) = 2.091 P=0.1663	F (1, 12) = 8.072 P=0.0149
Figure 10A	TRα1+m&TRβ KO vs. wt	2-way ANOVA, post hoc: Dunnett's multiple comparison		
		Interaction	Genotype	Time
		F (20, 150) = 2.636 P=0.0005	F (2, 15) = 29.79 P<0.0001	F (10, 150) = 10.51 P<0.0001
Figure 10B	TRα1+m&TRβ KO vs. wt	2-way ANOVA, post hoc: Dunnett's multiple comparison		
		Interaction	Genotype	Time
		F (20, 143) = 3.077 <0.0001	F (2, 15) = 27.03 <0.0001	F (10, 143) = 10.51 <0.0001
Figure 10C	TRα1+m&TRβ KO vs. wt	2-way ANOVA, post hoc: Dunnett's multiple comparison		
		Interaction	Genotype	Time
		F (20, 150) = 1.117 P=0.3383	F (2, 15) = 0.05501 P=0.9467	F (10, 150) = 2.827 P=0.0030
Figure 10D	TRα1+m&TRβ KO vs. wt	2-way ANOVA, post hoc: Dunnett's multiple comparison		
		Interaction	Genotype	Time
		F (20, 150) = 1.247 P=0.2248	F (2, 15) = 1.768 P=0.2044	F (10, 150) = 3.184 P=0.0010
Figure 10F	TRα1+m&TRβ KO vs. wt	Unpaired Student´s t-test		
TRβ KO vs. wt		Df	t	P value
		4.00	0.7754	0.4814
TRα1+m vs. wt		Df	t	P value
		5.00	2.273	0.0721

Figure	**Genotype**		**Statistical test**		
Figure 11A	TRα1+m&TRβ KO vs. wt		Unpaired Student´s t-test		
TRβ KO vs. wt		Gene	Df	t	P value
		Ucp1	8.00	2.104	0.068492
		Dio2	8.00	2.716	0.026419
		Adra1a	8.00	0.2892	0.779770
		Adrb2	8.00	0.3963	0.702278
		Adrb3	8.00	7.113	0.000101
		Cidea	8.00	1.287	0.234136
		Prdm16	8.00	1.503	0.171237
		Ppargc1a	8.00	6.563	0.000176
TRα1+m vs. wt		Gene	Df	t	P value
		Ucp1	10.00	2.104	0.023545
		Dio2	10.00	2.716	0.007512
		Adra1a	10.00	0.2892	0.668576
		Adrb2	10.00	0.3963	0.730414
		Adrb3	10.00	7.113	0.001240
		Prdm16	10.00	1.503	0.385226
		Cidea	10.00	1.287	0.704883
		Ppargc1a	10.00	6.563	0.049747
Figure 11B	TRα1+m&TRβ KO vs. wt		Unpaired Student´s t-test		
TRβ KO vs. wt		Gene	Df	t	P value
		Ucp1	9.00	1.054	0.319176
		Dio2	9.00	1.239	0.246788
		Adra1a	9.00	1.481	0.172647
		Adrb2	8.00	1.109	0.299563
		Adrb3	9.00	1.823	0.101608
		Cidea	9.00	1.271	0.235720
		Prdm16	8.00	3.807	0.005188
		Ppargc1a	9.00	1.057	0.318168
TRα1+m vs. wt		Gene	Df	t	P value
		Ucp1	11.00	1.676	0.121979
		Dio2	11.00	1.411	0.185909
		Adra1a	11.00	1.620	0.133479
		Adrb2	10.00	0.1276	0.900996
		Adrb3	11.00	0.8495	0.413729
		Prdm16	10.00	1.524	0.158406
		Cidea	10.00	0.1842	0.857500
		Ppargc1a	11.00	0.1405	0.890818
Figure 11C	TRα1+m&TRβ KO vs. wt		Unpaired Student´s t-test		
TRβ KO vs. wt		Gene	Df	t	P value
		Ucp1	9.00	1.767	0.111065
		Dio2	9.00	0.9806	0.352421
		Adra1a	9.00	1.129	0.287940
		Adrb2	9.00	0.6527	0.530243
		Adrb3	9.00	0.7866	0.451705

Figure	**Genotype**		**Statistical test**		
Figure 11C	TRα1+m&TRβ KO vs. wt		Unpaired Student´s t-test		
TRβ KO vs. wt		Gene	Df	t	P value
		Cidea	9.00	2.252	0.050842
		Prdm16	9.00	0.1915	0.852362
		Ppargc1a	9.00	2.027	0.073291
TRα1+m vs. wt		Gene	Df	t	P value
		Ucp1	11.00	0.2730	0.789889
		Dio2	11.00	1.203	0.254144
		Adra1a	11.00	1.114	0.289040
		Adrb2	11.00	2.090	0.060596
		Adrb3	11.00	2.614	0.024103
		Prdm16	11.00	0.4957	0.629872
		Cidea	11.00	1.068	0.308335
		Ppargc1a	11.00	0.9009	0.386949
Figure 11D	TRα1+m&TRβ KO vs. wt		Unpaired Student´s t-test		
TRβ KO vs. wt		Gene	Df	t	P value
		Pomc	9.00	0.9331	0.375130
		Npy	9.00	2.097	0.065451
		Lpl	9.00	2.585	0.029440
		Dio3	9.00	2.078	0.067487
		Dio2	9.00	2.753	0.022360
		Adrb2	9.00	4.663	0.001180
		Hcrt	9.00	2.382	0.041070
		Klf9	9.00	1.980	0.079062
TRα1+m vs. wt		Gene	Df	t	P value
		Pomc	9.00	0.3313	0.746626
		Npy	9.00	1.572	0.144311
		Lpl	9.00	0.8844	0.395409
		Dio3	9.00	2.205	0.049621
		Dio2	9.00	1.185	0.260939
		Adrb2	9.00	0.4233	0.680242
		Hcrt	9.00	0.1004	0.921827
		Klf9	9.00	3.048	0.011088
Figure 11E	TRα1+m&TRβ KO vs. wt		Unpaired Student´s t-test		
TRβ KO vs. wt		Gene	Df	t	P value
		Gk	9.00	10.18	0.000003
		Pck1	9.00	4.540	0.001406
		Dio1	9.00	10.55	0.000002
		Gys	9.00	5.403	0.000431
		Thrb	9.00	11.77	<0.000001
		Fasn	9.00	2.443	0.037186
		Thrsp	9.00	2.489	0.034488
		Cd5l	9.00	2.851	0.019051

Figure	**Genotype**		**Statistical test**		
Figure 11E	TRα1+m&TRβ KO vs. wt		Unpaired Student´s t-test		
TRα1+m vs. wt		Gene	Df	t	P value
		Gk	9.00	0.1340	0.895847
		Pck1	9.00	1.101	0.294393
		Dio1	9.00	0.4149	0.686224
		Gys	9.00	0.7233	0.484606
		Thrb	9.00	0.5880	0.568408
		Fasn	9.00	1.249	0.237523
		Thrsp	9.00	0.4021	0.695341
		Cd5l	9.00	0.3024	0.768017
Figure 12B	TRα1+m&TRβ KO vs. wt		Unpaired Student´s t-test		
	UCP1 TRβ KO vs. wt		Df	t	P value
			9.00	1.313	0.2217
	UCP1 TRα1+m vs. wt		Df	t	P value
			10.00	0.2805	0.7848
Figure 12C	TRα1+m&TRβ KO vs. wt		Unpaired Student´s t-test		
	OXPHOS Complexes TRβ KO vs. wt		Df	t	P value
	V		9.00	1.794	0.106351
	III		9.00	1.299	0.226302
	IV		9.00	3.975	0.003228
	II		9.00	3.703	0.004898
	I		9.00	6.981	0.000065
	OXPHOS Complexes TRα1+m vs. wt		Df	t	P value
	V		10.00	1.821	0.098567
	III		10.00	3.262	0.008547
	IV		10.00	0.7560	0.467062
	II		10.00	0.3429	0.738791
	I		10.00	2.668	0.023587
Figure 13	TRα1+m&TRβ KO vs. wt		Unpaired Student´s t-test		
	TRβ KO vs. wt		Df	t	P value
			7.00	4.857	0.0018
	TRα1+m vs. wt		Df	t	P value
			9.00	0.8573	0.4135
Figure 15B	DomNegTRα1 vs. cntrl		Unpaired Student´s t-test		
T3			Df	t	P value
			10.00	1.512	0.1616
T4			Df	t	P value
			11.00	1.492	0.1638
fT4			Df	t	P value
			7.00	2.177	0.0660

Figure	**Genotype**	**Statistical test**		
Figure 16A	DomNegTRα1 vs. cntrl	2-way ANOVA, post hoc: Bonferroni's multiple comparison		
		Interaction	Genotype	Time
		F (7, 77) = 7.077 P<0.0001	F (1, 11) = 11.94 P=0.0054	F (7, 77) = 5.031 P<0.0001
Figure 16B	DomNegTRα1 vs. cntrl	Unpaired Student´s t-test		
Food Intake		Df	t	P value
		11.00	0.9028	0.385954
Water Intake		Df	t	P value
		11.00	1.182	0.262124
Figure 16C	DomNegTRα1 vs. cntrl	Unpaired Student´s t-test		
Food Intake		Df	t	P value
		11.00	1.958	0.076098
Water Intake		Df	t	P value
		11.00	0.009531	0.992566
Figure 17B	DomNegTRα1 vs. cntrl	Unpaired Student´s t-test		
RQ Day		Df	t	P value
		11.00	0.8573	0.409544
RQ Night		Df	t	P value
		11.00	0.4147	0.686342
Figure 17C	DomNegTRα1 vs. cntrl	Unpaired Student´s t-test		
		Df	t	P value
		11.00	2.630	0.0234
Figure 17D	DomNegTRα1 vs. cntrl	Simple linear regression		
		Slope	Y-intercept	
		2.614	-15.13	
Figure 17F	DomNegTRα1 vs. cntrl	Unpaired Student´s t-test		
Oxygen Consumption Day		Df	t	P value
		11.00	1.837	0.093296
Oxygen Consumption Night		Df	t	P value
		10.00	1.649	0.127472
Figure 17G	DomNegTRα1 vs. cntrl	Simple linear regression		
		Slope	Y-intercept	
		0.5632	1.998	
Figure 17H	DomNegTRα1 vs. cntrl	Simple linear regression		
		Slope	Y-intercept	
		0.6791	2.849	

Figure	**Genotype**	**Statistical test**		
Figure 17I	DomNegTRα1 vs. cntrl	Unpaired Student´s t-test		
EE Day		Df	t	P value
		11.00	1.899	0.084092
EE Night		Df	t	P value
		11.00	1.548	0.149906
Figure 17J	DomNegTRα1 vs. cntrl	2-way ANOVA, post hoc: Šídák's multiple comparison		
		Interaction	Genotype	Time
		F (21, 231) = 1.845 P=0.0157	F (1, 11) = 3.905 P=0.0738	F (4.758, 52.34) = 32.86 P<0.0001
Figure 17K	DomNegTRα1 vs. cntrl	Unpaired Student´s t-test		
		Df	t	P value
		11.00	0.9611	0.3572
Figure 17L	DomNegTRα1 vs. cntrl	2-way ANOVA, post hoc: Šídák's multiple comparison		
		Interaction	Genotype	Time
		F (25, 275) = 0.9333 P=0.5590	F (1, 11) = 0.02224 P=0.8842	F (6.138, 67.52) = 24.64 P<0.0001
Figure 17M	DomNegTRα1 vs. cntrl	Unpaired Student´s t-test		
		Df	t	P value
		11.00	0.05459	0.9574
Figure 18A	DomNegTRα1 vs. cntrl	2-way ANOVA, post hoc: Šídák's multiple comparison		
		Interaction	Genotype	Time
		F (11, 121) = 2.374 P=0.0108	F (1, 11) = 16.10 P=0.0020	F (11, 121) = 13.70 P<0.0001
Figure 18B	DomNegTRα1 vs. cntrl	2-way ANOVA, post hoc: Šídák's multiple comparison		
		Interaction	Genotype	Time
		F (11, 121) = 1.706 P=0.0797	F (1, 11) = 8.275 P=0.0151	F (11, 121) = 22.54 P<0.0001
Figure 18C	DomNegTRα1 vs. cntrl	Unpaired Student´s t-test		
22°C		Df	t	P value
		11.00	3.410	0.005821
30°C		Df	t	P value
		11.00	4.215	0.001448
10°C		Df	t	P value
		11.00	1.651	0.126991

Figure	**Genotype**	**Statistical test**		
Figure 18E	DomNegTRα1 vs. cntrl	Unpaired Student´s t-test		
BAT Abs.		Df	t	P value
		11.00	1.800	0.099352
Tail Abs.		Df	t	P value
		11.00	0.6863	0.506712
Figure 18E	DomNegTRα1 vs. cntrl	Unpaired Student´s t-test		
BAT Norm.		Df	t	P value
		11.00	3.738	0.003276
Tail Norm.		Df	t	P value
		11.00	1.253	0.236287
Figure 19A	DomNegTRα1 vs. cntrl	Unpaired Student´s t-test		
	Gene	Df	t	P value
	Ucp1	11.00	0.6704	0.516419
	Dio2	11.00	0.6423	0.533817
	Adra1a	11.00	0.1259	0.902048
	Adrb2	11.00	0.9813	0.347535
	Adrb3	11.00	0.5938	0.564679
	Cidea	11.00	1.974	0.073974
	Prdm16	11.00	0.8486	0.414212
	Ppargc1a	11.00	1.842	0.092629
	Pparg	11.00	0.9758	0.350128
Figure 19B	DomNegTRα1 vs. cntrl	Unpaired Student´s t-test		
	Gene	Df	t	P value
	Adrb3	11.00	0.04867	0.962051
	Cidea	11.00	1.072	0.306790
	Prdm16	11.00	1.195	0.257113
	Fasn	11.00	0.4322	0.673941
Figure 19C	DomNegTRα1 vs. cntrl	Unpaired Student´s t-test		
	Gene	Df	t	P value
	Ucp1	11.00	1.093	0.297775
	Dio2	11.00	0.5284	0.607702
	Adrb3	11.00	0.6257	0.544255
	Cidea	11.00	0.5953	0.563713
	Prdm16	11.00	1.720	0.113364
	Fasn	11.00	0.2136	0.834798
Figure 19D	DomNegTRα1 vs. cntrl	Unpaired Student´s t-test		
	Gene	Df	t	P value
	Gk	11.00	1.559	0.147201
	Pck1	11.00	2.306	0.041615
	Dio1	11.00	2.034	0.066821
	Gys	11.00	0.6826	0.508986
	Thrb	11.00	0.4240	0.679724
	Fasn	11.00	2.332	0.039700

Figure	**Genotype**		**Statistical test**		
Figure 19D	DomNegTRα1 vs. cntrl		Unpaired Student´s t-test		
		Gene	Df	t	P value
		Thrsp	11.00	0.1945	0.849313
		Cd5l	11.00	0.06960	0.945758
		Fgf21	11.00	0.3616	0.724489
Figure 19E	DomNegTRα1 vs. cntrl		Unpaired Student´s t-test		
		Gene	Df	t	P value
		Myh1	11.00	1.206	0.252962
		Myh4	11.00	2.181	0.051749
		Gpd2	11.00	2.808	0.017041
		Atp2a1	11.00	3.819	0.002849
		Atp2a2	11.00	2.204	0.049753
		Ucp3	11.00	0.7991	0.441151
		Ryr1	11.00	1.089	0.299401
		Sln	11.00	0.3321	0.746022
		Mstn	11.00	2.537	0.027629
Figure 19F	DomNegTRα1 vs. cntrl		Unpaired Student´s t-test		
		Gene	Df	t	P value
		Myh1	11.00	0.6656	0.519370
		Myh4	11.00	0.7218	0.485501
		Gpd2	11.00	1.069	0.308043
		Atp2a1	11.00	0.4788	0.641465
		Atp2a2	11.00	1.132	0.281751
		Ucp3	11.00	0.4079	0.691207
		Ryr1	11.00	0.9762	0.349944
		Sln	11.00	0.7500	0.469010
		Mstn	11.00	0.09354	0.927156
Figure 20A	DomNegTRα1 vs. cntrl		Unpaired Student´s t-test		
			Df	t	P value
			11.00	0.3956	0.7
Figure 20B	DomNegTRα1 vs. cntrl		Unpaired Student´s t-test		
			Df	t	P value
			11.00	0.5377	0.6015
Figure 20C	DomNegTRα1 vs. cntrl		Unpaired Student´s t-test		
			Df	t	P value
			11.00	2.019	0.0685
Figure 20D	DomNegTRα1 vs. cntrl		Unpaired Student´s t-test		
			Df	t	P value
			11.00	0.8989	0.3898

Figure	Genotype	Statistical test		
Figure 20E	DomNegTRα1 vs. cntrl	Unpaired Student´s t-test		
		Df	t	P value
		11.00	0.3012	0.7689
Figure 21B	DomNegTRα1 vs. cntrl	Unpaired Student´s t-test		
	SERCA2	Df	t	P value
		11.00	0.1333	0.8964
Figure 21C	DomNegTRα1 vs. cntrl	Unpaired Student´s t-test		
	OXPHOS Complexes	Df	t	P value
	V	11.00	0.6189	0.548559
	III	11.00	0.5527	0.591521
	IV	11.00	0.5947	0.564074
	II	11.00	0.5359	0.602676
	I	11.00	1.244	0.239516
Figure 22A	DomNegTRα1 vs. cntrl	Unpaired Student´s t-test		
HR		Df	t	P value
		11.00	0.9353	0.3697
Figure 22B	DomNegTRα1 vs. cntrl	Unpaired Student´s t-test		
HRV		Df	t	P value
		11.00	0.1163	0.9095
Figure 22C	DomNegTRα1 vs. cntrl	Unpaired Student´s t-test		
R		Df	t	P value
		11.00	2.020	0.0685
Figure 22D	DomNegTRα1 vs. cntrl	Unpaired Student´s t-test		
Heart Weight		Df	t	P value
		11.00	0.6130	0.5524
Figure 22E	DomNegTRα1 vs. cntrl	Unpaired Student´s t-test		
	Complex name	Df	t	P value
	RR	11.000	1.020	0.329433
	PQ	11.000	1.998	0.071015
	PR	11.000	1.956	0.076287
	QRS	11.000	0.6589	0.523534
	QT	11.000	1.13	0.282380
	ST	11.000	1.178	0.263513
	QTC	11.000	0.8869	0.394131
	rMSSD	11.000	0.8956	0.389633
Figure 23B	T4-treated rats vs. control	Unpaired Student´s t-test		
	UCP1	Df	t	P value
		14.00	1.361	0.1951

Figure	**Genotype**	**Statistical test**		
Figure 23C	T4-treated rats vs. control	Unpaired Student´s t-test		
	OXPHOS Complexes	Df	t	P value
	V	14.00	3.515	0.003431
	III	14.00	0.6298	0.538991
	IV	14.00	1.348	0.199028
	II	14.00	1.117	0.282848
	I	14.00	0.9928	0.337637
Figure 23D	DomNegTRα1 vs. cntrl	Unpaired Student´s t-test		
	Gene	Df	t	P value
	Ucp1	14.00	0.9014	0.382600
	Adrb3	14.00	2.166	0.048065
	Dio2	14.00	1.486	0.159420
Figure 27A	Primary rat iBAT cells	2-way ANOVA, post hoc: Tukey's multiple comparison		
Gene	*Adrb3*	Interaction	b-CL treatment	T3 treatment
		F (3, 31) = 0.5143 P=0.6755	F (1, 31) = 9.927 P=0.0036	F (3, 31) = 0.9767 P=0.4163
Figure 27B	Primary rat iBAT cells	2-way ANOVA, post hoc: Tukey's multiple comparison		
Gene	*Adra1a*	Interaction	b-CL treatment	T3 treatment
		F (3, 29) = 0.3815 P=0.7671	F (1, 29) = 0.4615 P=0.5023	F (3, 29) = 0.4054 P=0.7503
Figure 27C	Primary rat iBAT cells	2-way ANOVA, post hoc: Tukey's multiple comparison		
Gene	*Dio2*	Interaction	b-CL treatment	T3 treatment
		F (3, 27) = 0.2643 P=0.8505	F (1, 27) = 0.9578 P=0.3364	F (3, 27) = 3.456 P=0.0302
Figure 27D	Primary rat iBAT cells	2-way ANOVA, post hoc: Tukey's multiple comparison		
Gene	*Ucp1*	Interaction	b-CL treatment	T3 treatment
		F (3, 28) = 0.4092 P=0.7476	F (1, 28) = 11.73 P=0.0019	F (3, 28) = 2.631 P=0.0696
Figure 28A	Primary rat iWAT cells	2-way ANOVA, post hoc: Tukey's multiple comparison		
Gene	*Adrb3*	Interaction	b-CL treatment	T3 treatment
		F (3, 24) = 0.2076 P=0.8901	F (1, 24) = 60.70 P<0.0001	F (3, 24) = 0.2266 P=0.8770
Figure 28B	Primary rat iWAT cells	2-way ANOVA, post hoc: Tukey's multiple comparison		
Gene	*Adra1a*	Interaction	b-CL treatment	T3 treatment
		F (3, 24) = 0,9274 P=0.4426	F (1, 24) = 0.07571 P=0.7856	F (3, 24) = 0.2059 P=0.8913

Figure	**Genotype**		**Statistical test**		
Figure 28C	Primary rat iWAT cells		2-way ANOVA, post hoc: Tukey's multiple comparison		
Gene		*Dio2*	Interaction	b-CL treatment	T3 treatment
			F (3, 24) = 1.378 P=0.2734	F (1, 24) = 6.707 P=0.0161	F (3, 24) = 2.683 P=0.0694
Figure 28D	Primary rat iWAT cells		2-way ANOVA, post hoc: Tukey's multiple comparison		
Gene		*Ucp1*	Interaction	b-CL treatment	T3 treatment
			F (3, 24) = 1.337 P=0.2858	F (1, 24) = 7.401 P=0.0119	F (3, 24) = 2.878 P=0.0570
Figure 29A	Primary mouse iBAT cells		2-way ANOVA, post hoc: Tukey's multiple comparison		
Gene		*Adrb3*	Interaction	b-CL treatment	T3 treatment
			F (3, 24) = 2.339 P=0.0988	F (1, 24) = 76.09 P<0.0001	F (3, 24) = 2.103 P=0.1264
Figure 29B	Primary mouse iBAT cells		2-way ANOVA, post hoc: Tukey's multiple comparison		
Gene		*Adra1a*	Interaction	b-CL treatment	T3 treatment
			F (3, 24) = 0.05244 P=0.9838	F (1, 24) = 5.112 P=0.0331	F (3, 24) = 0.3491 P=0.7901
Figure 29C	Primary mouse iBAT cells		2-way ANOVA, post hoc: Tukey's multiple comparison		
Gene		*Dio2*	Interaction	b-CL treatment	T3 treatment
			F (3, 24) = 1.120 P=0.3604	F (1, 24) = 18.41 P=0.0003	F (3, 24) = 0.7720 P=0.5210
Figure 29D	Primary mouse iBAT cells		2-way ANOVA, post hoc: Tukey's multiple comparison		
Gene		*Ucp1*	Interaction	b-CL treatment	T3 treatment
			F (3, 24) = 0.3640 P=0.7795	F (1, 24) = 117.8 P<0.0001	F (3, 24) = 1.122 P=0.3600
Figure 30A	Primary mouse iWAT cells		2-way ANOVA, post hoc: Tukey's multiple comparison		
Gene		*Adrb3*	Interaction	b-CL treatment	T3 treatment
			F (3, 24) = 0.9464 P=0.4338	F (1, 24) = 45.44 P<0.0001	F (3, 24) = 1.025 P=0.3991
Figure 30B	Primary mouse iWAT cells		2-way ANOVA, post hoc: Tukey's multiple comparison		
Gene		*Adra1a*	Interaction	b-CL treatment	T3 treatment
			F (3, 24) = 0.5178 P=0.6740	F (1, 24) = 4.076 P=0.0548	F (3, 24) = 0.08770 P=0.9661

Figure	**Genotype**		**Statistical test**		
Figure 30C	Primary mouse iWAT cells		2-way ANOVA, post hoc: Tukey's multiple comparison		
Gene		*Dio2*	Interaction	b-CL treatment	T3 treatment
			F (3, 23) = 0.07064 P=0.9751	F (1, 23) = 1.004 P=0.3268	F (3, 23) = 3.623 P=0.0282
Figure 30D	Primary mouse iWAT cells		2-way ANOVA, post hoc: Tukey's multiple comparison		
Gene		*Ucp1*	Interaction	b-CL treatment	T3 treatment
			F (3, 24) = 1.046 P=0.3904	F (1, 24) = 10.56 P=0.0034	F (3, 24) = 2.152 P=0.1201

Abbreviations in Supplementary Table 1: TRα1 = Thyroid hormone receptor α1; TRβ KO = Thyroid hormone receptor β knockout; wt = Wildtype; ANOVA = Analysis of variance; Df = Degrees of freedom; DomNegTRα1 = Dominant-negative TRα1; cntrl = Control; RQ = Respiratory quotient; EE = Energy expenditure; BAT Abs. = Absolute brown adipose tissue temperature; BAT Norm. = Normalized brown adipose tissue temperature; Tail Abs. = Absolute tail temperature; Tail Norm. = Normalized tail temperature; HR = Heart rate; HRV = Heart rate variability; R = R Amplitude; iBAT = Interscapular brown adipose tissue; iWAT = Interscapular white adipose tissue.

Acknowledgements

As the completion of scientific research projects and resulting publications are always the work of many, I would like to express my appreciation to a group of people that have supported me throughout my PhD journey.

First, I am immensely thankful to my supervisor Prof. Jens Mittag for his exceptional mentorship, constant encouragement, and trust throughout the last 3.5 years that flew by so fast. Your guidance has been instrumental to my academic growth and the successful completion of this PhD project.

Second, I am grateful to the entire “Adipocyte-Brain-Crosstalk” consortium (DFG-funded *Graduiertenkolleg* “GRK1957”), especially to Prof. Henrik Oster, my co-supervisors Dr. Helge Müller-Fielitz and Dr. Alexander Iwen, and my GRK mentor Prof. Jonas Obleser, for providing the opportunity to conduct research in a supportive and intellectually stimulating research environment.

Thirdly, my appreciation goes to Prof. Jan-Wilhelm Kornfeld and Hande Topel Batarlar (PhD), for the invaluable support during my stay at the University of Southern Denmark (SDU) as a visiting PhD student. Your expertise and willingness to share insights have been instrumental in shaping the direction of my future research.

Another special thanks is dedicated to Prof. Miguel López for his generosity in sharing murine samples and to Berenike Soehl (MSc) for helping me to conduct parts of the *in vitro* studies.

I would also like to express my appreciation to the entire *AG Mittag* for creating a cheerful, supportive, and collaborative environment that made saying *goodbye* so hard. A special thanks goes to Dr. Rebecca Oelkrug and Dr. Riccardo Dore for always having an open ear and for sharing your expertise in mouse physiology.

Lastly, I would like to thank all the people closest to me for supporting me throughout my academic journey. Thanks to all friends, family, and to my parents and my brother for your unconditional encouragement and support.